IMPROVED UPSCALING AND RESERVOIR SIMULATION OF ENHANCED OIL RECOVERY PROCESSES IN NATURALLY FRACTURED RESERVOIRS

MOHAMED AHMED ELFEEL

Submitted for the degree of Doctor of Philosophy

Institute of Petroleum Engineering

Heriot-Watt University

June 2014

To my beloved parents

ABSTRACT

Naturally fractured reservoirs (NFR) contain a significant amount of remaining petroleum reserves and are now considered for Enhanced Oil Recovery (EOR) schemes that involve three-phase flow such as water-alternating-gas (WAG) injection. Accurate numerical simulation of flow in NFR is essential for sound reservoir management decisions to maximise oil recovery and minimise the cost of field development. In this thesis, two important issues related to flow simulation in NFR are investigated. First, a step-wise upscaling approach is developed to evaluate the accuracy of dual porosity models in estimating matrix-fracture transfer during WAG injection. It was found that the classical dual porosity models generally overestimate recovery from matrix blocks. Hence, a double block model was developed and extended to a multi-rate dual porosity (MRDP). The multi-rate double block model showed significant improvements in matching detailed fine grid simulations of three-phase matrix-fracture transfer. Second, the accuracy of upscaling discrete fracture networks (DFN) is assessed and its impact on history matching was investigated on a real fractured reservoir. A new method to upscale the shape factors needed for MRDP models from DFN is presented. This method is a notable step towards more accurate but still efficient reservoir simulation in NFR.

PUBLICATIONS

This thesis contains excerpts from the following papers:

AHMED ELFEEL M. , Geiger S., Static and Dynamic Assessment of DFN Permeability Upscaling, SPE Paper 154369. In *SPE Europec/EAGE Annual Conference:Copenhagen, Denmark, 2012.*

AHMED ELFEEL M. , Al-Dhahli A., Geiger S., van Dijke M.I.J., Multi-scale Simulation of WAG Flooding in Naturally Fractured Reservoirs, SPE Paper 164837. In *SPE Europec/EAGE Annual Conference: London, United Kingdom, 2013.*

AHMED ELFEEL M. , Jamal M., Enemanna C., Arnold D., Geiger S., Effect of DFN upscaling on History Matching and Prediction of Naturally Fractured Reservoirs, SPE Paper 164838. In *SPE Europec/EAGE Annual Conference: London, United Kingdom, 2013.*

AHMED ELFEEL M. , Al-Dhahli A., Jiang Z., Geiger S., van Dijke M.I.J., Effect of Rock and Wettability Heterogeneity on the Efficiency of WAG Flooding in Carbonate Reservoirs, SPE Paper 166054. In S*PE Reservoir Characterisation and Simulation Conference and Exhibition, Abu Dhabi, UAE, 2013.*

AHMED ELFEEL M. , Al-Dhahli A., Geiger S., van Dijke M.I.J., Matrix-fracture interactions during immiscible three-phase flow. Submitted to *Journal of Petroleum Science and Engineering.*

AHMED ELFEEL M. , Agada S., Maier C., Geiger S., Integrating Discrete Fracture Models for Static and Dynamic Calibration of Fractured Reservoirs. In *Proceedings 76th EAGE Conference and Exhibition, Amsterdam, Netherlands, 2014.*

One can pay back the loan of gold,
but one dies forever in debt to those
who are kind

— A Malayan proverb

ACKNOWLEDGMENTS

This work would never be possible without the support and collaboration I found within the Carbonate Reservoir Group. First of all, I would like to express my gratitude to Prof. Sebastian Geiger for being an extraordinary supervisor. Your level of support was beyond any expectations. Thanks for giving me the autonomy to do what I like to do and for your leading by example style. I learned so much from you beside modelling fractured reservoirs.

I am also thankful to my secondary supervisor, Prof. Gary Couples for many good ideas I developed since my master's degree graduation project. I wish him great fun in his global lecture tour. Dr. Rink van Dijke's office was always open when I had questions regarding pore-network modelling. Thanks for reviewing some of the papers. Prof. Eric Mackay, I have learned a great deal from the three ECLIPSE tutorials. Thank you for that and for letting me keep my ECLIPSE support profession while I am studying.

A big thank you to Prof. Ken Sorbie and Prof. Leonhard Ganzer for agreeing to be my examiners. I tried my best to keep the thesis as simple and interesting as I could. I hope this was true. Thanks for your constructive criticism and the encouragement I received during the viva.

Thanks to Heriot-Watt University for the Ali Danesh scholarship, and for all the support I found. Thanks to the computer support group, despite their busy schedules and me being somewhat a naughty student, they have provided me with all software needed to do my PhD. Thanks to the career advisers for helpful tips, and the International Student Support Office for their help with accommodation and visa applications.

During my PhD I was fortunate enough to be one of the inhabitants of Planet R.1.16-EA. It has such a wonderful environment where one for all and all for one. THANK YOU to the inhabitants of R.1.16-EA for your true friendship and for an amazing experience. Christine, thanks for the occasional help with CSMP++, LaTex, ...etc. I will always remember our discussion in Notre-Dame de Paris! Claudia, thanks for being my neighbour for a long time. Many thanks for showing me how to plot with MATLAB and how to use the snipping tool, many

figures in the thesis would have been difficult without these. Thanks Karen for setting a standard on how a PhD work should impact the world! Viswa Santhi, it is true that you are peace to our world, thanks for arranging family engaging events, for the risk games which you won all :) , and for frequent RE discussions. Simeon, I will never forget our experience in St. Petersburg. Thanks for your help to digitise the fracture map in Chapter 8. By the way, are you Russian? :). Qing, my new neighbour, thanks for the Chinese lessons and for your critical advice. Robert, I admire your humbleness! thanks for always offering help even when you are busy - your quick fixes for CSP and LaTex always come handy. Alessandro, it was great to have a geologist inhabitant of R.1.16-EA. thank you for always offering help and for the subdomain figure in Chapter 2. Thanks for the memorable Halloween party. Yan, thanks for the first CSMP tour and for explaining the finite element method. I wish you and your family all the best. Chen, thanks for your honesty and sense of humour. Luiz and Alexandra et al., thanks for the presents, your visits and the BBQ. For you, I will support Brazil in the coming world cup. Adnan: you have been such a great help for me. Chapter 3 of the thesis wouldn't have seen the light without your collaboration even after finishing your PhD. Thank you very much and I wish you all the best for your wedding. My thanks are extended to the short visitors and neighbours of R.1.16-EA, Tannaz, Wessam, James, Obinna, Juliana, Martin and Roman.

I would like to thank the prayer room brothers for their support and help. Thank you Salem, Khaled, Khalid, Misfer, Mustapha, Usman, Adil, Abdeladim, Ali, Kamaran, and Amir. To those who left, Gamal, Saleh, Hassan and Dr. Arfan. Thank you all for your spiritual solidarity, frequent discussion and coffee breaks. Thanks are extended to my Sudanese friends at Heriot-Watt University. Thank you Mohamed Babikir, Musab, Nouren, Husam, Haitham, Hassan and Ahmed.

My brother Eltazy has been a great support without which my PhD would have been very difficult to endure. I wish him all the best in the reminder of his PhD. My brothers and sisters: Ayoub, Mugahid, Sondos, Khalid, Omer and Salma, thank you all for your support from a distance. I am glad that I will be meeting you soon. My sister Sondos and nephew Mohamed, you are such a relief to our lives! thank you for coming here to help us through some difficult times. Um Ayman's support was infinite, I simply can't thank you enough for always looking after me and my son. I am heavily indebted to my parents for every success in my life. Without your love, care and support I would have achieved nothing. All what I hope for in this life, is to make you pleased with me.

All praise is due to Allah, the creator of the heavens and the earth. I ask Him to forgive my failures and shortcomings, endow me with knowledge and wisdom, and guide me to the better, always. Amen.

ACADEMIC REGISTRY
Research Thesis Submission

Name*:*	Mohamed Ahmed		
School/PGI:	IPE		
Version: *(i.e. First, Resubmission, Final)*	Final	Degree Sought (Award **and** Subject area)	PhD in Petroleum Engineering

Declaration

In accordance with the appropriate regulations I hereby submit my thesis and I declare that:

1) the thesis embodies the results of my own work and has been composed by myself
2) where appropriate, I have made acknowledgement of the work of others and have made reference to work carried out in collaboration with other persons
3) the thesis is the correct version of the thesis for submission and is the same version as any electronic versions submitted*.
4) my thesis for the award referred to, deposited in the Heriot-Watt University Library, should be made available for loan or photocopying and be available via the Institutional Repository, subject to such conditions as the Librarian may require
5) I understand that as a student of the University I am required to abide by the Regulations of the University and to conform to its discipline.

* *Please note that it is the responsibility of the candidate to ensure that the correct version of the thesis is submitted.*

Signature of Candidate*:*		Date:	

Submission

Submitted By *(name in capitals):*	
Signature of Individual Submitting:	
Date Submitted:	

For Completion in the Student Service Centre (SSC)

Received in the SSC by *(name in capitals):*			
Method of Submission *(Handed in to SSC; posted through internal/external mail):*			
*E-thesis Submitted (**mandatory for final theses)***			
Signature:		Date:	

Please note this form should bound into the submitted thesis.

Updated February 2008, November 2008, February 2009, January 2011

CONTENTS

LIST OF FIGURES

LIST OF TABLES

NOMENCLATURE

A	area	$[m^2]$
b	shrinkage factor	$[m^3_{SC}/m^3]$
B	formation volume factor	$[m^3/m^3_{SC}]$
C	Oda's percolation parameter	[-]
D	matrix block height	$[m]$
e	fracture aperture	$[m]$
g	gravity acceleration constant	$[m/s^2]$
G	gravity potential	$[Pa]$
h	Dynamic fluid level	$[m]$
k	absolute permeability	$[mD]$
k_r	relative permeability	[-]
L	length, fracture spacing	$[m]$
M	Oda's correction multiplier	[-]
p	pressure	$[Pa]$
p_c	capillary pressure	$[Pa]$
q	production / injection rate	$[m^3/s]$
S	fluid saturation	[-]
t	time	$[s]$
T	transmissibility	$[m^3/s/Pa]$
V	volume	$[m^3]$
V_b	bulk volume	$[m^3]$
x, y, z	Cartesian coordinates	
γ	specific weight	$[Pa/m]$
δ	time-step difference	
Δ_x	spatial difference	
$\Delta/2$	Thickness of the outer matrix block	$[m]$
λ	matrix-fracture transmissibility	$[m^3/s/Pa]$

μ	fluid viscosity	[Pa.s]
ρ	density	[Kg/m^3]
σ	matrix shape factor, imbibition	[m^{-2}]
σ_z	matrix shape factor, gravity drainage	[m^{-2}]
ϕ	porosity	[-]
Φ	potential	[Pa]
Superscripts		
n	time step level	
Subscripts		
f	fracture	
g	gas	
m	matrix	
M1	outer matrix block	
M2	inner matrix block	
o	oil	
r	residual	
w	water	

1

INTRODUCTION

Fractures are ubiquitous in almost all rock formation outcrops (Fig. 1.1). The majority of subsurface reservoirs are therefore assumed to contain fractures to some degree. It is often said that *"all reservoirs should be considered fractured until proven otherwise"* (e.g. Narr et al., 2006; Nelson, 2001). The term Naturally Fractured Reservoirs (NFR) is often used to denote reservoirs where fractures have a significant impact on fluid flow. Fractures can alter the porosity and/or permeability of the reservoir (Nelson, 2001), resulting in a more complex fluid flow compared to unfractured reservoirs. Numerical simulation of flow processes in NFR is of prime interest for a number of reasons including ground water management, CO_2 storage, nuclear waste management, hydrothermal energy exploitation, and the recovery of hydrocarbon resources. The latter is the primary focus of this thesis.

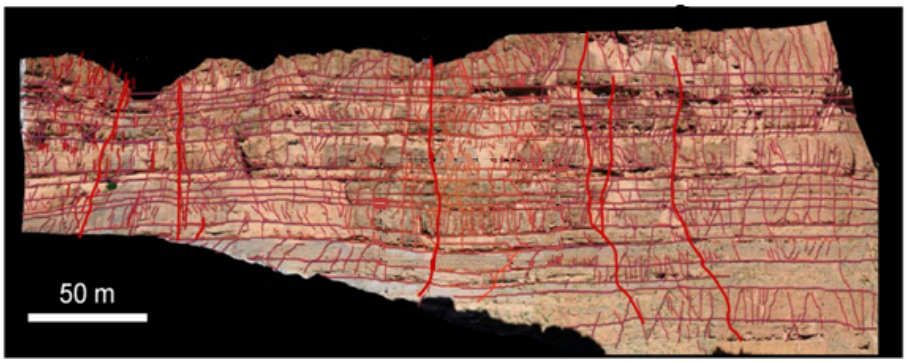

Figure 1.1: A carbonate fractured formation outcrop. The horizontal lines represent bed boundaries. The fractures are sub-vertical. Detailed fracture geometries were identified using the LiDAR technology (LIght Detection And Ranging). Taken from Agar et al. (2010).

Today, the world consumes nearly 90 million barrels of oil per day (IEA, 2014). If this is kept constant, conventional oil reserves will become progressively scarce and are set to be finished in 50 years time, unless the reserves increase. The current booked reserves are estimated at 1.669 trillion barrels worldwide (BP, 2012). There are two ways to increase reserves: discovering new fields and increasing ultimate recovery from existing reservoirs. The former is becoming increasingly

difficult and involves exploring environmentally sensitive areas such as the arctic and deepwater reservoirs. Hence, the deployment of enhanced oil recovery (EOR) and improved oil recovery (IOR) techniques is inevitable to increase the world's reserves. It is also conjectured that oil prices stay high because of the limited oil supply (Muggeridge et al., 2014), rendering many EOR/IOR techniques viable.

Schlumberger (2007) estimates that carbonate reservoirs contain more than 60% and 40% of the remaining oil and gas, respectively. Carbonate reservoirs are typically naturally fractured. Recovery in these reservoirs is generally lower than sandstone reservoirs (Montaron, 2008). Early reservoir engineering and geology studies (e.g. Bulnes and Fitting, 1945; Imbt and Ellison, 1947; Pirson, 1953) analysed the possible reasons and suggested that the two sedimentary rock types should be studied separately.

The role of secondary porosity and diagenesis in carbonate reservoirs is more significant and hence leads to porosity-permeability relationships that are very different to sandstone reservoirs (Lucia, 1995, Chandra et al., In press). Furthermore, the multi-phase flow functions, such as wettability, relative permeability and capillary pressure, are also different. Carbonates tend to be more oil-wet than sandstone reservoirs (e.g. Chilingar and Yen, 1983; Lichaa et al., 1993; Bennion et al., 2002; Hollis et al., 2010) (Fig. 1.2). Recovery as a result of water injection, the widely used method for secondary recovery, strongly depends on the wettability state of the reservoir rock. The more oil-wet the rock is, the less the matrix recovery will be. As more and more water flows in the fractures, this will lead to early water breakthrough (e.g. O'Neill , 1988; van Dijkum and Walker, 1991).

Figure 1.2: Pie charts showing wettability preferences obtained from over 60 sandstone and carbonate formations in Canada. Data taken from Bennion et al. (2002).

Gas oil gravity drainage (GOGD) provides an important drive mechanism in such cases because it can increase recovery factors irrespective of the reservoir wettability (e.g. Hagoort, 1980). Fractures extend the exposure of the injected gas with oil in reservoir rock, which renders GOGD more effective compared to unfractured reservoirs. Hence gas injection has been applied in many NFR (e.g. O'Neill, 1988; van Dijkum and Walker, 1991; Jakobsson and Christian, 1994; Saidi, 1996). However, as the gas mobility is very high compared to water and oil, so is the risk of by-passed oil and gravity override, which can lead to very early gas breakthrough (e.g. Panda et al., 2009). In addition, the lack of availability of gas may limit the implementation of a recovery scheme that solely relies on gas injection.

Water-alternating-gas (WAG) injection, both at miscible and immiscible conditions, combines the merits of the two injection fluids described above on macroscopic and microscopic scales while stabilizing the injection front, delaying breakthroughs, and therefore leading to increased oil recovery compared to continuous water or gas injection. This has been demonstrated in micromodel experiments that mimic multi-phase flow in conventional (Sohrabi et al., 2004) and fractured porous media (Er et al., 2010; Dehghan et al., 2012). In almost all reported cases, WAG application on the field-scale was observed to improve recovery (Christensen et al., 2001, Awan et al., 2008, Brodie et al., 2012).

WAG injection and tertiary gas injection are widely applied as EOR techniques (Christensen et al., 2001). In the North Sea, WAG injection has been regarded as the most successful EOR method (Awan et al., 2008, Muggeridge et al., 2014). In the United States, the above two methods constitute more than 80% of all EOR applications in carbonate reservoirs (Manrique et al., 2007). WAG injection has already been piloted in the Middle East (Arayni et al., 2013, Rawahi et al., 2012, Kalam et al., 2011), the preliminary results are very promising (Al Shamsi et al., 2012). WAG injection is also considered for the vast untapped carbonate reservoirs offshore Brazil (Pizarro and Branco, 2012).

WAG injection is known to improve micro- and macro-scale oil recovery (Christensen et al., 2001). However, the recovery mechanisms are still not fully understood due to the complexity of three-phase flow. A recent overview of multi-

scale evaluation of WAG recovery mechanisms has been presented by Skauge and Sorbie (2014). Pore-scale observations are used to understand why residual oil saturation during WAG is usually less than continuous water or gas injection (Fig. 1.3). Pore-network models have been developed to decipher the complexity of three-phase flow as experimental evaluations are extremely difficult and costly (van Dijke et al., 2004, Al-Dhahli et al., 2013). Three-phase flow functions, i.e. relative permeability and capillary pressure, couple the pore- and lab-scale to the reservoir-scale flow simulations. These flow functions have a significant impact on matrix-fracture transfer and are fundamental for accurate reservoir simulations.

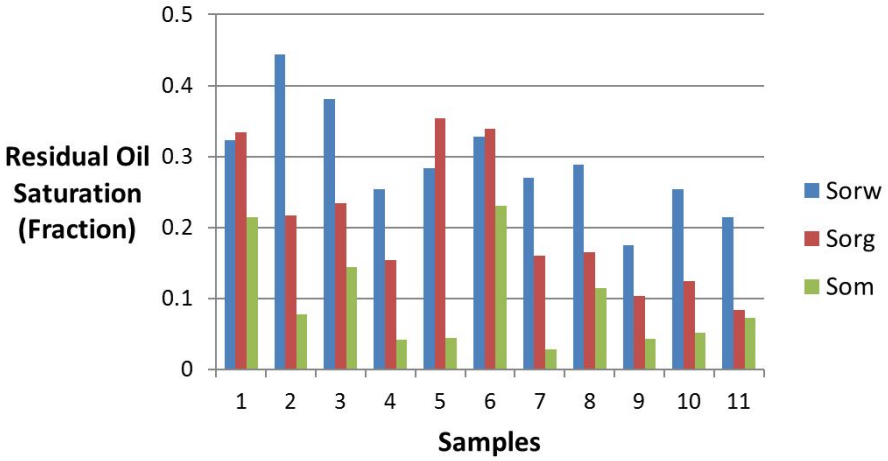

Figure 1.3: Comparison of residual oil saturation, S_{or}, due to WAG injection (Som), continuous gas injection (Sorg) and continuous water injection (Sorw). Data from Skauge and Sorbie (2014)

1.1 CONTEMPORARY MODELLING OF FRACTURED RESERVOIRS

In this section, a brief introduction into the modelling approaches of NFR is presented. These approaches will be reviewed in greater detail in Chapter 2 of the thesis. A note is given here on the critical impact of three-phase flow functions in numerical simulation of NFR. The role of three-phase flow functions will also be discussed in detail later in the thesis.

1.1.1 *The dual porosity model*

Fractured reservoirs can be viewed as a combination of two entities: fractures that have a significant impact on the reservoir flow capacity, but which holds a small fraction of the reservoir storage capacity; and matrix blocks that hold the majority of the reservoir storage capacity, but have a little influence on the flow capacity. A model that combines the two entities is called a dual porosity (DP) model (Barenblatt et al., 1960, Warren and Root, 1963). Although this model was introduced half a century ago, it is still the industry standard to model flow in fractured reservoirs. The interaction between fractures and matrix blocks is modelled through sink/source terms known as transfer functions (Kazemi et al., 1976, Thomas et al., 1983)(Fig.1.4a).

1.1.2 *Discrete fracture models*

The advances made in computational software and hardware in the past three decades facilitated seemingly realistic models to be built where fractures are explicitly honoured as discrete objects. These models are classified into two main groups: Discrete fracture network (DFN) models (e.g. Long et al., 1982; Robinson, 1984; Dershowitz et al., 1998; Sabathier et al., 1998; Dershowitz et al., 2000) and discrete fracture and matrix (DFM) models (e.g. Kim and Deo, 2000; Juanes et al., 2002; Bogdanov et al., 2003; Karimi-Fard et al., 2004; Hoteit and Fairoozabadi, 2006; Matthai et al., 2007; Geiger et al., 2009).

In DFN models, the matrix blocks are not represented in the numerical model (Fig. 1.4b). Hence, like the dual porosity model, these models require transfer functions to simulate flow in fractured porous media. The transfer functions are not required when DFN models are applied to simulate flow and transport in fractured metamorphic or igneous rocks where rock porosity is infinitely small (e.g. Niemi et al., 2000). The DFN approach has been used as a platform for static modelling of fractured reservoirs (Dershowitz et al., 2000, Sabathier et al., 1998), where fracture networks are generated to match observation data (e.g. image logs, outcrop data, dynamic well tests and production logging), and to upscale

fracture properties to continuum scale properties. These properties are fracture porosity, fracture permeability and matrix shape factors. Before the introduction of DFN upscaling, it was common to use these properties as history matching parameters without a direct link to geological observations. DFN modelling tools are readily available in standard petroleum reservoir modelling software.

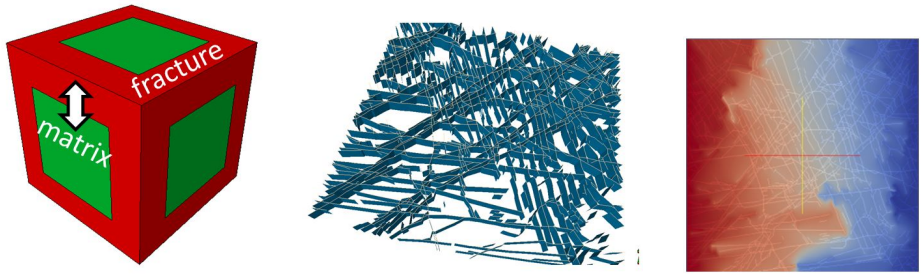

(a) (b) (c)

Figure 1.4: Types of fracture models. (a) A dual porosity (DP) model where fractures and matrix blocks are modelled separately and linked with a transfer function. (b) A discrete fracture network (DFN) model where only fractures are considered in the numerical model. (c) A discrete fracture and matrix model (DFM) showing pressure distribution in both fractures and matrix blocks.

DFM models explicitly account for fracture and matrix block flow (Fig. 1.4c). Hence, they require additional gridding and computational cost, but overcome assumptions generally applied to model flow in the matrix blocks. The DFM approach can hence serve as a numerical laboratory, where hypotheses related to fracture properties are tested and conceptual models are evaluated. DFM simulations have been used to upscale single and multi-phase flow in fractured reservoirs (Karimi-Fard et al., 2006, Gong et al., 2008, Matthäi and Nick, 2009, Ahmed Elfeel et al., 2010, Ahmed Elfeel and Geiger, 2012).

1.1.3 *Three-phase flow*

In NFR, capillary pressure and relative permeability functions have a major impact on fluid exchange between matrix blocks and fractures. Fluid transfer between fractures and matrix blocks is dominated by capillary and gravity forces. Since most oil is contained inside the matrix, capillary and gravity forces can be more important in NFR compared to unfractured reservoirs. For example, capil-

lary forces may either enhance or reduce recovery from matrix blocks depending on wettability (e.g. Gilman and Kazemi, 1988; Gang and Kelkar, 2008).

Three-phase flow modelling is challenging as saturation functions are difficult to measure in the lab. Commonly, three-phase relative permeability is estimated using empirical models such as Stone I and II (Stone 1970, 1973) and the saturation weighted interpolation method (Baker, 1988). Improvements have been made to increase the accuracy of these empirical models for WAG injection applications (Larsen and Skauge, 1998, Skauge et al., 1999, Blunt, 2000, Shahverdi and Sohrabi, 2013). WAG injection numerical simulation results are highly dependent on the choice of the empirical model. It has been shown that uncertainty in recovery can be as large as 20% absolute, only due to the use of different empirical models (Shahverdi and Sohrabi, 2013). This significant uncertainty necessitates the verification of the flow functions before employing them in reservoir simulation.

Pore-network modelling (PNM), sometimes referred to as digital rock physics, has been developed recently to estimate three-phase flow functions (e.g. Mani and Mohanti, 1998; van Dijke et al., 2004; Piri and Blunt, 2005; Al-Dhahli et al., 2013). The flow functions predicted by PNM are in close matches to the experimentally derived flow functions for water-wet rocks (e.g. Oak, 1990); or micro-model experiments for different wettability configurations (e.g. van Dijke et al., 2004). PNM, hence, offer an alternative to empirical models (Fig. 1.5) and its results can be used as input in commercial reservoir simulators (see Chapter 3).

1.2 CHALLENGES AND LIMITATIONS IN MODELLING FLOW IN NFR

1.2.1 *Characterisation and geological uncertainty*

The effect of fractures on flow can range anything from complete hindrance, as in mineral-filled fractures, to the other extreme where fractures constitute major flow conduits. This is exacerbated by the tremendous difficulty encountered when characterising fracture properties at reservoir conditions. Uncertainty quan-

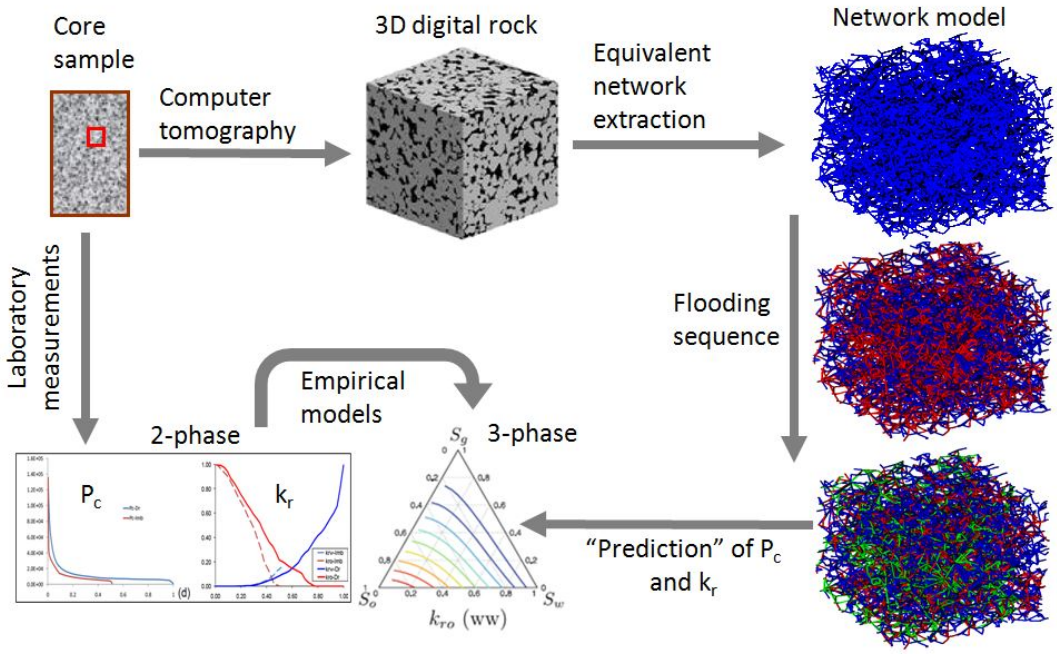

Figure 1.5: Three-phase pore-network modelling as an alternative to empirical models. From Al-Dhahli (2013)

tification is therefore highly recommended to accompany any attempt to model flow in NFR (e.g. Mäkel, 2007). This necessitates building equi-probable realizations of static and dynamic fracture models to explore the possible range in simulation results due to the geologic uncertainty.

DFM models become unfavourable in stochastic frameworks where multiple models are generated, upscaled and run because of the computational cost needed. In some cases, the generation of the unstructured grid is very challenging and may not be achieved without simplifying assumptions (e.g. Mallison et al., 2010), or increasing the number of nodes to high numbers in order to resolve the complex fracture geometries.

DFN models link the dual porosity parameters to geological parameters. The computational cost of DFN, by definition, is smaller than DFM models. Therefore, the DFN approach provides a reasonable compromise between efficiency and accuracy. The fact that they are readily available in industry standard reservoir modelling software means that implementing new DFN-based upscaling methodology or improvement will be relatively fast and straightforward. The DFN models are well suited for stochastic frameworks for uncertainty quantification and for matching observations. DFN upscaling can follow one of two

methods: analytical and flow-based upscaling. The DFN upscaling is very efficient when analytical methods are used (Oda, 1985).

1.2.2 *Upscaling related challenges*

Continuum modelling of flow in porous media assumes the existence of a representative elementary volume (REV), above which the media properties are uniform within the simulation cell size. However, real fracture distributions show a scaling behaviour in fracture length and connectivity (e.g. Odling, 1997; Bonnet et al., 2001; Berkowitz, 2002; Neuman and Di Federico, 2003)(Fig. 1.6). Therefore, the upscaling of fracture networks might depend on the simulation cell size. As will be discussed in detail in Chapter 2, the analytic DFN upscaling method of Oda (1985) is known to overestimate the fracture connectivity (Dershowitz et al., 2000, Cottereau et al., 2010, Ahmed Elfeel and Geiger, 2012). On the other hand, flow-based upscaling depends on boundary conditions (Dershowitz et al., 2000). The upscaling dependency necessitates a quantitative measure to assess the DFN upscaling errors in a given situation, but so far only qualitative approaches have been developed.

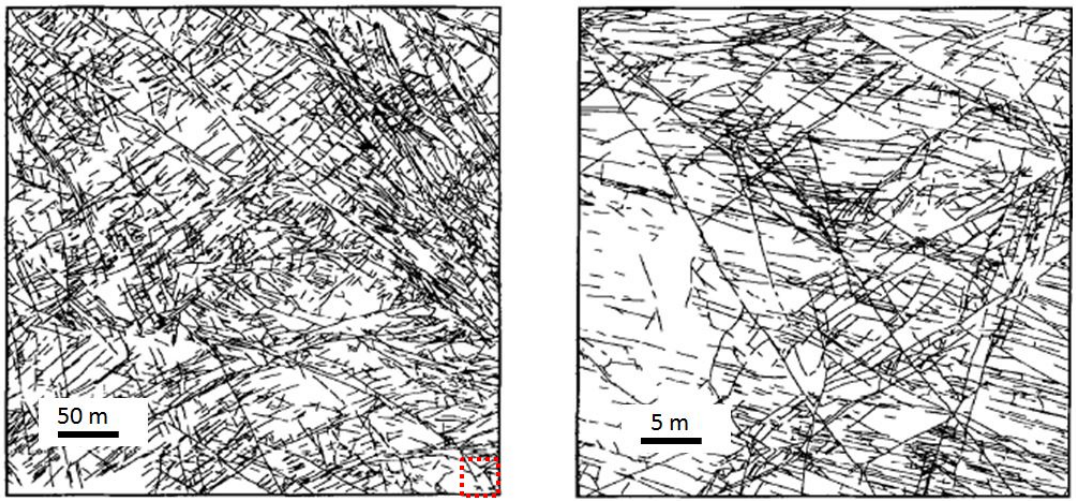

Figure 1.6: Scaling of fracture distributions in the Hornelen Basin in Norway. The relative location of the small scale fracture map (right) is indicated by the red square in the large scale fracture map (left). From Odling (1997).

Karimi-Fard et al. (2006), Gong et al. (2008) presented a DFM-based upscaling method. Both DFN and DFM flow-based upscaling can feed into dual porosity

models to simulate flow in fractured reservoirs. These DFN/DFM flow-based methods could be accurate, but might not be applicable to full field scales and uncertainty quantification workflows because flow-based methods are computationally expensive.

1.2.3 *Challenges related to three-phase flow functions*

One last, but important, challenge related to three-phase flow modelling remains. The empirical models usually employed, e.g. Stone I, II (Stone 1970, 1973) and the saturation weighted interpolation method (Baker, 1988), were mainly developed based on available published data, the majority were for water-wet rock. Since carbonate reservoirs are less water-wet than sandstone reservoirs, an evaluation of the performance of empirical models becomes necessary. This is particularly true when the oil saturation is small, as this is exactly the region of interest when applying the EOR methods (Blunt, 2000, Spiteri and Juanes, 2006). Moreover, under some conditions, WAG may lead to water and gas displacing each other, while leaving the oil phase located in the matrix in place. Simple extrapolation of two-phase flow functions might fail to capture such fluid displacement processes.

1.3 OBJECTIVES AND STRUCTURE OF THE THESIS

The aim of the thesis is to improve the reliability of upscaling and reservoir simulation of fractured reservoirs. This is achieved by the quantification and possibly removal of upscaling and model concept errors so that the focus is only on evaluating the geological uncertainty. Accuracy and efficiency are the two main areas to improve the state-of-the-art modelling capabilities. First, the accuracy of existing methods is evaluated by quantitative analysis of simulation models (e.g. comparing a reference fine grid model with an equivalent classical dual porosity model). The primary focus is on implementing new improvements in the upscaling methods and numerical models to enhance the accuracy of the prediction.

Second, efficiency is taken into consideration by focusing on the combination of DFN-based upscaling and classical dual porosity models. This combination is less computationally demanding compared to full DFM models and DFM-based upscaling methods. Furthermore, new improvements in DFN-upscaling and classical dual porosity models can be implemented easily in conventional reservoir simulators and modelling packages.

The thesis aims to specifically achieve the following:

- Investigate PNM application to predict matrix-fracture transfer during WAG injection. This enables the evaluation of the accuracy of the empirical models. PNM is also used to explore the effect of various pore structures and wettability to analyse their influence on relative permeability and capillary pressure curves and the subsequent impact on matrix-fracture transfer.

- Improve the classical dual porosity model to simulate three-phase matrix-fracture transfer more accurately. This improvement should facilitate the application of dual porosity models in reservoirs with multi-scale heterogeneity.

- Improve DFN-based upscaling methods to estimate fracture permeability and matrix shape factors. Develop a new workflow to assess DFN upscaling accuracy and quantify the impact of upscaling errors on history matching.

The thesis is divided into two parts: The first concerns three-phase matrix-fracture transfer and the effect of multi-scale heterogeneity, including different heterogeneities at the pore-scale. It encompasses the first and second objectives of the thesis. The second part is focused on the evaluation of DFN based upscaling and the development of improvements in upscaling methods. In total, the thesis has 9 chapters.

Chapter 1 is the current chapter. It shows the importance of fractured reservoirs and three-phase flow modelling. A brief overview is given on the stat-of-the-art fractured reservoirs modelling tools followed a discussion of limitations

and challenges. This paves the way to introduce the objective of the thesis and explain its structure.

Chapter 2 reviews the methods to model fractured reservoirs in detail. A critical review is provided on the different approaches proposed in the industry to model flow in fractured reservoirs. A special emphasis is given to the development of the classical dual porosity model. DFN and DFM modelling approaches are also discussed and highlights are provided on the limitations of each approach.

PART I: MATRIX-FRACTURE TRANSFER UNDER THREE-PHASE FLOW

Chapter 3 discusses the effects of wettability and pore-scale heterogeneity on three-phase matrix-fracture transfer. A novel pore-network modelling tool is used to estimate three-phase relative permeability and capillary pressure. These are then used in fine grid single porosity simulations to quantify the impact on matrix-fracture transfer during three-phase flow. A comparison is made between the pore-network derived results and the empirical models.

Chapter 4 discusses the effects of heterogeneity at the scale of a simulation cell on three-phase matrix-fracture transfer. The fine grid single porosity model used in Chapter 3 is used here again to quantify the impact of sub-cell heterogeneities, common to fractured carbonate reservoirs, on matrix-fracture transfer. These heterogeneities include permeability, wettability distribution and matrix block sizes. The results are then compared with equivalent dual porosity models.

In Chapter 5, an improved dual porosity model is developed to improve the accuracy of matrix-fracture transfer during WAG injection. The transfer term is derived and compared with to a commercial reservoir simulator's calculations. The configuration of the new parameters is discussed followed by extension of the model to simulate matrix-fracture transfer when matrix blocks are of different sizes.

PART II: DFN UPSCALING ASSESSMENT AND IMPROVEMENT

Chapter 6 highlights the uncertainty that arises due to DFN permeability upscaling. A workflow to assess the upscaling accuracy is shown.

Chapter 7 assesses the impact of DFN upscaling on history matching. Data from the Tensleep Formation in the Teapot Dome Field is gathered to history match the field production data in a geologically consistent manner. The model building is described followed by discussion of the history matching results.

Chapter 8 revisits the DFN permeability upscaling workflow in relation to the reservoir engineering data normally available. An improved upscaling methodology for matrix shape factors is shown that feeds into the multi-rate dual porosity models. The utility of the improved upscaling method is demonstrated using a realistic 2D fracture outcrop model.

Chapter 9: A summary of the key outcomes of the thesis and concluding remarks are given. This is followed by an outlook on how this research can develop in the future.

2

RESERVOIR SIMULATION OF FLOW IN FRACTURED RESERVOIRS

2.1 BACKGROUND

During the early twentieth century, as more and more petroleum reservoirs were discovered and developed, geoscientists and reservoir engineers started to notice a disparity in reservoir response to developments in carbonate and sandstone reservoirs. They started developing hypotheses to explain why carbonate reservoirs usually yield lower recovery than sandstone reservoirs. Since carbonate reservoirs are typically naturally fractured, fracture related issues were sometimes discussed under carbonate versus sandstone comparisons. Having recognized the differences in terms of porosity-permeability relationship, relative permeability and capillary pressure curves, Bulnes and Fitting Jr (1945) suggest that carbonate and sandstone reservoirs should be studied separately.

Imbt and Ellison Jr (1947) attributed the disparity in reservoir quality to the secondary porosity created by dissolution. However, the first 'dual porosity' hypothesis was put forward by Pirson (1953). He envisaged two parallel porosity-permeability relationships: One that constitutes 90% of reservoir pore volume, but posses a permeability in the order of 1 mD or less, and another that occupies the remaining 10% of the pore volume but has permeability in the order of 100 mD or more.

In unfractured reservoirs with a single porosity-permeability relationship, the single phase flow is governed by the continuity equation (e.g. Bear, 1972):

$$\frac{\partial}{\partial x}(\rho v) = \frac{\partial}{\partial t}(\rho \phi). \tag{2.1}$$

For simplicity, a one dimensional flow problem is considered here. ρ is the fluid density, v is flow velocity and ϕ is the porosity. $\rho = \rho_{SC}/B$ where ρ_{SC} is the

fluid density at standard conditions and B is the fluid formation volume factor (the ratio between a unit volume in the reservoir to the volume at the standard conditions). Since ρ_{SC} is constant, ρ is replaced by $1/B$ in both sides of Eq. 2.1. Also, v can be substituted using Darcy's law. As a result, the continuity equation takes the following form

$$\frac{\partial}{\partial x}\left(\frac{k}{\mu B}\frac{\partial \Phi}{\partial x}\right) = \frac{\partial}{\partial t}\left(\frac{\phi}{B}\right). \tag{2.2}$$

k is the rock absolute permeability, μ is the fluid viscosity and Φ is the flow potential. For completeness, a source/sink term, q', is added to account for injection/production wells in a simulation cell

$$\frac{\partial}{\partial x}\left(\frac{k}{\mu B}\frac{\partial \Phi}{\partial x}\right) - q' = \frac{\partial}{\partial t}\left(\frac{\phi}{B}\right). \tag{2.3}$$

Each term in Eq. 2.3 has a unit of $(1/t)$ and therefore q' is the injection/production rate normalized by the bulk volume of the control volume, V_b. If Eq. 2.3 is discretised and multiplied by V_b, one obtains

$$\Delta_x\left(\frac{k}{\mu B}A\frac{\Delta \Phi}{\Delta x}\right) - q = \frac{V_b}{\Delta t}\delta\left(\frac{\phi}{B}\right). \tag{2.4}$$

Here, Δt is the time increment, δ represents the change with respect to Δt and Δ_x represents the change with respect to x. It is often more convenient to use transmissibility of the simulation cells when descritising Eq. 2.4. The transmissibility is defined as $T = kA/(\mu B \Delta x)$. Also, when the potential Φ is split into its pressure and gravity components, $\Phi = p - \gamma D$, the equation becomes

$$\Delta_x\left(T(\Delta p - \gamma D)\right) - q = \frac{V_b}{\Delta t}\delta\left(\frac{\phi}{B}\right). \tag{2.5}$$

2.2 DEVELOPMENT OF THE DUAL POROSITY MODEL

Inspired by the work of Pirson (1953), Barenblatt et al. (1960) developed the first model for a dual porosity system. The model assumes that at any spatial location, there exist two pressure values: one represents the fracture and the other represents the matrix blocks. The exchange between the two domains, fractures and matrix, is characterized by a geometrical factor that relates to the fracture density and hence the size of the matrix blocks. The denser the fracture spacing, the smaller the matrix blocks are. Hence, the matrix-fracture interface area increases, and therefore the exchange rate increases as well. Later, Warren and Root (1963) established an analytical solution for the dual porosity model. The purpose was to identify and quantify the additional parameters needed to describe the flow behaviour during well testing. Hence, this was developed for single phase flow.

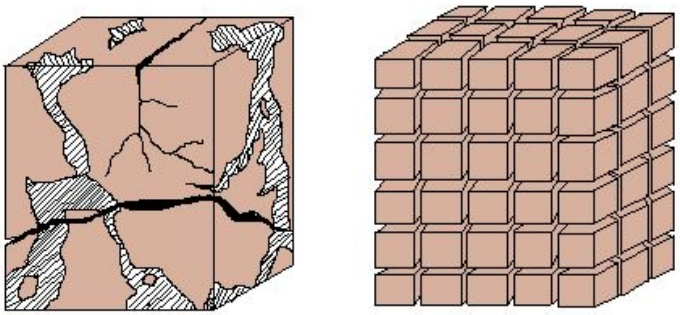

(a) Actual reservoir containing fractures and vugs

(b) Model reservoir with idealised fracture geometry

Figure 2.1: Idealization of a heterogeneous fractured porous medium. Redrawn from Warren and Root (1963)

Barenblatt et al. (1960) and Warren and Root (1963) set the following assumptions to derive the dual porosity equations:

1. Flow between the matrix and fractures is governed by a pseudo steady-state relationship, i.e. flow changes constantly with the potential difference between the fractures and the matrix.

2. The matrix blocks are homogeneous, isotropic and are in a systematic array of identical rectangular parallelepipeds (Fig. 2.1).

3. Fractures can be considered equivalent to porous media

They coupled the equations for matrix and fracture flow by additional source/sink terms in the fracture flow equation:

$$\Delta_x(T(\Delta p - \gamma D)_f) - q_f + \lambda(p_m - p_f) = \frac{V_{bf}}{\Delta t}\delta\left(\frac{\phi}{B}\right)_f. \tag{2.6}$$

$$\Delta_x(T(\Delta p - \gamma D)_m) - q_m - \lambda(p_m - p_f) = \frac{V_{bm}}{\Delta t}\delta\left(\frac{\phi}{B}\right)_m. \tag{2.7}$$

The subscripts f and m denote fracture and matrix blocks, respectively. λ is a transmissibility term equivalent to T but for matrix-fracture exchange and is given by:

$$\lambda = \left(\frac{k}{\mu B}V_b\right)_m \sigma, \tag{2.8}$$

where σ is the shape factor which describes the surface area per unit volume. It has a unit of $1/L^2$. Eqs. 2.6 – 2.7 account for fracture-fracture flow, matrix-matrix flow and matrix-fracture exchange through $\lambda(p_m - p_f)$. This model is the original model proposed by Barenblatt et al. (1960). It is referred to as the dual porosity – dual permeability model (DP–DK). Such formulation was later implemented by Hill and Thomas (1985) for reservoir simulation in fractured media. However, in Warren and Root's (1963) model and in reservoirs with low matrix permeability matrix-matrix flow is negligible and the first two terms in LHS of Eq. 2.7 are ignored. This is called the dual porosity (DP) model and is the main focus in this thesis. It should be noted that the DP model lacks the direct matrix-matrix connections and hence there is no capillary continuity. When the matrix permeability is high, matrix-matrix connections become important and DP–DK models should be considered.

The driving forces for single-phase model matrix-fracture flow are pressure difference and fluid expansion. However, most reservoir engineering problems,

and indeed the focus of this thesis, involve multi-phase flow. This gives rise to other driving forces: capillary and gravity forces that will influence the physics of matrix-fracture exchange and hence the transfer term (Fig. 2.2).

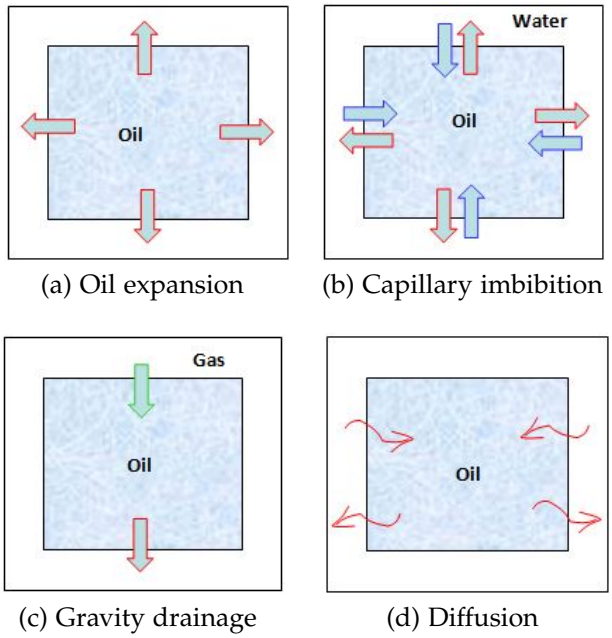

(a) Oil expansion (b) Capillary imbibition

(c) Gravity drainage (d) Diffusion

Figure 2.2: Different recovery mechanism associated with a matrix block and surrounding fractures exchange under multi-phase flow. Modified after Lu et al. (2008).

One approach to study and model multi-phase was pioneered by Mattax and Kyte (1962). Spontaneous imbibition experiments in laboratory are used to model matrix-fracture exchange. It is common to use dimensionless analysis to derive scaling groups that enable reservoir scale predictions based on the laboratory results. Various scaling groups have been developed (e.g. Kazemi and Gilman, 1993; Zhang et al., 1996) for different rock types and fluids involved. The scaling can be used to estimate sink/source terms that define the transfer functions, such as in de Swaan (1978) and Di Donato et al. (2003). Recently, Schmid and Geiger (2012, 2013) found a universal scaling group based on the analytical solution for spontaneous imbibition. Hence, matrix-fracture transfer can be computed for any fluid or rock properties. This makes the scaling approach very promising when predicting recoveries in reservoirs with arbitrary rock and fluid properties. A dual porosity model incorporating this analytical solution has already been implemented (Maier et al., 2013, Maier and Geiger, 2013). In this thesis, the aim is to improve conventional reservoir simulation methods in

NFR which is dominated by the classical dual porosity model. Therefore, scaling of experimental results is not discussed further.

The first multi-phase extension of the classical dual porosity model was presented by Kazemi et al. (1976). The model is three-dimensional and considers a two-phase (oil and water) system. It accounts for relative fluid mobilities, gravity forces (only in the fracture domain) and imbibition in matrix blocks. In Kazemi's model, the dual porosity equations are updated as follows:

$$\Delta_x(T_\alpha(\Delta p_\alpha - \gamma_\alpha D)) - q_{\alpha f} + \lambda_\alpha(p_{\alpha m} - p_{\alpha f}) = \frac{V_{bf}}{\Delta t}\delta\left(\frac{\phi S_\alpha}{B_\alpha}\right)_f, \tag{2.9}$$

and

$$-\lambda_\alpha(p_{\alpha m} - p_{\alpha f}) = \frac{V_{bm}}{\Delta t}\delta\left(\frac{\phi S_\alpha}{B_\alpha}\right)_m. \tag{2.10}$$

The subscript α denotes oil or water phases. T_α is updated from the single phase form by multiplying by $k_{r\alpha}$

$$T_\alpha = \frac{k k_{r\alpha} A}{\mu B \Delta x}. \tag{2.11}$$

The phase pressures are linked through the capillary pressure term

$$p_c = p_o - p_w. \tag{2.12}$$

If Eq. 2.12 is substituted in 2.10 for the water phase, the following is obtained

$$-\lambda_w(p_{om} - p_{of} + (p_{cf} - p_{cm})) = \frac{V_{bm}}{\Delta t}\delta\left(\frac{\phi S_w}{B_w}\right)_m. \tag{2.13}$$

The transfer term in Eq. 2.13 models matrix-fracture transfer due to spontaneous imbibition, a main recovery mechanism in water-wet reservoirs. As noted

above, Kazemi's model does not account for gravity forces inside matrix-fracture transfer. Kazemi et al. (1976) saw their model capturing fractured reservoirs heterogeneity since, in principle, each grid block has a unique shape factor based on fracture distribution in the reservoirs.

Thomas et al. (1983) presented a three-phase dual porosity model that accounts for capillary, gravity and viscous forces for fracture-fracture flow. The equations were essentially similar to Equations 2.9 and 2.10, in addition to the gas phase equations. Thomas et al. (1983) also provided provisions as to how gravity forces can be accounted for in the matrix-fracture exchange terms. Taking the equation for the water phase for comparison with Eq. 2.13, the gravity term is added as follows

$$-\lambda_w(p_{om} - p_{of} + (p_{cf} - p_{cm}) + C\Delta p_{gravity}) = \frac{V_{bm}}{\Delta t}\delta\left(\frac{\phi S_w}{B_w}\right)_m, \tag{2.14}$$

where C is a constant that depends on the distance over which $\Delta p_{gravity}$ acts and the characteristic length of the matrix blocks. Gilman and Kazemi (1983) used the simulation cell thickness, D, and fluid pressure gradients, γ, to account for the gravity forces in the matrix-fracture transfer function

$$-\lambda_w(p_{om} - p_{of} + (p_{cf} - p_{cm}) + (\gamma_{wf}D_f - \gamma_{wm}D_m)) = \frac{V_{bm}}{\Delta t}\delta\left(\frac{\phi S_w}{B_w}\right)_m. \tag{2.15}$$

However, it was not clear why they defined separate constants for matrix block thicknesses of the fractures and matrix blocks. Also, their gravity term is constant. Ideally, the gravity potential may increase or decrease, depending on the type of fluid in the fractures and matrix blocks. Sonier et al. (1988) introduced a 'dynamic' matrix-fracture gravity drainage term. Based on the assumption of fluid segregation, they used fluid saturations to derive the gravity potential as follows

$$-\lambda_w(p_{om} - p_{of} + (p_{cf} - p_{cm}) + \gamma_w(h_{wm} - h_{wf})) = \frac{V_{bm}}{\Delta t}\delta\left(\frac{\phi S_w}{B_w}\right)_m, \tag{2.16}$$

where,

$$h_w = \left(\frac{S_w - S_{wc}}{1 - S_{wc} - S_{or}} \right) L_z. \tag{2.17}$$

In Eq. 2.17, S_{wc} is the connate water saturation, S_{or} is the residual oil saturation and L_z is the vertical fracture spacing. Gilman and Kazemi (1988), Quandalle and Sabathier (1989) presented improvements in viscous flow calculations for matrix-fracture transfer. The improved model uses weighting functions to simulate a gradient of pressure, where fracture pressure is higher than the matrix pressure at one face and lower at the opposite face. Gilman and Kazemi (1988) revisited the gravity drainage process and recommended the use of multiple sub-domains, discussed later, or through dual porosity-dual permeability model that accounts for matrix flow in the vertical direction only. Quandalle and Sabathier (1989) separated vertical and horizontal flow to derive an improved shape factor. van Heel and Boerrigter (2006), Ramirez et al. (2009), Al-Kobaisi et al. (2009) used different shape factors for imbibition and gravity drainage. The transfer term, therefore, has the following form:

$$-\lambda_w(p_{om} - p_{of} + (p_{cf} - p_{cm}) + \frac{\sigma_z}{\sigma}\gamma_w(h_{wm} - h_{wf})) = \frac{V_{bm}}{\Delta t}\delta \left(\frac{\phi S_w}{B_w} \right)_m, \tag{2.18}$$

where σ_z is the gravity drainage shape factor, while σ is for viscous/imbibition shape factor. Lu et al. (2008) evaluated the four recovery mechanisms as in Fig. 2.2 and combined them to present the General Transfer Function. In a comparative study, AbuShaikha and Gosselin (2008) found that General Transfer Function and that of Quandalle and Sabathier (1989) performed better than the earlier transfer functions (Kazemi et al., 1976, Gilman and Kazemi, 1983, Sonier et al., 1988). In general, accounting for gravity forces in the DP model is considered to be simple and can lead to modelling errors, especially when Gas Oil Gravity Drainage (GOGD) is the main driving mechanism (e.g. Matthäi and Bazrafkan, 2013). Hence, more attention should be given to examine the gravity

terms in Eq. 2.18 and that they are capable of capturing the recovery mechanism in GOGD applications.

2.3 LIMITATIONS OF THE DP MODEL AND WORKAROUND SOLUTIONS

Dual Porosity (DP) models are widely used to model flow in fractured reservoirs. The strength of this model stems from the parsimony of the conceptual model, its efficiency and the ease with which it can be implemented in reservoir simulators. However, the three assumptions made in order to develop the DP model limit its applicability. (1) The pseudo steady-state assumption of the classical dual porosity model remains the centre of discussions and has been steering research efforts to seek workaround solutions, or possibly an alternative approach to model flow in fractured reservoirs (Saidi, 1983, Pruess and Narasimhan, 1985, Sarma and Aziz, 2006, Rangel-German and Kovscek, 2006, Karimi-Fard et al., 2006, Hui et al., 2013). (2) Another important limitation is the assumption of uniformity of matrix block sizes and geometries within the scale simulation grid block. Many fractured formation outcrops show that matrix block sizes are not uniform in that scale (e.g. Odling, 1997; Geiger et al., 2013). (3) The third assumption is related to the representation of fractures as an equivalent porous medium.

2.3.1 *The pseudo steady-state assumption*

The matrix blocks have a single pressure and fluid saturation values. This implies that fluids are distributed equally inside the matrix blocks. In single phase flow modelling, immediate pressure dispersion inside the matrix blocks and pseudo steady-state assumption could be a valid estimate, particularly, when the matrix permeability is high. Multi-phase flow however is complicated as relative permeability and capillary pressure values are affected by the saturation distribution in the matrix blocks. Therefore, a pseudo steady-state relationship as that of Eq. 2.18 may fail to accurately describe the flow behaviour. Many of the published work on DP models cited here used experimental data or fine-grid single poros-

ity simulations to provide reference solutions in order to verify the dual porosity models. When a match cannot be obtained, i.e. due to pseudo steady-state assumptions, a number of techniques were followed to change the DP parameters so that it fits the reference solution. These techniques are (1) varying the shape factor, (2) the use of pseudo capillary pressure or relative permeability curves, (3) the use of time dependent shape factors, and (4) increased discretisation inside the matrix blocks.

2.3.1.1 *Varying a constant shape factor*

As noted before, the shape factor quantifies the matrix block geometry or fracture spacing. If the matrix-fracture transmissibility, λ, is equated to the fracture-fracture / matrix-matrix transmissibility, T (see Eqs. 2.4 and 2.8), the following is obtained

$$\sigma = \frac{1}{V_b}\frac{A}{\Delta x}. \tag{2.19}$$

A similar term is used by Kazemi et al. (1992). Here, Δx represents the total distance the fluid front can reach during imbibition or gravity drainage. This is useful as it shows the geometrical elements affecting the shape factor. Assuming that the matrix blocks are uniform sugar cubes as in Fig. 2.1, it can be proved that for imbibition

$$\sigma = 4\left(\frac{1}{L_x^2} + \frac{1}{L_y^2} + \frac{1}{L_z^2}\right). \tag{2.20}$$

Here, L represent the matrix block sizes (or fracture spacing) in the three principal dimensions. If $L_x = L_y = L_z$, then σL^2 is constant and is equal to 12 (Kazemi et al., 1976). This characteristic constant has been estimated differently in different studies, e.g. Warren and Root (1963) used 60, Coats (1989), 24, Chang (1993), Lim and Aziz (1995), 29.6. Ueda et al. (1989) proposed to use a multiplier to Kazemi's et al. shape factor to match experimental data. Thomas et al. (1983) adjusted the shape factor constant to 25 to match fine grid simulation results.

The lack of consensus on the shape factor in published technical reports has contributed somehow to the use, or probably *'abuse'*, of the shape factor as a *'legitimate'* history matching parameter. This has been exacerbated by the lack of information about fracture distributions in the subsurface that led to the often made assumption that σ is the same for all cells (e.g. keywords like *SIGMA* and *DIFRAC* in *ECLIPSE* and *CMG* software, respectively). However, real fractured formation outcrops show that fracture intensity can vary spatially (see Fig. 1.6). Clearly, this is an area that could be improved to increase the reliability of dual porosity models. In this thesis, the approach is to honour the physical concept of the shape factor by relating it solely to fracture spacing.

Another problem with commonly used simulation parameters like *SIGMA* and *DIFRAC*, is the implicit assumption that the fracture domain is continuous throughout the reservoir. This assumption is not always true. In some fractured formation outcrops, there are regions where fractures do not persist. Such regions are better represented using the conventional single porosity model. Adaptive dual porosity models (e.g. von Pattay and Ganzer, 2001; Ganzer, 2002) combine the single and dual porosity models. These combinations are available in commercial reservoir simulators (e.g. *DPNUM* in *ECLIPSE*). Honouring the multi-scale nature of fracture connectivity, Bourbiaux et al. (2002) presented a workflow to use single porosity, dual porosity (DP) or dual porosity-dual permeability (DP-DK) depending on the fracture lengths and matrix properties. However, this does not treat modelling errors arising as a result of the pseudo steady-state assumption.

2.3.1.2 *The use of pseudo flow functions*

In addition to the shape factor, the transfer term in Eq. 2.18 contains relative permeability and capillary pressure terms. Hence, another workaround solution to improve the accuracy of dual porosity models is to change the capillary pressure and relative permeability values to fit experimental or fine grid simulations of matrix-fracture transfer. Dean and Lo (1988) followed an iterative process to estimate the capillary pressure curves by history matching fine grid single porosity models. Rossen and Shen (1989) presented a pseudoisation method for gas

oil gravity drainage and water oil imbibition. This method requires performing fine grid simulation of a single matrix block only once. The objective is to derive the matrix block saturation gradient with time (dS/dt). The derivative is used to calculate a pseudo capillary pressure curve that takes gravity and capillary displacement into account. Hence, this method is more efficient than that of Dean and Lo (1988) as it only requires the fine grid simulation once.

Gurpinar and Kossack (2000) tested many options to match single porosity fine grid simulations and recommended the use of pseudo capillary pressure curves. Pseudoisation of capillary pressure curves was also recommended by other authors (e.g. Sabathier et al., 1998, Abu Shaikha and Gosselin, 2008) to correct for simulation errors during gas oil gravity drainage. The error is caused because the capillary pressure in a simulation cell is evaluated at the cell centre (Fig. 2.3). However, the actual matrix blocks height could be larger as shown in the fine grid representation. The error increases with the thickness of simulation grid blocks and it is dependent on the shape of the gas oil capillary pressure. This correction is already implemented in commercial reservoir simulators (AbuShaikha and Gosselin, 2008).

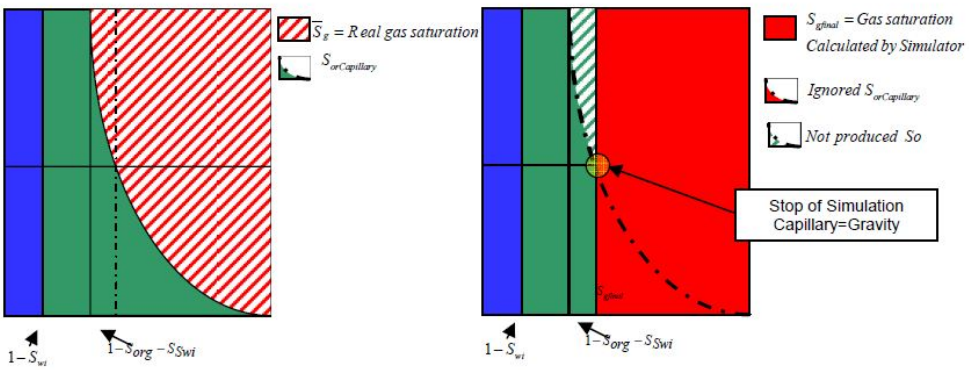

Figure 2.3: Capillary pressure pseudoisation to correct for simulation errors during gas oil gravity drainage. Comparison of a single matrix block fine grid results (left) and a dual porosity model (right) at the end of gas oil gravity drainage. The dual porosity model error is represented by the difference of the red hatched area in the fine grid results (left) and the red area in the dual porosity model (right). From Abu Shaikha and Gosselin (2008)

There are three limitations for the application of pseudoisation. The first is the cost of calculating the pseudo curves. Given the wide range of heterogeneity in fractured reservoirs, calculating pseudo curves for all the rock properties could mount to a formidable computational cost. The second limitation is that the use

of pseudo curves makes the reservoir simulation process specific, e.g. one can model either water oil imbibition or gas oil gravity drainage. If the recovery process changes, new pseudo curves have to be obtained. Finally, capillary pressure and relative permeability are related to pore-scale structure and heterogeneity; and are very expensive to obtain. By using pseudo flow functions, we may eliminate the physical basis of multi-phase matrix-fracture transfer. As with the shape factors, one may use pseudo curves as history matching parameters (e.g. Gurpinar and Kossack, 2000) instead of focusing on the geologic understanding and the physics of the displacement process.

2.3.1.3 *The use of time-dependent shape factors*

The pseudo steady-state describes the fluid saturation evolution in a linear fashion (e.g. the term $\lambda(p_m - p_f)$ in Eqs. 2.6 and 2.7). To overcome this assumption, the shape factor σ, embedded in λ, is made a function of time to capture transient effects. Penuela et al. (2002) derived a time-dependent shape factor which matched a 1D imbibition single porosity simulation results. In addition to a dimensionless time variable, the shape factor was a function of relative permeability parameters. Sarma and Aziz (2006) partitioned the matrix-fracture transfer into two terms. The first models fluid expansion and uses a constant shape factor. The second term captures recovery due to imbibition and is time-dependent. The summation of the two terms gave a more accurate recovery curve when compared to a reference solution. Rangel-German and Kovscek (2006) followed a similar approach but derived a time-dependent shape factor by dimensional analysis of experimental data.

Derivation of time-dependent shape factors usually involves solving an analytical equation which could be complex for immediate implementation in current reservoir simulators. Due to this difficulty, the validation of these shape factors is done with relatively simple models (1D simulation models) or simple experiments. In all three cases cited above, gravity forces were not considered, although the possibility of including them in the future was not ruled out.

Another transient shape factor has been suggested by Sabathier et al. (1998) to capture the physics of the water oil imbibition process. The shape factor is made saturation dependent, such that:

$$\sigma(S_\alpha) = \frac{1}{V_b}\frac{A}{X(S_\alpha)}, \tag{2.21}$$

where $X(S_\alpha)$ is evaluated based on geometrical considerations and the recovery process. Sabathier et al. (1998) used the saturation-dependent shape factor and found it performing better than the constant shape factor in matching a single block fine grid reference solution. However, contrary to these results, Bourbiaux et al. (1999) reported a case where the classical shape factor gave a closer match to fine grid simulations than this saturation dependent shape factor.

2.3.1.4 *Increased discretisation inside matrix blocks*

A natural solution to the model errors in the classical dual porosity approach, arising from the pseudo steady-state assumption, is to increase the discretisation inside matrix blocks. Saidi (1983) presented a fully implicit three-phase 2D cylindrical model to simulate flow in matrix blocks in fractured reservoirs. He explicitly gridded the matrix blocks and criticised the use of transfer functions. His model was able to history match 22 years of production from the Haft Kel field in Iran.

The justification for Saidi's approach comes from the fact that the majority of hydrocarbons in place (over 90%) are in the matrix blocks and that it is essential to capture the displacement processes accurately. He described transfer functions as *"lumped parameters"* that could introduce errors. In his simulations, full fluid segregation was assumed in the fractures. The fluid contacts were set as boundary conditions to solve for flow in the matrix blocks. The dual porosity model was not used in Saidi's work. His work can be considered as a full matrix discretisation method (Fig. 2.4b).

Other matrix sub-domain methods were based on the dual porosity model and were aimed at extending the dual porosity concept. Pruess and Narasimhan (1985) presented a multiple interacting continua (MINC) model, where matrix

blocks are sub-gridded into rings based on proximity to fractures (Fig. 2.4c). This extension is used to simulate imbibition and heat flow in fractured porous media numerically. The MINC model can be applied to more representative fracture geometries, i.e. not necessarily only the idealised sugar cubed model. Shape factors are not used. Instead, cross-sectional areas of the sub-domain rings, their volumes and nodal distances between them are used to calculate the flux across the sub-domains. Wu and Pruess (1988) showed that the classical dual porosity model may result in large errors, particularly, when the matrix permeability is low or when the matrix block sizes are large. This is because the transient effects take longer times in these two cases. Generally, they showed that recovery is overestimated when the matrix domain is not divided into sub-domains and a constant shape factor is used.

The reason for the overestimation can be explained by considering a one dimensional capillary diffusion process

$$\phi \frac{\partial S}{\partial t} = \frac{\partial}{\partial x}\left(D \frac{\partial S}{\partial x}\right), \tag{2.22}$$

where D is the capillary diffusion factor. If the matrix block size is large, the classical dual porosity model underestimates the imbibition rate, whereas in fine grid simulations (or the MINC approach) steep saturation gradient develops close to the matrix-fracture interface as a result of the imbibition rate. Subsequently, the increased water saturation diminishes the imbibition rate and the hence the actual recovery is less than estimated by the classical dual porosity model. Results that confirm this analysis will be presented in Chapter 4.

Two other sub-domain methods were presented by Gilman (1986). The first is similar to the MINC model but it uses shape factors to calculate fluxes across the sub-domains. This could be suitable for heat flow, water oil imbibition, fluid expansion and pressure difference driven matrix-fracture exchange. The geometry, however, is not suitable for gas oil gravity drainage. The reason is that the direction of gas oil gravity drainage is always vertical, while the MINC is developed for radial flow processes. Therefore, the second sub-domain method of Gilman (1986) was dividing the matrix blocks vertically to a number of stacked layers

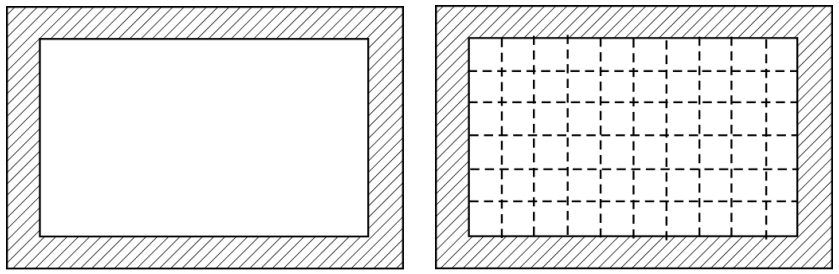

(a) Classical dual porosity model. Barenblatt et al. (1960), Warren and Root (1963)

(b) Full matrix discretisation. Saidi (1983)

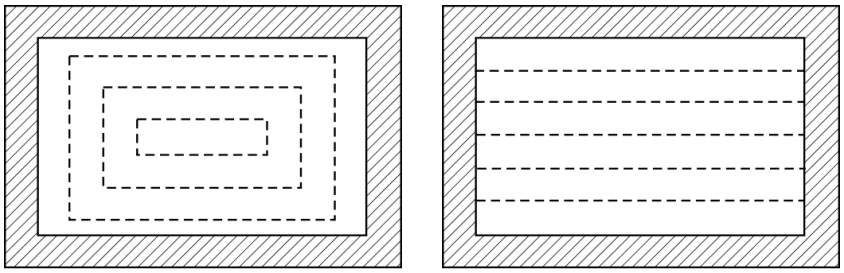

(c) MINC model. Pruess and Narasimhan (1985), Gilman (1986)

(d) Stacked layers model. Gilman (1986)

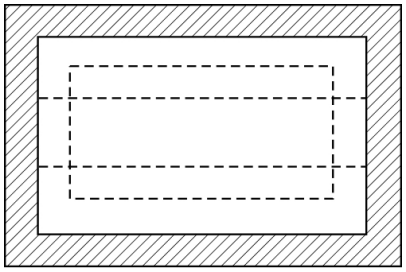

(e) Hybrid model. Beckner et al. (1991)

Figure 2.4: Types of matrix sub-domain methods. The hatched outer boundary represents the fractures.

(Fig. 2.4d). The fluxes between the sub-domains were also calculated using shape factors. However, the characterization methodology of the shape factors for the different domains was not discussed by Gilman (1986), nor was its relationship to the fracture spacing.

So far, the sub-domain methods facilitated either water oil imbibition or gravity drainage processes. Beckner et al. (1991) therefore presented a discretisation method suitable for both imbibition and gravity driven displacements (Fig. 2.4e). They reported errors as high as 30% in calculated recovery when the classical dual porosity models are used. Similar to the previous methods, no provisions were given on how the sub-domain transmissibilities relate to fracture spacing.

The increased accuracy as a result of the sub-domain methods is at the expense of increased computational cost. One extreme is to use the classical dual porosity model without matrix discretisation, which is not accurate in all cases. The other extreme is to fully discretise all matrix blocks in the reservoir, which might be intractable and unnecessary. The computational cost added can be manageable using today's computers. Another challenge is the characterisation of shape factors for the sub-domains depending on fracture spacing.

2.3.2 *The assumption of uniform matrix block sizes and properties*

The second assumption of the classical dual porosity model considered here is that all matrix block geometry and properties are uniform within each simulation cell. State variables such as pressure and saturation are also assumed to be uniform. However, a look at any fractured formation outcrop would suggest otherwise. Matrix blocks within a scale of a reservoir simulation cell (on the order of 100 m horizontally and 10 m vertically), come in all shapes and sizes (Fig. 2.5a). Hence, a more geologically appealing and realistic conceptual model is one that honours the variety of matrix blocks' geometries and properties (Fig. 2.5c).

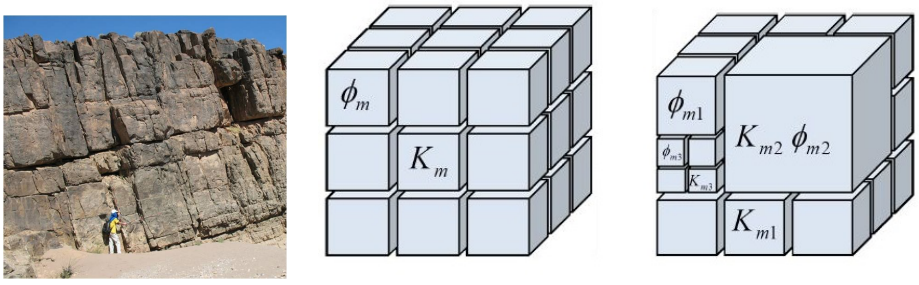

(a) (b) (c)

Figure 2.5: Heterogeneity of matrix block sizes in outcrops and two dual porosity conceptual models. (a) An image of a fractured carbonate outcrop showing matrix blocks of various sizes at a scale below the size of a single reservoir simulation grid block (Image courtesy of H. Boro, see Geiger et al., 2013). (b) A classical dual porosity conceptual model where matrix block sizes are uniform as well as the matrix properties (e.g. ϕ_m and k_m) (c) A multi-rate dual porosity conceptual model. (b) and (c) are taken from Maier et al. (2013).

To overcome the uniformity of matrix block sizes and properties assumption in dual porosity models, Pirker et al. (2007) and Pirker and Heinemann (2008)

used recovery curves derived from fine grid simulations. The recovery curves replace the constant shape factor transfer functions in classical dual porosity. Recovery curves for matrix blocks of different sizes can be combined to account for multiple matrix block sizes or different matrix properties (e.g. permeability). However, this method can be limited by the numerical cost added by carrying out the fine grid simulations. Further, the recovery curves are valid for a specific recovery process i.e. water imbibition, only.

Haggerty and Gorelick (1995) pioneered a multi-rate mass transfer (MRMT) model. The model is developed for single-phase flow. The main concept behind the model is that a distribution of transfer rates exists between the mobile domain (fractures) and the immobile domain (matrix blocks). Hence, allows capturing heterogeneous matrix blocks within each simulation cell. The model is considered as a generalization of the dual porosity concept and was used to interpret tracer tests in a fractured dolomite formation (Haggerty et al., 2001). It was found that the MRMT is consistent with available data and capable of matching the observed recovery curves, while the classical single rate model was orders of magnitude off.

Di Donato et al. (2007) applied the multi-rate concept for two-phase flow. They used up to three different transfer rates in a dual porosity model using a streamline based simulator. They studied flow in a Chinese naturally fractured reservoir. The multi-rate models predicted low recoveries as the imbibition takes longer for a given fracture spacing. In a single-rate dual porosity models, the fracture spacing is normally taken as the average. This assumption could lead to erroneous recovery estimation.

Geiger et al. (2013) extended the MRMT model to two-phase flow in fractured porous media. They applied the model on a realistic fracture model featuring a range of matrix block sizes. Geiger et al. (2013) also generalized the application of MRMT to account for saturation gradients that develop in matrix blocks under multi-phase flow. The model gave decent matches with the reference solution. Thus, the multi-rate dual porosity has a great potential for applications in the future as it does not only overcome the REV limitation, but also the pseudo steady state assumption. The number of applications of the model has been growing

recently. The multi-rate dual porosity model (MRDP) was implemented with spontaneous imbibition for two-phase simulations in reservoirs with multi-scale heterogeneity (Maier et al., 2013). In the comparison cases, the MRDP models gave higher and lower recoveries compared to a single rate dual porosity model. Therefore, the MRDP offers greater flexibility in matching production data from NFR. The MRDP model has been extended to include gas oil gravity drainage (Maier and Geiger, 2013).

2.3.3 *Fractures as an effective porous medium*

In dual porosity models, fractures are considered equivalent to porous media. In continuum modelling of flow in porous media, the simulation cell sizes must be above the scale of a representative elementary volume (REV) of the rock properties (e.g. Hubbert, 1956; Bear, 1972; Caers, 2005). For real porous media, this condition can be met easily because the REV scale is small and comparable to that of pore-scale. However, fractures in outcrops appear in different scales, larger and smaller than reservoir simulation cells (Fig. 1.6). As noted before, the multi-scale approach of Bourbiaux et al. (2002) treats different fracture length scales differently. For example, if the fractures are disconnected and their length smaller than simulation cell size, they only enhance permeability of the matrix. If the fractures are equal or larger in scale than the simulation cell, they can contribute the fracture permeability in a dual porosity model. The simulation cell size is, however, usually limited by external factors (e.g. heterogeity in the rock matrix properties, or the available CPU time) such that the REV of the fracture geometries may never exist.

2.4 DISCRETE FRACTURE NETWORKS

The general lack of a REV (e.g. Berkowitz, 2002) for continuum models to simulate flow in fractured porous media has prompted research to seek alternatives to the dual porosity model and avoid the assumptions in modelling matrix-fracture transfer. The single porosity approach with structured orthogonal grids cannot

resolve the complex fracture geometries seen in the outcrops and present in the subsurface. Hence, discrete fracture models with unstructured grid commonly using the finite element and/or finite volume discretisation are sought after as alternatives to the dual porosity model.

There are two main classes of discrete fracture models. The first is the discrete fracture networks (DFN) approach, where only fractures are considered in the flow calculations. The second is the discrete fracture and matrix (DFM) approach, where fractures and matrix blocks are considered in the flow calculations. In the remainder of this chapter, more detail is provided on how these models are built, their flow equations and their upscaling to single and dual porosity models.

2.4.1 *DFN generation*

Combinations of fractures of various orientations, lengths and apertures produce a complex fracture network through which fluid flow can occur. DFN models aim to characterize such networks and evaluate their connectivity, permeability and matrix block sizes for a number of engineering problems. Due to the limited information available on each single fracture, DFN are usually generated as multiple fracture sets. Each set is characterized by unique geometrical properties, such as orientation, fracture intensity, apertures, length and height. The generated fracture sets must satisfy the input statistical distributions that are commonly available from image log, outcrop data, geomechanical models and seismic data.

An example for a DFN generation process can be described as follows (e.g. Long et al., 1982): The location of each fracture is found by assuming that the centres of the fractures are distributed according to an intensity map. The fractures orientation is assigned next based on a statistical model. A commonly used fracture orientation model is Fisher's model (Dershowitz, 1984) which contains a dispersion parameter to model the observed variability of fracture orientations within each fracture set. Fractures length, height or radius is assigned afterwards, usually using power-law or log-normal distributions. Finally, aperture values are assigned, satisfying a log-normal distribution or other type of distributions. They

can also be correlated with fracture length (e.g. Olson et al., 2001). DFN models are usually generated stochastically, although it is possible to honour deterministic fracture geometries (Golder Associates Inc., 2010).

2.4.2 *DFN as a modelling platform*

Geometrical and analytical methods are used in the DFN approach to evaluate fracture intensity, connectivity, matrix block sizes and equivalent porous medium permeability (Dershowitz, 1984, Oda, 1985, Dershowitz et al., 1998). Percolation theory can be used to evaluate the connectivity of fracture networks (e.g. Berkowitz, 2002). These evaluations are computationally cheap and hence very valuable tools to estimate fracture connectivity. Permeability upscaling can follow analytical or flow-based methods. Oda (1985) presented a method to compute equivalent fracture permeability analytically. This method is widely used in DFN upscaling due to its efficiency (Dershowitz et al., 2000, Cottereau et al., 2010, Ahmed Elfeel and Geiger, 2012). This is discussed in detail below.

Other geometrical analyses available in the DFN approach, such as cluster analysis and the number of intersected fractures by a well path facilitate matching generated DFNs with available image-log and outcrop data. Fracture connectivity can be observed qualitatively from production data in fractured reservoirs (e.g. high well productivity index with permeability exceeding the rock matrix permeability by orders of magnitude). The cluster analysis is a geometrical tool that helps evaluating the connectivity of a DFN. For example, if production data supports a hypothesis that the fractures are well connected, the cluster analysis can be used to evaluate fracture connectivity for a given DFN without running flow simulations. The number of intersected fractures in an observation point (e.g. a well) is another useful geometrical tool to condition generated DFN.

As a result of the efficient and useful features available in the DFN approach, it is now commonly used as a modelling platform to build models for fractured reservoirs (e.g. Dershowitz et al., 2000; Sabathier et al., 1998; von Pattay; Ganzer, 2001; Ganzer, 2002)(Fig. 2.6). The static modelling consists of generating a DFN that is conditioned by the observation data available including well test and

seismic data (Casciano et al., 2004, Delorme et al., 2013, Sayers and den Boer, 2012). This is followed by DFN-based upscaling process to calculate parameters for single and dual porosity model. The fracture modelling workflow comes on top of the usual matrix properties characterisation workflow.

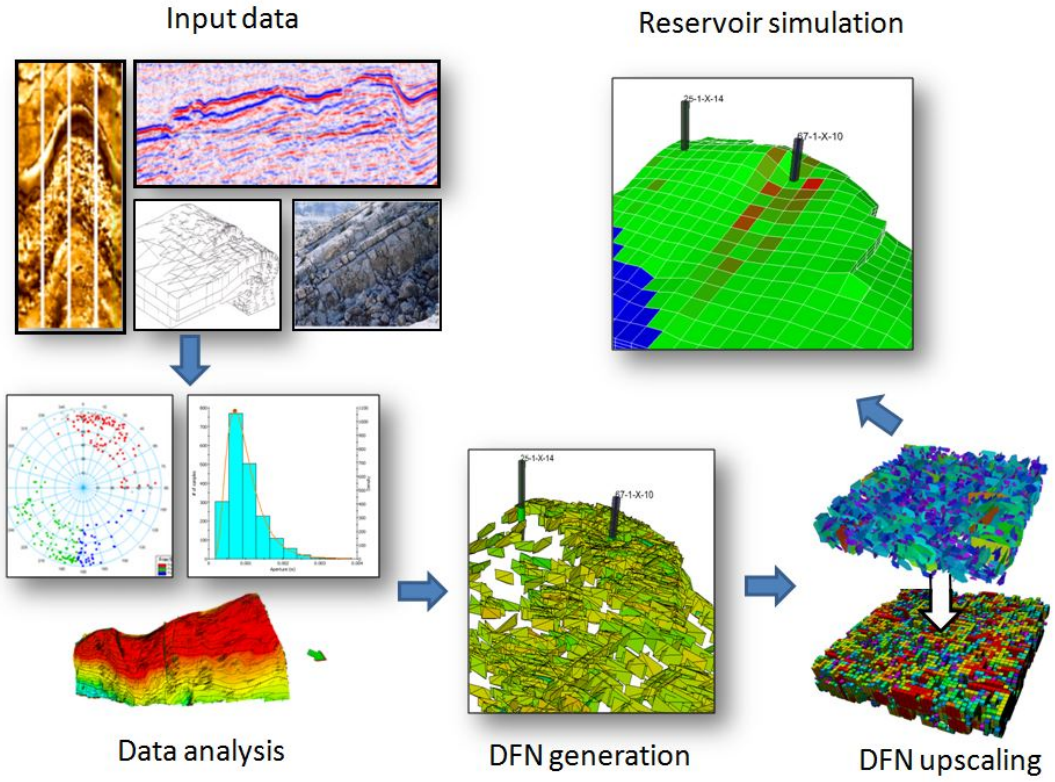

Figure 2.6: Workflow to build fractured reservoir models incorporating DFN generation and upscaling. Input data comprise image logs, outcrop analogues, geomechanical models and seismic interpretation. In the data analysis, fracture orientations, length and intensity maps are analyzed based on the input data to define statistical models. Then the DFN is generated honouring the statistical models. DFN upscaling computes the fracture porosity, permeability and matrix shape factors. Finally, DP or DP-DK reservoir simulation is performed based on DFN upscaling results.

2.4.3 *DFN upscaling*

As noted before, in addition to the modelling capabilities available, the DFN approach can be used to upscale the fracture properties to grid properties suitable for numerical simulation models. Three properties are evaluated in this upscaling process: fracture porosity, fracture permeability and matrix shape factors.

2.4.3.1 *Fracture porosity*

The fracture porosity is calculated using the fracture geometrical properties as in the following relationship (Dershowitz et al., 2000)

$$\phi_f = P_{32} \times e. \tag{2.23}$$

P_{32} is a measure of fracture intensity expressed as total fracture area per unit volume. e is the aperture of the fractures.

2.4.3.2 *Oda permeability upscaling method*

Oda (1985) used Darcy's velocity to calculate the equivalent fracture permeability

$$v_i = -\frac{k_{ij}}{\mu}\nabla\Phi, \tag{2.24}$$

where v_i is the Darcy velocity of the ith dimension, k_{ij} is the permeability tensor, μ is the fluid viscosity and Φ is the flow potential. The equivalent porous media velocity is given by

$$v_i = \frac{1}{V}\int_V v_i.dV. \tag{2.25}$$

Oda then introduced a probability density function (PDF), E, that is a function of fracture orientation, fracture size and aperture. It satisfies the following integral

$$\int_0^\infty \int_0^\infty \int_\Gamma E(n, A, e).d\Gamma.dA.de = 1. \tag{2.26}$$

Fracture orientations are represented by unit normal vectors n inside an angle Γ corresponding to the surface of a unit sphere. A and e represent fracture sur-

face area and aperture, respectively. In the above expression, the limits of infinity must be replaced by the maximum sizes of A and e. To calculate the number of fractures N located inside the control volume, the PDF is multiplied by the total number of fractures N^f:

$$N = N^f \times E(n, A, e).d\Gamma.dA.de. \tag{2.27}$$

Now the total void volume V^t can be calculated using fracture geometries

$$V^t = A \times e \times N. \tag{2.28}$$

If the expression for N in Eq. 2.28 is substituted from Eq. 2.27, one obtains

$$V^t = A \times e \times N^f \times E(n, A, e).d\Gamma.dA.de \tag{2.29}$$

The Darcy velocity inside fractures can be calculated using the law of parallel plate (Snow, 1969)

$$v_i = \frac{e^2}{12\mu}\nabla\Phi. \tag{2.30}$$

The fracture velocity in Eq. 2.30 and the fracture void volume in Eq. 2.29 are substituted into Eq. 2.25 to obtain

$$v_i = \frac{N^f}{V}\frac{1}{12\mu}\nabla\Phi \int_0^\infty \int_0^\infty \int_\Gamma A \times e^3 \times E(n, A, e).d\Gamma.dA.de, \tag{2.31}$$

and introduce F_{ij}, a second rank tensor relating only to the fracture geometry, defined as

$$F_{ij} = \frac{N^f}{V} \int_0^\infty \int_0^\infty \int_\Gamma A \times e^3 \times E(n, A, e).d\Gamma.dA.de. \tag{2.32}$$

Oda introduced the Kronecker delta, δ_{ij}, to normalize fracture orientation relative to the control volume (e.g. a simulation cell). By substituting ν_i back in Eq. 2.24 the upscaled DFN permeability is given by

$$k_{ij} = \frac{1}{12}(F_{kk}\delta_{ij} - F_{ij}), \tag{2.33}$$

where F_{kk} defines the principal directions of permeability. A limitation of Eq. 2.33 is that fractures of any length will contribute to the permeability value even if fractures do not percolate in a cell (e.g. the green fractures in Fig. 2.7). This is because the disconnected fractures will still contribute to the value of E and subsequently to the permeability value. To overcome this limitation, Oda introduced two factors that, if properly characterized, can increase the reliability of Oda's method. Oda considered situations where fractures are not connected and introduced the multiplier M, which has the range: $0 \leqslant M \leqslant 1/12$. To account for the fact that this equation produces non-zero permeabilities even when F_{ij} becomes negligibly small (as in the case of disconnected fractures), another parameter, C, was introduced so that

$$k_{ij} = \begin{cases} M(F_{kk}\delta_{ij} - F_{ij}) - MC(F_{kk}\delta_{ij} - F_{ij}) & C > C_0 \\ 0 & C \leqslant C_0 \end{cases}, \tag{2.34}$$

where C_0 is a threshold value below which the fractures are not connected. Oda's method application is commonly based on Eq. 2.33. An improved Oda's method exists which is based on equation Eq. 2.34. This method performs checks on the connectivity, evaluating C_0, of the fractures in a cell and if the fractures

are not percolating, the upscaled permeability is overridden by a value of zero (Golder Associates Inc., 2010). The latter is referred to as the Improved Oda's method in this thesis.

However, the improved Oda's method evaluation of fracture connectivity is not accurate. For example, if the fractures are percolating in a cell, there still might be fractures that do not contribute to fluid flow (Fig. 2.7b). These are considered in the probability function E (Eq. 2.26) in the improved Oda's method. Hence, flow-based upscaling is used to evaluate DFN models and provide reference solutions (Long et al., 1982, Robinson, 1984, Dershowitz, 1984).

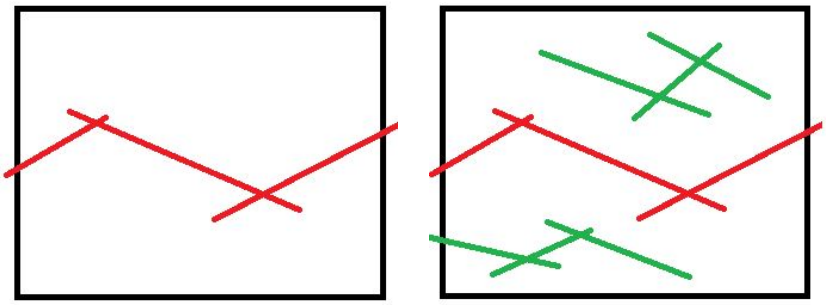

(a) $k_{Oda} = k_{Gold} = k_a$ (b) $k_{Oda} = k_{Gold} = k_b; k_b > k_a$

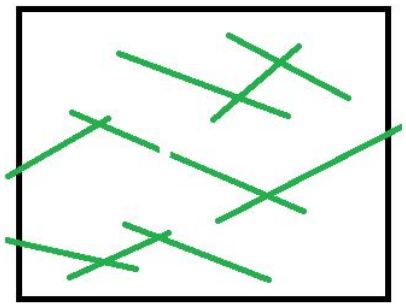

(c) $k_{Oda} = k_c \approx k_b; k_{Gold} = 0$

Figure 2.7: An example of a 2D discrete fracture networks and qualitative comparison of the Oda's method with and without the improvement in three DFN models. The improved Oda's method is denoted as k_{Gold}. (a) A DFN model where all fractures are connected. (b) A DFN model where some fractures are connected. (c) A DFN model where no fracture is connected. The colours denote fractures that contribute to fluid flow (red) and the isolated fractures (green).

2.4.3.3 *Flow-based upscaling methods*

In flow-based upscaling, boundary conditions for the region of interest (Fig. 2.7) can be assigned as no-flow boundaries or a pressure gradient is specified across the region. This boundary conditions enable the calculation of the pressure distri-

bution in the fractures. The pressures are computed at the fracture intersections, which represent the nodes. The nodes are connected by fractures of a given length and aperture. Under incompressible flow at each node, j, mass balance implies that

$$\sum_{i=1}^{I} v_{ij} = 0, \tag{2.35}$$

where v_{ij} is the flow velocity from the node i to j and I is the total number of nodes connected to j. For fracture flow, assuming the parallel plate rule (Eq. 2.30) is applicable, the flow velocity is related to the pressure difference by the following equation

$$v_{ij} = \frac{e_{ij}^2}{12\mu L_{ij}}(p_i - p_j). \tag{2.36}$$

Here, e_{ij} is the effective aperture of the link between i and j , L_{ij} is its length, and p is the node pressure. If the total number of nodes is N , Eq. 2.36 is evaluated N times. This forms a matrix of $N \times N$, the solution of which provides pressure values at each node and the total flow velocity, v_t, across the domain. Removing the nodes for the fractures that do not contribute to the total flow (Fig. 2.7) is common to increase the efficiency of the computation (Dershowitz, 1984, Robinson, 1984). The equivalent porous media permeability is then evaluated using Darcy's law as

$$k_{eq} = \frac{v_t \mu L}{\Delta p}, \tag{2.37}$$

where Δp is the pressure difference across the sides of the simulation cell, and L is the distance between the sides. Although three-dimensional modelling of flow in porous media requires the use of three-dimensional elements. Two-dimensional elements can be used in DFN models to represent the fractures because the fractures are essentially two-dimensional surfaces in a three-dimensional

reservoir model. Generating two-dimensional grids for the DFN is easier than three-dimensional grids needed for the DFM, and can be automated for arbitrary DFN geometries. This is a great advantage of the DFN approach, as it facilitates the use of DFN generation and DFN-related analysis in stochastic frameworks. However, flow-based upscaling is still computationally intensive. Table 2.1 shows the CPU time for flow-based upscaling and upscaling using Oda's method for a DFN with 2000 fractures. The total number of cells on which flow-based upscaling was successful is limited to a few thousand.

Table 2.1: Comparison of DFN upscaling CPU time for a HP workstation with an 2.67 GHz Intel Xeon processor and 8 GB RAM. The model contains 2000 fractures.

	CPU Time	
Number of cells	Analytical	Flow-based
50	< 1	395
200	1	262
1250	2	775
5000	3	2730
20000	8	12240
125000	20	*NA*
500000	67	*NA*
2000000	247	*NA*

Flow-based upscaling is also sensitive to the type of boundary conditions used during the flow calculations. It is well known that, depending on the heterogeneity of the geological model, boundary conditions impact on the resulting equivalent permeability (Renard and deMarsily, 1997, Durlofsky, 1991). Four types of boundary conditions are commonly used. These are: No flow boundaries, linear (uniform) boundary conditions, constant pressure, and periodic boundary conditions (Fig. 2.8). Depending on the upper and lower sides' boundary conditions, these four boundary conditions can be grouped into two: Closed side boundary (no flow) and open side boundary (all other conditions).

2.4.3.4 *Shape factor upscaling*

Finally, the matrix block size is evaluated using a number of methods (Dershowitz et al., 1998) including the mutli-directional spacing (MDS) method and

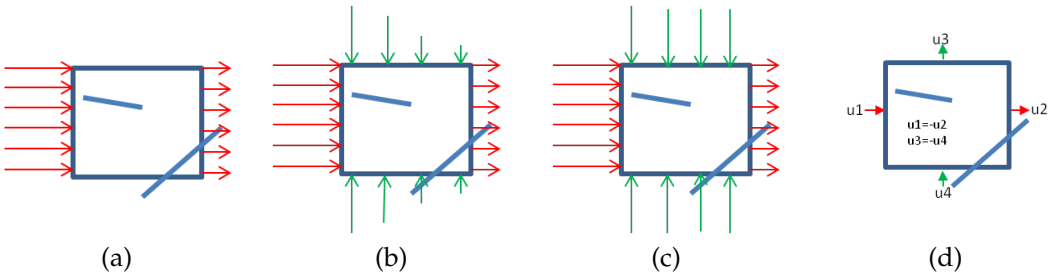

Figure 2.8: Types of boundary conditions commonly used in flow-based DFN permeability upscaling. (a) No side flow boundary (b) Linear pressure (c) Constant pressure (d) Periodic boundaries. Upscaling results in this particular fracture geometry and for no flow boundary condition (a) gives $k = 0$ as no flux is coming from the sides, this is contrary to other types of boundary conditions.

an image processing methodology that was introduced by Sarda et al. (1997). The MDS is widely used because it is efficient. It is a geometrical method where fracture intersections with imaginary lines are calculated in all principal directions (Dershowitz et al., 2000). The imaginary lines are placed uniformly across the cell principal directions (Fig. 2.9). The spacing between the fractures is statistically analysed to evaluate the matrix block dimensions. The shape factor can then be calculated based on Eq. 2.20 for example.

Another method is based on an image processing approach. In analogy to the water-oil capillary imbibition mechanism, 2D horizontal matrix block dimensions can be estimated by establishing a relationship between invaded area and distance from the fracture (Sarda et al., 1997, Sabathier et al., 1998, Sarda et al., 2002)(Fig. 2.10a). Pixels corresponding to fractures are initialized with zero values. Then, for all matrix pixels, the distance is calculated to the nearest zero pixel. The invaded area is equal to the cumulative distance normalized by matrix area (Fig. 2.10b). Another normalized equivalent invasion area A_{eq} (Fig. 2.10a) is calculated based on an idealized block geometry

$$A_{eq}(x) = \begin{cases} 1 - \frac{1}{L_x L_y}(L_x - 2x)(L_y - 2x) = 2(\frac{1}{L_x} + \frac{1}{L_x})x - \frac{4}{L_x L_y}x^2 & x < \min(\frac{L_x}{2}, \frac{L_y}{2}) \\ 1 & x \geqslant \min(\frac{L_x}{2}, \frac{L_y}{2}) \end{cases}. \tag{2.38}$$

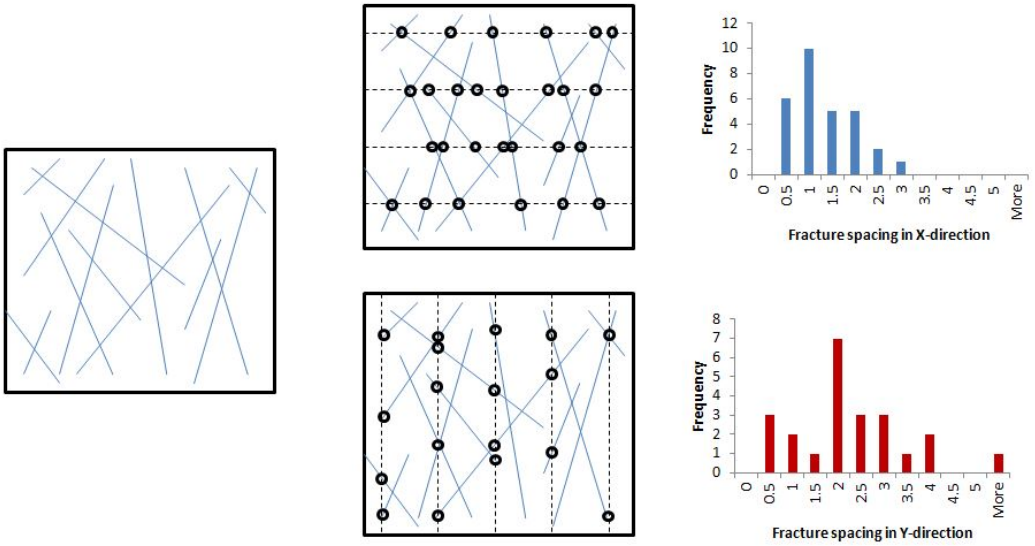

Figure 2.9: Calculation of fracture spacing using the Multi-Dimensional Spacing (MDS) method. A DFN model for which fracture spacing is calculated is shown (left). Imaginary lines based on the orientation of the grid block cell are generated (dashed lines) and fracture intersection points are recorded (small circles) (centre). The spacing between the intersection points is analysed statistically to determine fracture spacing in X and Y dimensions (right). Note that the method is equally applicable in three-dimensional fracture model. The method is applied here on a two-dimensional fracture model for illustration purposes.

For values of A_{eq} less than unity, the equivalent invaded area can be rewritten in the following format

$$A_{eq} = ax + bx^2, \tag{2.39}$$

where

$$a = 2\left(\frac{1}{L_x} + \frac{1}{L_y}\right) \tag{2.40}$$

and

$$b = -\frac{4}{L_x L_y}. \tag{2.41}$$

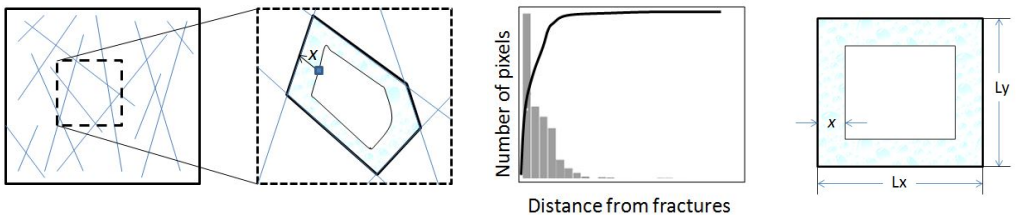

(a) (b) (c)

Figure 2.10: An image processing technique to evaluate the matrix shape factor in DFN models. (a) The image processing technique to collect pixel data. (b) Evaluation of $A(x)$ using the pixel data. (c) Using an ideal block geometry with fracture spacing L_x in the x-direction and L_y in the y-direction to calculate $A_{eq}(x)$. The values of L_x and L_y that best represent the DFN model are calculated by equating the two areas $A(x)$ and $A_{eq}(x)$.

$A_{eq}(a, b, x)$ is then equated to $A(x)$ evaluated by an image processing technique (Fig. 2.10b). Hence, one obtains the following the quadratic equation

$$ax + bx^2 - A(x) = 0. \tag{2.42}$$

The values for a and b are obtained by solving Eq. 2.42. Subsequently, L_x and L_y are found by solving Eqs. 2.40 and 2.41 simultaneously.

2.4.4 *Limitations of the DFN approach*

The stochastic generation of fracture networks in the reservoir typically does not follow geomechanical constrains. Hence, there is a need to condition the DFN generation to honour the known geomechanical controls. For example, it has been observed that DFN generation might place multiple fractures in the same location or within a minimally small space (Fig. 2.11).

The analytical DFN upscaling methods overestimate equivalent fracture permeability while flow-based upscaling can be intractable for full field models. The DFN upscaling methods are sensitive to simulation cell sizes (e.g. due to fracture scaling as in Fig. 1.6) and boundary conditions used (Dershowitz et al., 2000). Qualitative measures have been presented to select a suitable cell size (Dershowitz et al., 2000), while others tried to incorporated scale dependency in

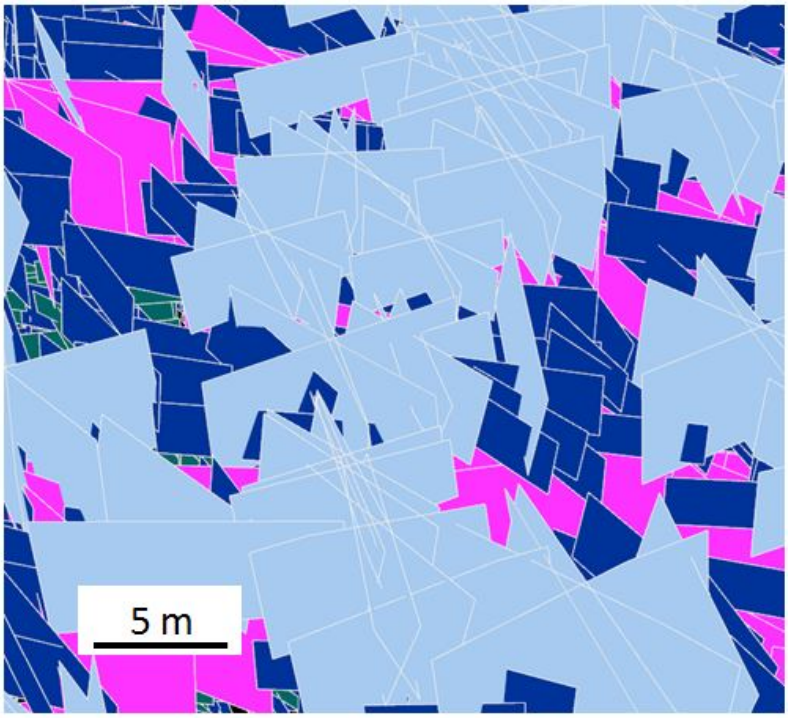

Figure 2.11: Example of a stochastic DFN model showing multiple fractures at approximately the same spatial location

the effective permeability calculations (Garcia et al., 2007). However, no quantitative measure to assess the accuracy of DFN upscaling has been proposed and the possible propagation of uncertainty due to upscaling errors has not been studied.

In many reservoirs, matrix permeability is large and can connect what was otherwise disconnected fractures. Bogdanov et al. (2003) found that matrix permeability can affect the percolation of fluid flow in fractured porous media by connecting isolated fractures. In such reservoirs, DFN models do not capture the full flow unless transfer functions are used to estimate flow in the matrix. DFM models explicitly account for matrix flow and hence are free of transfer functions.

2.5 DISCRETE FRACTURE AND MATRIX MODELS

2.5.1 *DFM models generation*

All DFN generation methods are essentially applicable here, because discrete fracture and matrix (DFM) models are inclusive of the DFN geometry and properties. To resolve the complex fracture geometries, DFM/DFN models use spatially adaptive unstructured grid, typically with finite element and/or finite volume methods (e.g. Kim and Deo, 2000; Juanes et al., 2002; Bogdanov et al., 2003; Karimi-Fard et al., 2004; Hoteit and Fairoozabadi, 2006; Matthai et al., 2007; Geiger et al., 2009). Fractures are generally represented as lower-dimensional elements (e.g. as 1D lines in 2D models or 2D surfaces in 3D models). However, elements that represent the rock matrix are equi-dimensional (e.g. 2D elements such as triangles and quadrilaterals in 2D models (Fig. 2.12); 3D elements, such as tetrahedrons, prisms and hexahedrons, in 3D models). Three-dimensional mesh generation is a significant challenge and disadvantage of the DFM approach because matrix blocks are discretised too.

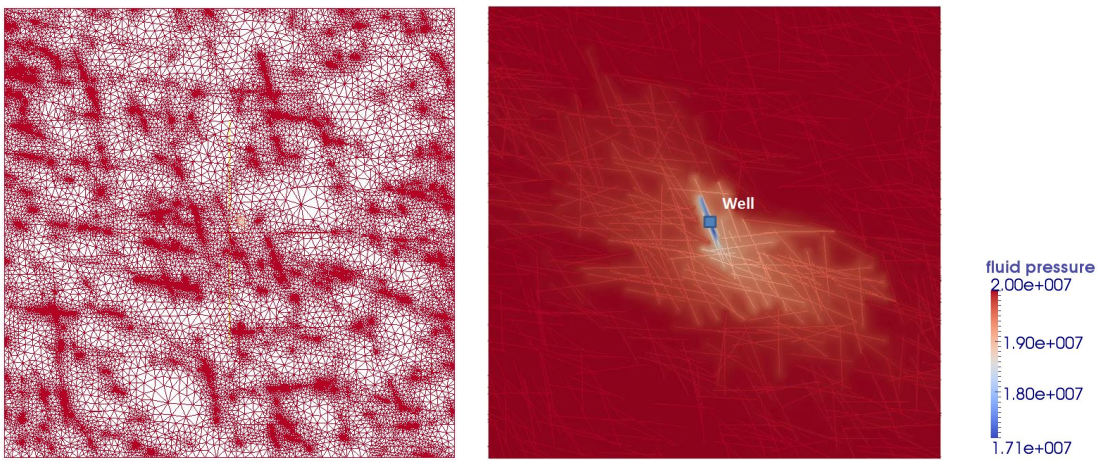

(a) (b)

Figure 2.12: A 2D example (map view) of a discrete fracture and matrix (DFM) model. (a) The finite element mesh with spatial adaptation to resolve the complex geometry of the fractures. (b) The pressure distribution as a result of well testing. The fluid pressure is in Pascals.

2.5.2 *Applications of DFM models*

DFM models can be geologically more realistic because fewer assumptions are necessary to model flow in fractured porous media, including matrix-fracture transfer. Therefore, DFM models are very useful in studying flow behaviour in fractured porous media (Matthäi et al., 2007, Agar et al., 2010, Geiger et al., 2013, Matthäi and Bazrafkan, 2013), investigating pressure transient responses in fractured media and interpreting them (Matthäi et al., 1998, Corbett et al., 2010, Biryukov and Kuchuk, 2012, Ahmed Elfeel et al., 2014) and providing reference solutions for upscaling and quantitative comparisons with other modelling approaches (Bourbiaux et al., 1999, Matthäi and Nick, 2009, Geiger et al., 2013).

The technological advances in computer software and hardware have enabled field scale simulations using the DFM approach (Hui et al., 2008, Mallison et al., 2010, Hui et al., 2013). To facilitate the workflow to field-scale DFM simulations, a number of advanced solutions were introduced. These include an efficient mesh generation method, accurate upscaling to dual porosity models and a next-generation reservoir simulator. Hui et al. (2013) used the DFM approach to simulate EOR methods including three-phase flow in fully compositional model (Fig. 2.13). The DFM simulations were compared against the dual porosity model using DFM-based upscaling methods and a classical dual porosity model. The average errors for a new DFM-based upscaling method and the classical dual porosity dual permeability models are 14% and 65%, respectively. The reported running times for the upscaled two models were comparable.

2.5.3 *DFM-based upscaling*

Karimi-Fard et al. (2006), Gong et al. (2008), Tatomir et al. (2011) presented a DFM-based upscaling method. This approach is based on the MINC model of Pruess and Narasimhan (1985) and is referred to as the Multiple Sub-Region (MSR) method. The upscaling is performed in two steps. The first step aims at upscaling matrix-fracture transfer using single-phase DFM upscaling within each simulation grid block (Fig. 2.14). Results are used to partition the matrix

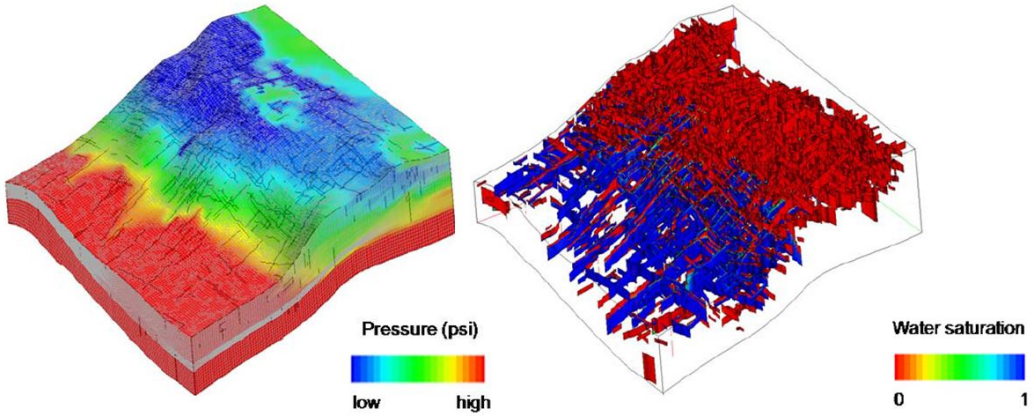

Figure 2.13: Visualization of DFM simulation results in a reservoir comprising 4500 discrete fractures. The results show matrix pressure distribution (left) and water saturation inside the fractures (right) after 30 years of water injection. From Hui et al.(2013).

into a number of sub-domains to increase the accuracy of calculation, as discussed for the MINC model before. This is done by using pressure distributions from fine grid single phase simulations (Fig. 2.14). The shape of the sub-regions hence depends on the fracture geometry and matrix permeability (Karimi-Fard et al., 2006).

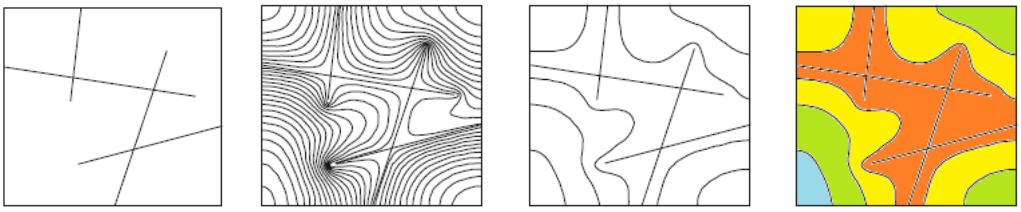

(a) Fracture distribution (b) Pressure contours (c) Reduced contours (d) Sub-regions

Figure 2.14: Matrix-fracture transfer upscaling using DFM models. A single-phase simulation is performed in each cell until a pseudosteady state is reached. The pressure contours then are used to define the sub-regions. The different colours denote different sub-regions. From Karimi-Fard et al. (2006).

The second step concerns the fracture-fracture and matrix-matrix flow between the simulation cells. Flow between two adjacent simulation cells is calculated (Fig. 2.15). Again a single-phase flow is carried out to evaluate the transmissibility between the two cells. This implicates that each cell will have as many transmissibility evaluations as the number of cells it is connected to. Typically, transmissibility is calculated based on the permeability of the cells. Hence, DFM-

based upscaling is computationally more demanding than DFN-based upscaling, but also more accurate.

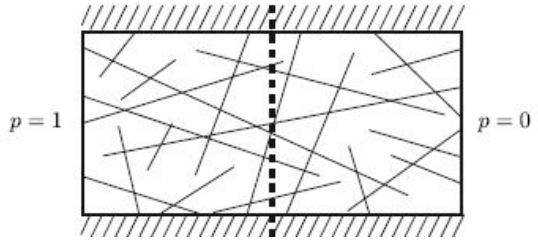

Figure 2.15: Block to block transmissibility calculation in the Multiple Sub-Region (MSR) method. Fixed pressure boundary conditions are applied in the transmissibility direction, all other boundaries are no flow. From Karimi-Fard et al. (2006).

2.5.4 *Limitations of the DFM approach*

The mesh generation is very challenging for 3D models and often requires additional correction and quality checking. Hence, this may hinder any stochastic approach, where a large number of models are generated to quantify the geological and other uncertainties. In addition, assumptions such as all fractures are sub-vertical, are also necessary to simplify the fracture geometry (Mallison et al., 2010).

After the mesh has been generated successfully, the computational cost to run the DFM models or the DFM-based upscaling can be high. Parallelisation can help (e.g. Geiger et al, 2009) but only for a sector scale . High CPU times still prevent any automated reservoir simulation workflow and uncertainty quantification with DFM models. It is noted that full field application of the DFM approach (e.g. Fig. 2.13) consider large scale fractures that are not fully connected in part of the reservoir grid. However, it is the fractures with lengths that are usually less than the simulation grid block size that defines the dual porosity behaviour.

Commonly, the large scale fractures are few but associated with smaller to medium fractures that affect fluid flow. Simulation of flow through the large scale features is of prime importance and is best achieved through deterministic modelling. These large features are easily identifiable from seismic data with

little uncertainty. However, DFM simulation of all small to medium fractures is neither tractable nor required. A more generic approach therefore is to combine DFM simulations and dual porosity modelling (e.g. Maier et al., 2013; Maier and Geiger, 2013) to capture the multi-scale nature of flow in fractured reservoirs.

2.6 SUMMARY AND CONCLUSION

In this chapter, the early development of the classical dual porosity model is reviewed together with its extension to multi-phase flow. The solutions offered to overcome three major limitations are examined: the pseudo steady-state assumption, the uniformity of matrix block sizes and geometries, and the treatment of fractures as an equivalent porous medium. The DFN method and its upscaling applications were reviewed, and similarly, the DFM method and its applications.

The solutions offered to improve the classical dual porosity model are (1) varying a constant shape factor, (2) the use of pseudo capillary pressure curves, (3) transient shape factors or (4) increased matrix discretisation. The latter could be considered within the multi-rate dual porosity approach. The first two entail changing a physical parameter heuristically to match laboratory experiments or fine grid simulation results. Transient shape factors are difficult to implement in reservoir simulators, while more matrix discretisation require additional characterisation constants to control the flow between the matrix sub-domains.

The multi-rate dual porosity model overcomes the uniform matrix block size and geometry limitation. This also incurs the need for additional storage capacities during numerical simulation. Recent advances in computer hardware easily absorb the additional storage needed for matrix discretisation and multi-rate dual porosity models. It is also important to develop characterization and upscaling methods to drive shape factors for the sub-domains of the matrix blocks, and provide the needed input to inform multi-rate dual porosity model.

Discrete fracture (DFN and DFM) models introduce additional realism and accuracy to the modelling, upscaling and simulation of fractured reservoirs. DFN models are already used for static modelling of fractured reservoirs, thanks to the geometrical analysis capabilities and analytical and flow-based upscaling

methods. More investigations are needed to study the impact of different DFN-based upscaling methods, cell sizes and boundary conditions on history matching and development of fractured reservoirs. DFM simulations provide insights to understand the nature of multi-phase flow in fractured media. The application of DFM for full field simulation is still limited because it poses significant technical challenges and limitations, especially with respect to gridding and CPU time.

Capillary and gravity forces dominate multi-phase matrix-fracture transfer. This makes relative permeability and capillary pressure curves key factors in determining recovery in fractured reservoirs. The next chapter will discuss how these parameters are affected by pore-scale heterogeneity and evaluate their subsequent impact on matrix-fracture transfer.

Part I

MATRIX-FRACTURE TRANSFER UNDER THREE-PHASE FLOW

In this part, a step-wise upscaling approach is developed to evaluate the accuracy of classical dual porosity models for estimation of three-phase flow in NFR. First, the pore-scale heterogeneity is examined and a pore-network model is used to estimate three-phase flow functions. These functions are used in detailed fine grid simulations to analyse matrix-fracture transfer as a result of WAG injection. Based on the upscaling results, a new extension of the multiple interacting continua (MINC) model, called the double block model is developed and extended to a multi-rate dual porosity (MRDP) model. The combination of MINC and MRDP results in a significantly better agreement with detailed fine grid simulation results compared to the classical dual porosity model.

3

EFFECT OF PORE-SCALE HETEROGENEITY ON MATRIX-FRACTURE TRANSFER

3.1 INTRODUCTION

Carbonates form the majority of NFR. Carbonate reservoirs can be extremely heterogeneous; because carbonate sediments are susceptible to diagenetic modifications, which result in multi-scale heterogeneities (Fig. 3.1)(e.g., Choquette and Pray, 1970; Lucia, 1983, 1995; Kerans et al., 1994; Jennings and Ward, 2000). They are also chemically more active than sandstone reservoirs, which leads to wettability alteration and a wide range of wettabilties, from weakly water-wet to strongly oil-wet (e.g., Chilingar and Yen, 1983; Lichaa et al., 1993; Esfahani and Haghighi, 2004) . The presence of fractures and vugs at various length scales affects the connectivity and/or storage capacities of a carbonate reservoir and increases the complexity of heterogeneity even further. Such variable and multi-scale heterogeneities render modelling carbonate reservoirs, and hence their evaluation and management, very difficult. Furthermore, many carbonate reservoirs have been producing for decades and are increasingly entering mature production phases where Enhanced Oil Recovery (EOR) techniques including WAG injection are required to sustain oil and gas production (Burchette, 2012).

WAG flooding establishes three-phase flow regions in the reservoir. This necessitates using three-phase relative permeability and capillary pressure functions, hereafter termed *"flow functions "*, in order to model the displacement processes at the continuum scale. Commonly, these functions are obtained by empirical interpolation of two-phase functions such as the Stone models (Stone, 1970, 1973) and saturation weighted interpolation method (Baker, 1988), see Blunt (2000) for an overview of empirical three-phase flow functions. They are usually employed for reservoir simulation because three-phase flow functions are very difficult to measure in the laboratory (Shahverdi and Sohrabi, 2013).

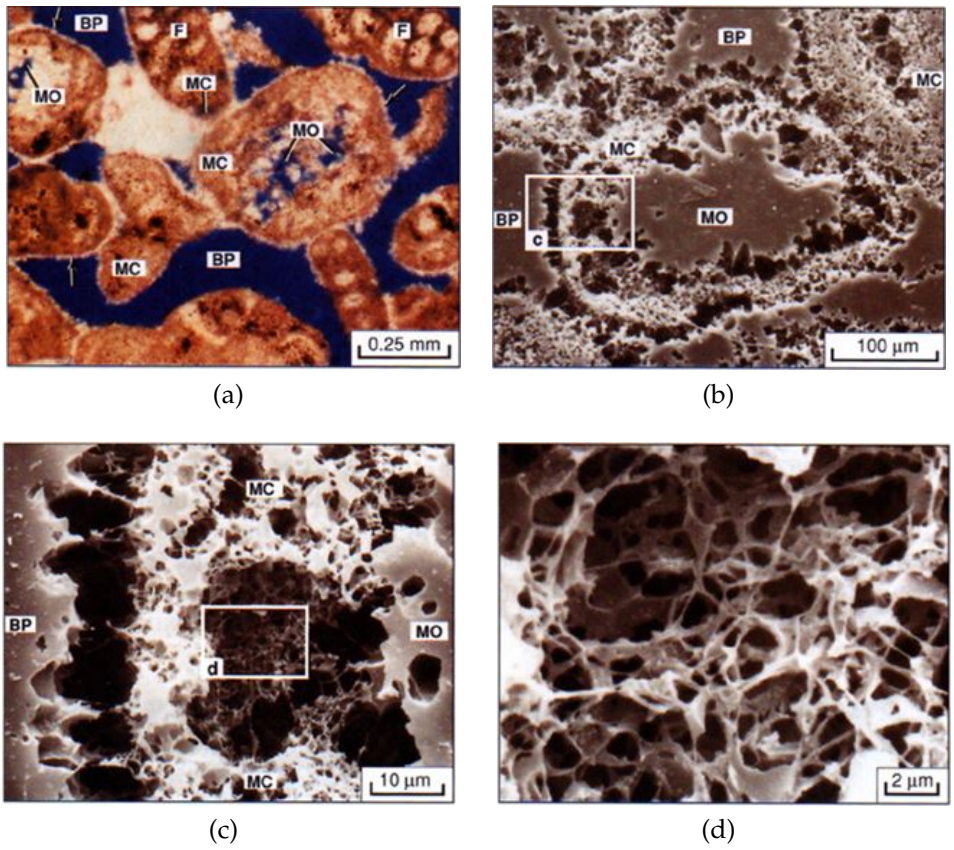

Figure 3.1: Heterogeneity between the millimeter and micrometer scales in Arab Formation carbonates, Saudi Arabia. Figure taken from Cantrell and Hagerty (1999)

In empirical models, the oil relative permeability for three phase flow is interpolated from two two-phase displacement experiments: the oil relative permeability from a water-oil experiment $k_{row}f(S_w)$ and from gas-oil experiment $k_{rog}f(S_g)$. Hence, the empirical models relates the three-phase k_{ro} to S_w and S_g.

Pore-network modelling offers the possibility to compute physically consistent three-phase flow functions. The resulting three-phase flow functions can readily be used in commercial reservoir simulators. This is achieved by establishing two-dimensional tables where $k_{ro} = f(S_w, S_g)$ (see Appendix A) from the pore-network modelling results. Hence, this enables us to compare the results against empirical models (Al-Dhahli et al., 2013a, Al-Dhahli et al., 2013b).

Recently, Jiang et al. (2013a, 2013b) presented a methodology to create multi-scale pore-networks efficiently. Such pore-systems are typical for carbonate rocks, for example comprising micro- and macro-porosity such as those shown in Fig. 3.1. This enables a more quantitative investigation of the effect of pore scale het-

erogeneities on flow functions. Furthermore, it is now possible to study the flow functions for different rock types. Rock typing is a very important component in carbonate reservoirs characterisation. The aim is to link the geologic concepts (e.g. diagenesis) to the obtained petrophysical measurements (e.g. porosity and permeability) and to study their subsequent impact on fluid flow.

Previous carbonate rock type characterization workflows have demonstrated the importance of including pore-size distributions and emphasised the need to distinguish between interparticle (micro-pores) and vuggy porosity (macro-pores) (e.g., Lucia, 1995; Gomes et al., 2008; Hollis et al., 2010; Al-Ameri and Shebl, 2011). Some studies highlighted the impact of diagenetic modification on petrophysical properties, including the impact of wettability change on capillary pressure function (Gomes et al., 2008), while others stressed the importance of incorporating the geologic evolution of pore geometries in the rock typing process (Hollis et al., 2010).

The matrix-fracture transfer terms shown in Chapter 2 contain flow function variables. Hence, the changes in flow functions can directly affect flow between fracture and matrix blocks. In this chapter, the effect that the wettability and pore-scale heterogeneity have on the matrix-fracture transfer is quantified. A state-of-the-art pore-network modelling tool is employed to estimate the flow functions for different wettability and pore structures. The resulted flow functions are then used in fine grid simulations matrix-fracture transfer in a scale of a simulation cell (Fig. 3.2). Although the majority of applied WAG injection cases are miscible, only immiscible WAG injection is considered in this thesis. The aim is to increase accuracy of reservoir simulation of the simple case (immiscible) first before approaching cases with additional complexities (near miscible and miscible three-phase flow).

3.2 PORE-NETWORK MODELLING

A novel pore-network model is used to compute the three-phase flow functions (Al-Dhahli et al., 2013a, 2013b). The model encompasses a number of features that enables us to capture a wide range of pore-scale physics. Firstly, the model

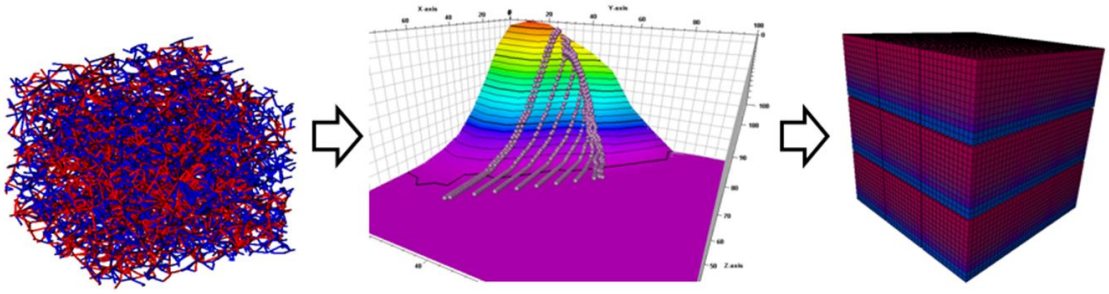

Figure 3.2: Step-wise upscaling procedure of matrix-fracture transfer during three-phase flow in carbonate reservoirs. Left: Pore-scale modelling is used to generate three-phase flow functions. Centre: three phase gas relative permeability (Z-axis) as a function of two saturations (X- and Y-axes). The data points represent the pore-network calculation results. The fitted surface is used to generate a two-dimensional table as input for reservoir simulation. Right: fine grid simulation of matrix-fracture exchange during WAG injection.

uses realistic pore-network geometries from complex 3D digital rocks as inputs. This is based on the work of Jiang et al. (2013a, 2013b). Secondly, the model comprises an improved pore shape characterization, which allows representation of complex pore throats and hence the computation of hydraulic conductivities through them more accurately (Ryazanov et al., 2009). Thirdly, a novel thermodynamic criterion for oil layer formation and collapse (van Dijke and Sorbie, 2006) has been incorporated that allows for more accurate calculation of flow functions at low oil saturation. The model also accounts for multiple displacement processes during three-phase flow, which has been observed in micro-model experiments and is a key process that generates low oil saturations (Sohrabi et al., 2004). Furthermore, the model has been benchmarked against published three-phase relative permeability data for water-wet sandstone and oil-wet micromodel experiments (Al-Dhahli et al., 2013a, 2013b).

To investigate the impact of heterogeneity at the pore-scale, two fundamentally different pore systems are considered. The first network comprises pores between grains and/or crystals, i.e. interparticle porosity (Lucia, 1983). This is common to sandstone and grainstones. Permeability of such pore system is largely determined by the grain/crystal sizes. However, the grain/crystal size has little effect on porosity. The second network represents vuggy porosity. Examples of vugs can include intrafossil pore space, moldic pore space and intragranular micro porosity (Lucia, 1995). Such a pore-system comprises different

characteristics compared to interparticle pore-system; the presence of separate vugs tends to change porosity but can have little effect on permeability. The purpose of this section is to study how the presence of separate vugs and variations in wettability affect the three-phase flow functions. To investigate pore-scale heterogeneity, we consider three different pore-networks, two of them representing interparticle porosity and one vuggy porosity.

3.2.1 *Description of pore-networks*

The three pore-networks are shown in Fig. 3.3. The first network with interparticle porosity is the homogeneous Berea sandstone; the second is a heterogeneous carbonate rock. These are labelled Berea sandstone and Carbonate 1, respectively. The first network has been extracted using a process-based reconstruction of the Berea sandstone (Øren and Bakke, 2003). The Berea sandstone is used here as a proxy for grainstone carbonate rock. The second pore-network was extracted from a micro-CT rock image of a real carbonate rock at 2.86 μm resolution (Jiang et al., 2013a). The third pore-network, Carbonate 2, represents vuggy porosity in which micro and macro pore systems are joined together based on micro-CT scans of rock images at 2.86 and 14.29 μm resolution, respectively (Jiang et al., 2013a). The micro-scale network is the statistical equivalent of the heterogeneous Carbonate 1 pore system described above. Therefore Carbonate 1 and 2 could be considered as a carbonate pore system that has undergone different stages of diagenesis, i.e. where vuggy porosity was created at later stages. Carbonate 2 is comparable to Berea sandstone in terms of porosity whereas it is comparable to Carbonate 1 in terms of permeability (Table 3.1).

Table 3.1: Properties of pore-networks for a homogeneous sandstone, heterogeneous carbonate, and multi-scale carbonate rock, respectively

Properties	Berea sandstone	Carbonate 1	Carbonate 2
Number of nodes	12349	11518	36334
Number of bonds	26146	17929	54588
Coordination number	4.19	3.08	2.99
Porosity, %	18.30	13.67	17.88
Permeability, mD	2673	135.56	143.40

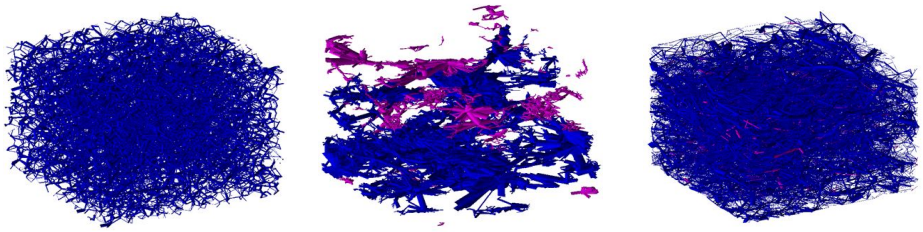

(a) Berea sandstone (b) Carbonate 1 (c) Carbonate 2

Figure 3.3: The extracted pore-networks for three rock types. Pink regions denote isolated pores

The effect of wettability is investigated by considering two wettability cases for each network, a strongly water-wet case and a strongly oil-wet case. For water-wet cases, the oil-water contact angles are between 0 and 60 degrees. For oil-wet cases, oil-water contact angle are changed after the drainage process; these contact angles are between 120 and 140 degrees. Note that the interfacial tension values considered here are as follows: oil-water, 48; gas-oil, 19 and gas-water, 67 mN/m. The three-phase wetting order is water-oil-gas for the water-wet case and oil-gas-water for the oil-wet case.

To generate three-phase flow functions for the different pore-networks, it is assumed that all pore-networks are initially water-wet and saturated with water. Oil is then injected to simulate oil-water drainage until the irreducible water saturation is reached. At this point, the contact angles are changed to simulate wettability alteration *("ageing")* for the oil-wet cases. This is followed by repeated water injection up to predefined water saturations. Each water injection is followed by a gas injection, which results in a series of three-phase saturations paths that map the regions where three fluid phases can coexists and provides the corresponding relative permeabilities and capillary pressures. Hence, the effect of hysteresis due to a decrease in water and oil saturation during gas injection is automatically accounted for in the three-phase flow functions. However, hysteresis during subsequent water injections is not represented in the fluid injection sequence presented above.

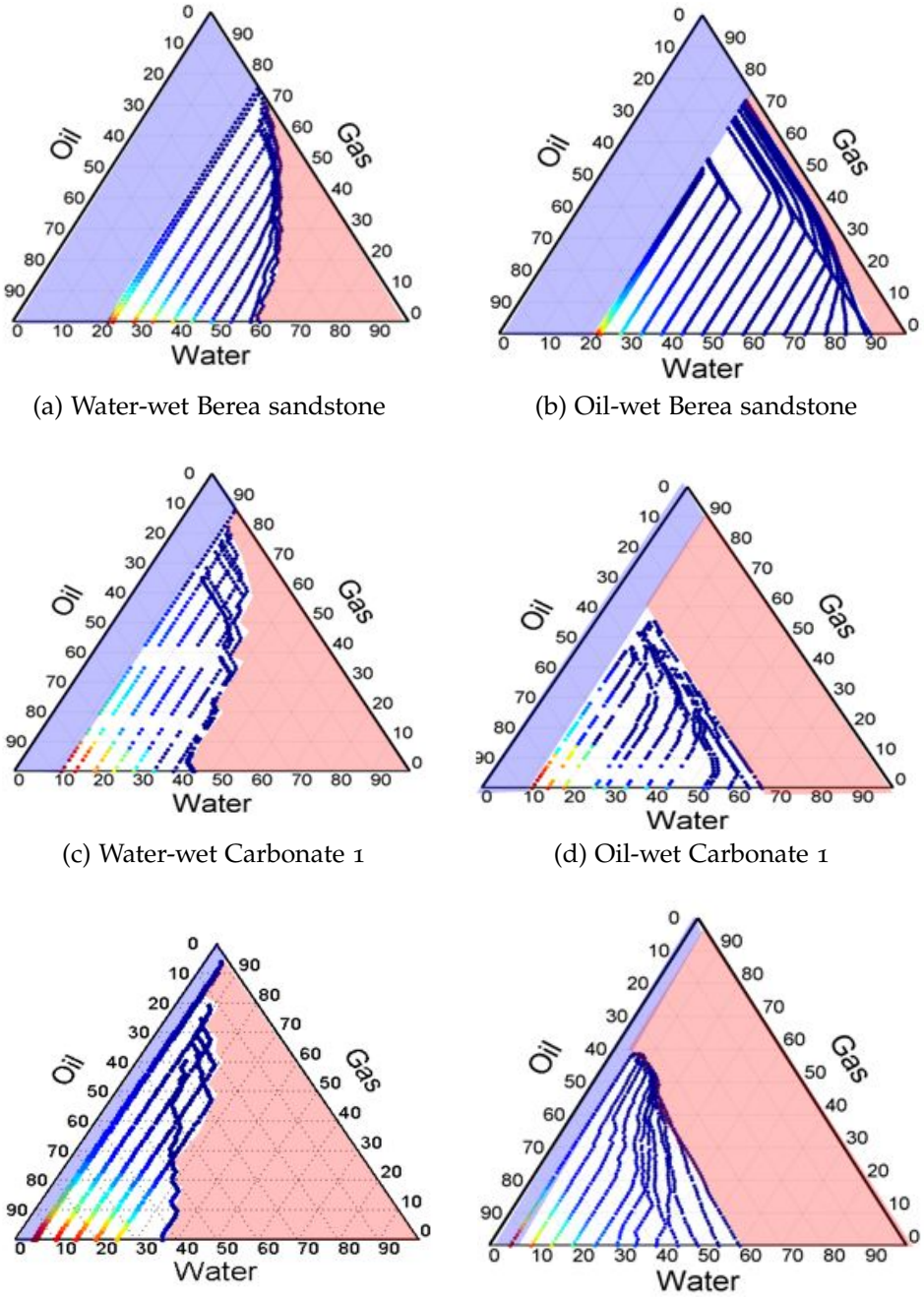

(a) Water-wet Berea sandstone

(b) Oil-wet Berea sandstone

(c) Water-wet Carbonate 1

(d) Oil-wet Carbonate 1

(e) Water-wet Carbonate 2

(f) Oil-wet Carbonate 2

Figure 3.4: Three-phase oil relative permeability and the saturation paths for the three rock types predicted by pore-network modelling. The figure enables the comparison of regions where three fluid phases coexist and the corresponding oil relative permeability (k_{ro}) as predicted from pore-network modelling (kro values between 0 (blue) and 1 (red)). Results also include gas and water relative permeabilities and three-phase capillary pressure functions (not shown in this figure). Each line represents a single saturation path after water injection up to predefined water saturations, followed by gas injection. The irreducible water saturation areas are shaded by light blue, the residual oil saturation areas are shaded by light red.

3.2.2 *Effect of pore system heterogeneity*

The petrophysical properties of Carbonates 1 and 2 (Table 3.1) are in agreement with the observations that separate vugs tend to increase porosity while permeability remains unchanged (Lucia 1995). It should be noted that both, Carbonate 1 and 2, reach low connate water saturation (Fig. 3.4). Again, this is consistent with field observations. Clerke et al. (2013) reported connate water saturation as small as 5% for vuggy carbonates from the Middle East. A direct comparison of the connate water saturation between the Carbonates 1 and 2 samples and the Berea sandstone is not straightforward due to the existence of clay and capillary bound water in the sandstone. Drainage oil-water capillary pressure (Fig. 3.5a) shows significant steps in the capillary pressure for Carbonate 2 due to the vuggy porosity. This is also true, but to a lesser degree, for Carbonate 1 where this behaviour is caused by the heterogeneity of the pore sizes. Step-changes in capillary pressure are typical for carbonates with separate vugs (Lucia 1995). As expected, the Berea sandstone capillary pressure curve is smooth due to the relatively homogeneous pore-size distribution.

The residual oil saturation (S_{or}) after water injection is highest in Carbonate 2 and lowest in the Berea sandstone. This holds for both, oil-wet and water-wet cases. The high S_{or} is due to the trapping of the oil phase in large separate vugs in Carbonate 2 and the bypassing of oil in the larger pores of Carbonate 1. The saturation paths for Berea sandstone are mostly parallel following a constant water saturation line in the ternary diagram. This indicates that mostly only oil phase is displaced during gas injection. However, for Carbonate 2 and particularly for the oil-wet case, the saturation paths indicate that both water and oil are displaced simultaneously during gas injection. Hysteresis effects are larger in Carbonate 2 with vuggy porosity (compare drainage and imbibition curves in Figs. 3.5b–3.5d. In this case, the oil relative permeability curves have multiple saturation plateaus, which correspond to the sequential filling of the vugs. It is to be expected that the combination of the above factors will impact the shape of the three-phase flow functions and therefore influence the continuum-scale flow behaviours significantly.

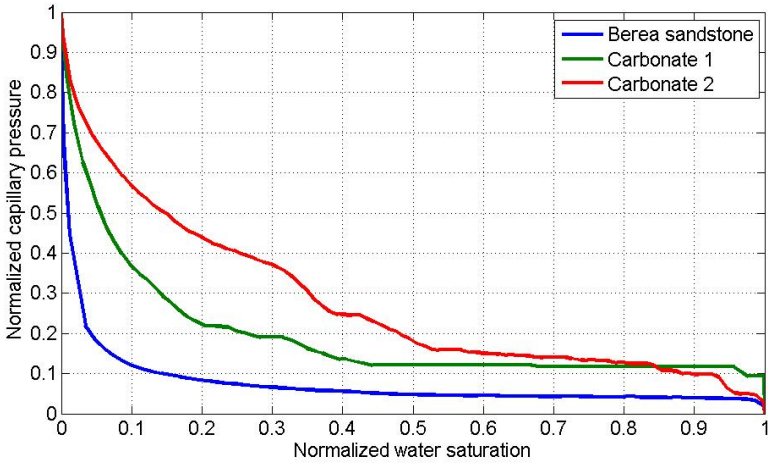

(a) Normalized oil-water capillary pressure curves during oil-water drainage for all three pore-networks.

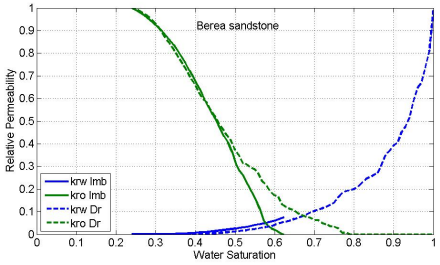

(b)

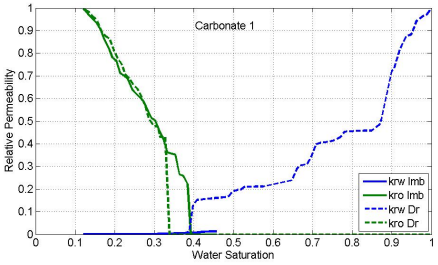

(c)

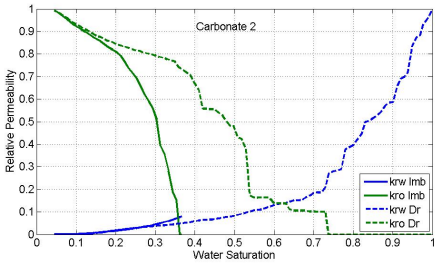

(d)

Figure 3.5: Comparison of capillary pressure and two-phase relative permeability predicted by the pore-network model for the three rock types. The results in (a) can be considered analoguos to Mercury Injection Capillary Pressure (MICP) laboratory measurement. (b), (c) and (d) show the computed two-phase oil-water relative permeability during drainage (Dr) and imbibition (Imb) for Berea sandstone, Carbonate 1 and Carbonate 2, respectively.

3.2.3 *Effect of wettability alteration ("ageing")*

Fig. 3.4 further demonstrates how variation in wettability impacts the shape, extension and location of three-phase saturation region. Note that the there are two residual oil saturations. One represents the remaining oil after the water

injection, denoted as S_{orw}. The other represents S_{or} after gas injection, denoted as S_{org}. The controlling parameter on the shape of the region where the three-phases coexist is S_{orw}. Water-wet Carbonates 1 and 2 have very high S_{orw} because of the water snaps off the oil phase. The snap-off occurs because water can move through the wetting films and as a bulk in piston-like displacements (e.g. Mohanty et al., 1987). This leads to the entrapment of the oil phase in the large pores, particularly when micro-pores are present. In oil-wet cases, the displacement is controlled more by piston-like displacements resulting in a lower S_{orw} compared to the water-wet case.

During gas-oil displacement in the water-wet networks, S_{org} values are very low because oil moves as a bulk phase and / or through intermediate layers (van Dijke et al., 2007; Al-Dhahli et al., 2013b). In the oil-wet cases, these intermediate layers still exist but they seem to be limited. The results are counter-intuitive and show that S_{orw} and S_{org} values are comparable.

3.3 MATRIX-FRACTURE TRANSFER

A fine grid model was constructed for a grid-block scale of 50× 50× 50 ft with 27 (3× 3× 3) matrix blocks. The dimensions of a single matrix block are 12× 12× 12 ft. The model, hereafter termed the *"intermediate-scale model"*, resembles the classical dual porosity model of Warren and Root (1963) (Fig. 3.6). The intermediate-scale model enables us to upscale results from the pore-scale, in the form of flow functions, to continuum scale where fractures and matrix blocks are present in the form of transfer functions. This will further enable direct comparison against the dual porosity model (see Chapter 4). Numerical dispersion effects were investigated and selected simulations were performed on three times finer model but only negligible differences were observed.

To simulate three-phase flow, the fractures are initially filled with water. The initial distribution is the same in all models. For subsequent cycles the initial phase saturations of all three phases in the matrix are taken from the previous cycle results. However, the fracture saturation is changed instantly between gas and water phases. Matrix blocks were assigned the three-phase flow functions

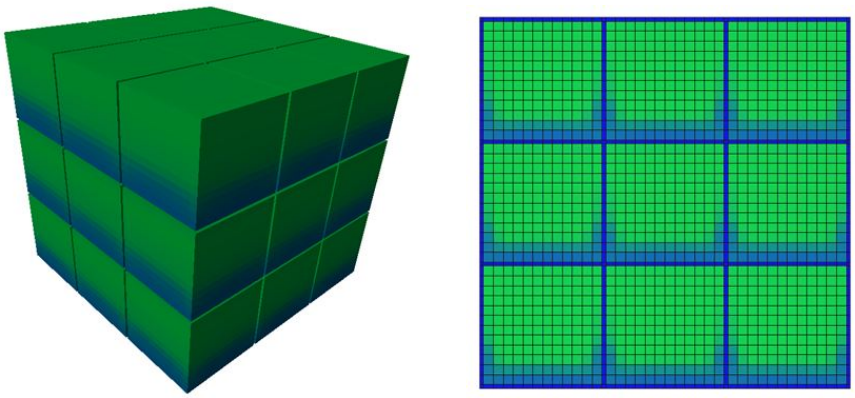

(a) (b)

Figure 3.6: Fine grid model used to simulate matrix-fracture multiphase transfer. Left: a three-dimensional view. Right: a cross-sectional view of the model showing the distribution of the phases (green = oil, blue = water) in fractures (shown in dark blue as they are filled with water) and matrix after a water injection cycle in an oil-wet matrix (right).

discussed in the previous section. The fractures were represented as high permeability features (1000 mD) in which linear relative permeability curves were used. Capillary pressure in the fractures is assumed to be negligible. Further rock and fluid properties are summarized in Table 3.2. The commercial reservoir simulator *ECLIPSE* (Schlumberger, 2012) was used.

Table 3.2: Rock and fluid properties of the intermediate-scale model

Matrix porosity	0.2	(Fraction)
Matrix permeability	1	mD
Matrix rock compressibility	0.36×10^{-10}	Pa^{-1}
Fracture permeability	1000	mD
Viscosity, oil	52.3×10^{-5}	Pa.s
Viscosity, water	52.3×10^{-5}	Pa.s
Viscosity, gas	$17.0E-6$	Pa.s
Formation volume factor, oil	1.00	m^3/sm^3
Formation volume factor, water	1.00	m^3/sm^3
Formation volume factor, gas	3.65×10^{-3}	m^3/sm^3
Density, oil	801	Kg/m^3
Density, water	1000	Kg/m^3
Density, gas	0.673	Kg/m^3

Previous work has already investigated how the choice of hysteresis models impacts the predicted oil recovery during WAG in unfractured reservoirs (Spi-

teri and Juanes, 2006). Additionally, the difference between empirical models and pore-network results for predicting recovery from a clastic reservoir during gas flooding after a prolonged waterflood was studied recently (Al-Dhahli et al., 2013a, 2013b). Here, similar objectives are sought but in the context of matrix-fracture transfer. This is of interest because, as noted in Chapters 1 and 2, flow functions control the matrix-fracture transfer and are hence more influential on the numerical simulation results than in unfractured reservoirs. Firstly, a comparison with empirical models is performed and results are analysed based on recovery from matrix blocks. Secondly, we evaluate the effects of pore-network heterogeneity on the intermediate-scale. The WAG cycles length in all simulations is two to three years to allow water and/or gas fronts to advance deep into the matrix blocks.

3.3.1 *Comparisons with empirical models*

In this comparison, only Berea sandstone network is considered. This rock is used because of the availability of three-phase experimental data and also because the flow functions of this rock are well reported in the literature (e.g. Oak et al., 1990; Blunt, 2000; Spiteri and Juanes, 2006; Spiteri et al., 2008). Four two-phase displacements simulations were carried out to compute flow functions that provide the input for empirical three-phase models. These two-phase simulations are: drainage and imbibition during water-oil flow as well as drainage and imbibition during gas-oil flow. The resulting flow functions match the experimental results of Oak et al. (1990) well, as discussed in Al-Dhahli et al. (2013a). It should be emphasized that the two-phase flow functions are special cases of three-phase flow functions, i.e. when only two phases coexist, two- and three-phase flow functions are identical (see Appendix A). In total, we consider three different empirical models: Stone I and II (Stone 1970, 1973) and the saturation weighted interpolation (SWI) method of Baker (1988). Hysteresis was implemented by using Carlson's model (Carlson, 1981) for the two-phase flow functions. Carlson's model is based on Land's trapping relationship (Land, 1968) and is simpler than other hysteresis models (e.g. Killough, 1976).

The resulting oil recovery from the matrix during WAG is shown in Fig. 3.7. Empirical models without hysteresis yield lower recoveries than the pore-network derived flow functions. When hysteresis is incorporated in the empirical models, the predicted recovery during the second WAG cycle (gas injection) is comparable to the results that employ pore-network derived flow functions. However, the oil recovery continues to increase in subsequent WAG cycles. Ultimately, this causes up to 10% difference in recovery depending on which empirical three-phase flow model is chosen.

When hysteresis is not accounted for, we do not honour trapping of the water and gas phases during gas and water injection, respectively. This leads to inaccurate results as water and gas displace each other, leaving behind significant volumes of oil in the matrix. It is noted that the flow functions that have been computed from the pore-network model account for the hysteresis effect of a generic flow path; in this case, when gas saturations increase after water injection. Recovery predictions that employ pore-network derived flow functions show hardly any increase during the third and later WAG cycles. This is because the saturation paths used to estimate flow functions do not account for hysteresis and phase trapping during higher-order WAG cycles when the gas saturation decreases. Simulating hysteresis during higher-order WAG cycles with pore-network models could be achieved, in principle, by computing two-dimensional relative permeability tables for different saturation paths increasing and decreasing gas saturations and interpolating between the tables, but this remains subject to further research.

When hysteresis is accounted for in any of the empirical three-phase flow models using Carlson's hysteresis model, the observed recovery depends strongly on the choice of empirical model; up to 10% absolute difference in recovery have been observed during higher-order WAG cycles. This highlights the choice of three-phase relative permeability models is a key uncertainty in predicting oil recovery from fractured reservoirs during WAG.

The reason for the high uncertainty in oil recovery when considering hysteresis effects can be explained as follows: Hysteresis allows for water and gas phases trapping. This trapping can reduce the oil saturation to low values. A

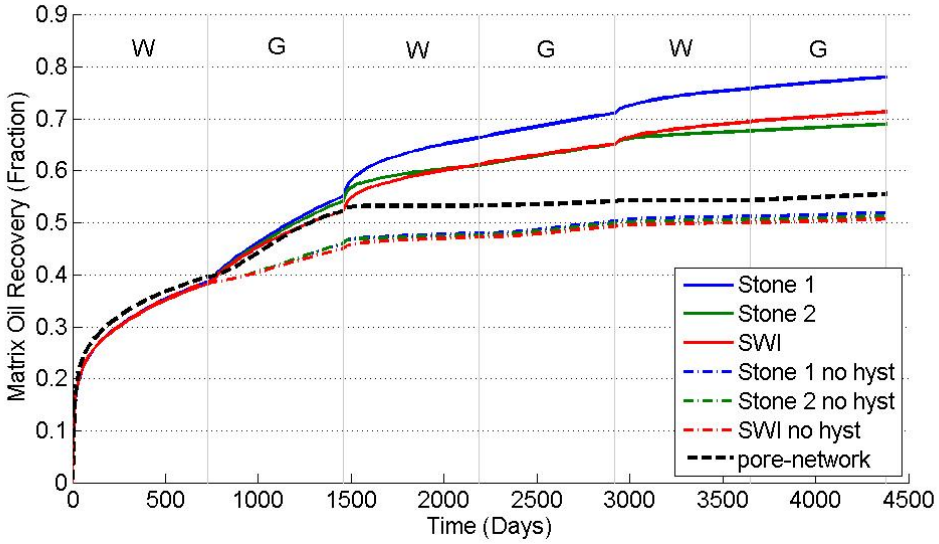

Figure 3.7: Comparison of oil recovery from water-wet matrix blocks in the intermediate scale model predicted using three-phase flow functions from different empirical models, with and without hysteresis, and the pore-network model. Vertical grey lines show the boundaries between individual WAG cycles with 2 years length each. (G = gas, W = water).

comparison between the three empirical models and pore-network results is given in Fig. 3.8 at high and low oil saturations. Clearly, there are significant differences of oil relative permeability values estimated by empirical models when the oil saturation is low. This is the saturation region of interest during WAG injection.

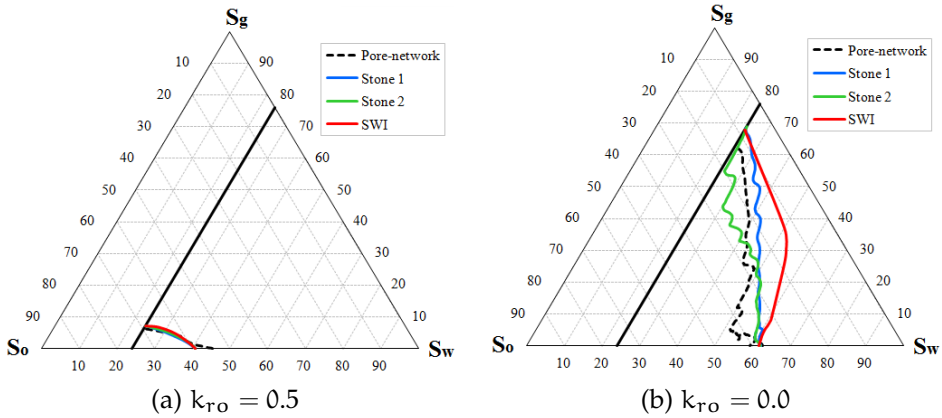

(a) $k_{ro} = 0.5$ (b) $k_{ro} = 0.0$

Figure 3.8: Oil iso-perms (lines of constant relative permeability) for water-wet Berea sandstone computed using pore-network modelling and using three empirical models. The black solid line represents the initial water saturation.

As noted above, flow functions that were estimated from the pore-network model only account for hysteresis during increasing gas saturations, not decreas-

ing ones which are encountered when water is reinjected. Since the recovery predictions using empirical three-phase models also vary greatly during later WAG cycles, only the first two WAG cycles are considered in the following analyses.

3.3.2 *Effects of pore-scale heterogeneity on the intermediate-scale*

Away from producing or injecting wells, capillary and gravity forces control recovery from matrix blocks in NFR. In such regions of the reservoir, accurate capillary pressure and relative permeability functions are keys to representing recovery mechanisms adequately. The flow functions computed by pore-network modelling are applied in the intermediate scale model. We do this by simulating water injection for three-years followed by gas injection for the same period and compare water-wet with oil-wet cases (Fig. 3.9)

Generally, the recovery profiles in Fig. 3.9 show that spontaneous imbibition is only effective in water-wet reservoirs as illustrated by the high oil recovery factors during the water injection cycle. In the oil-wet cases, the recovery was very low. As noted before in Chapter 1, the majority of carbonate reservoirs are mixed to oil-wet (Chilingar and Yen, 1983; Lichaa etal., 1993; Esfahani and Haghighi, 2004). Hence improved recoveries are commonly obtained by gas injection due to gravity forces that dominate and enhance oil production from the rock matrix. This explains why more than 80% of EOR applications in carbonate reservoirs in the US involve WAG injection or gas injection.

During water injection in the water-wet cases, capillary and gravity forces simultaneously displace oil from the matrix blocks, and the higher the capillary forces the higher the recovery. Flow functions computed for Carbonate 1 and Carbonate 2 pore-networks have higher capillary pressure values due to the presence of micro-pores. However, Carbonate 1 and 2 have higher S_{or}, which also affects the overall recovery. The latter seems to have a stronger effect and hence the flow functions for the Berea sandstone network result in higher overall recovery during water injection. During the gas injection cycle, the incremental recovery behaves similarly and the residual oil to gas, S_{org} is comparable for the three pore-networks (Fig. 3.4).

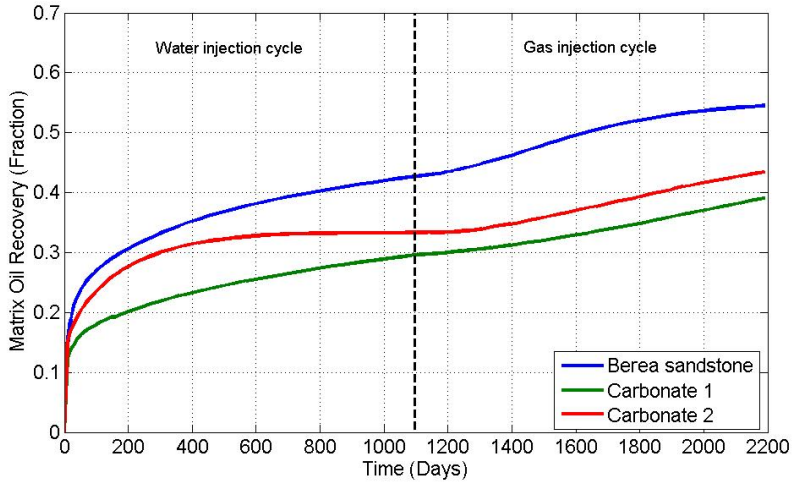

(a) Water-wet

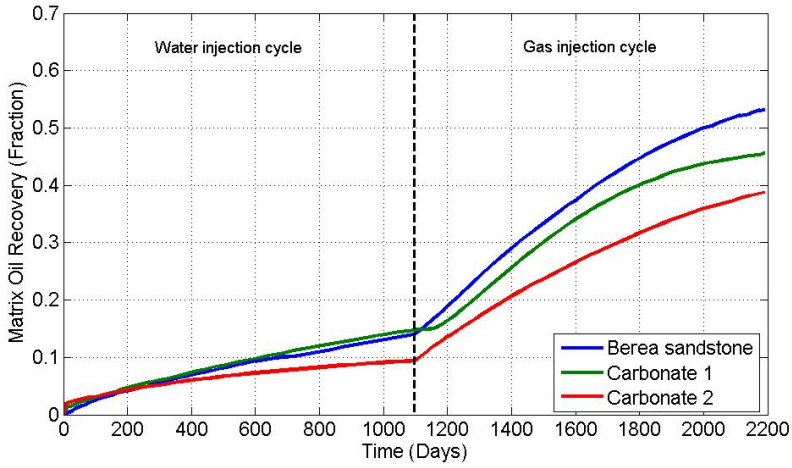

(b) Oil-wet

Figure 3.9: Comparison of recovery profiles of two WAG cycles for the three pore-networks: Berea sandstone, Carbonate 1 and Carbonate 2.

For the oil-wet cases, capillary forces act against recovery and recovery is only due to gravity forces being higher than capillary forces. Contrary to the water-wet cases, the flow functions for Carbonate 1 therefore yield recoveries that are higher than those from Carbonate 2. The highest recoveries are observed for the Berea sandstone network because of its lower value of S_{org} (Fig. 3.4).

3.4 CONCLUDING REMARKS

In this Chapter, pore-scale heterogeneity and wettability has been investigated and their effects on matrix-fracture transfer has been shown. The simulation

results highlight that pore-scale heterogeneity has a direct impact on matrix-fracture transfer in fractured reservoirs. The knowledge of the wettability state is essential for the design of effective recovery methods in NFR. Residual oil saturation, capillary pressure and relative permeability should hence lie at the heart of matrix-fracture transfer calculations. An important step towards more reliable three-phase flow simulation in NFR is to verify the three-phase flow functions. Results in this chapter show that empirical models, which are widely used for three-phase flow, are generally sufficient to predict oil relative permeability when the oil saturation is high.

However, residual oil saturation is associated with a high uncertainty when the oil saturation is low (Fig. 3.8b). A similar observation was made by Zhou et al. (2013). The oil iso-line corresponding to a relative permeability of zero in Figure 3.8b is of paramount importance in this context because it defines the residual oil saturation. Skauge et al. (1999) suggested that Stone 1 model can be modified to match observed residual oil saturation. This technique can be used to calibrate the empirical models so that they reproduce the experimental or pore-network modelling observations when the oil saturation is low.

The next chapter builds on the methodology adopted in this chapter to investigate heterogeneity at the intermediate-scale level, and compare the intermediate-scale simulation results with equivalent dual porosity models.

4

EFFECT OF INTERMEDIATE SCALE HETEROGENEITY

4.1 INTRODUCTION

In the intermediate-scale model in Chapter 3, it was assumed that matrix blocks are homogeneous media of single porosity, permeability and a uniform wettability distribution. The fractures spacing, hence matrix block sizes, are also uniform. The design of the intermediate-scale model facilitates direct comparisons with the dual porosity sugar cube model. However, in reality, fractured carbonate reservoirs show heterogeneity in porosity, permeability and wettability distribution at the intermediate-scale. For example, Lichaa et al. (1993) measured the petrophysical and wettability indices of cores from a Middle Eastern carbonate reservoir (Fig. 4.1). Their results show that for matrix permeabilities varying over several orders of magnitude, the wettability indices cover the full range from strongly water- to strongly oil-wet. Most notably, these cores were taken from a total length of less than 20 m, i.e. a length that is typically at or below the intermediate-scale.

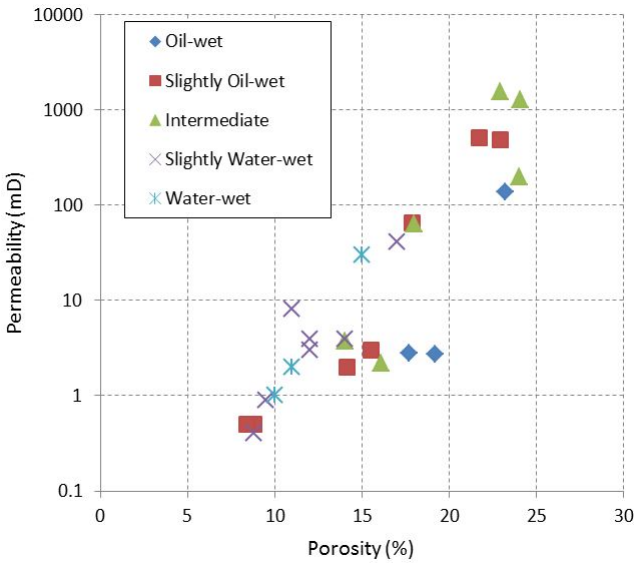

Figure 4.1: Permeability, porosity and wettability indices from a 20 m section in a real carbonate reservoir. Data from Lichaa et al (1993).

Fracture spacing is seldom uniform in fracture formation outcrops. For example, in the real fracture distribution shown in Fig. 1.6 and 2.5a, matrix block sizes are anything but uniform. However, matrix porosity, permeability, wettability and block sizes are considered as uniform in the classical dual porosity model (Chapter 2). The purpose of this chapter is to investigate the effect of heterogeneity at the intermediate-scale, then evaluate the classical dual porosity model reliability in modelling these heterogeneities. The latter is performed by a comparative study of fine grid explicit simulations using the intermediate-scale model and an equivalent dual porosity model. An attempt is made to source the range of heterogeneous parameters from real reservoir properties. Hence, data from a carbonate rock outcrop is used for the comparative study. The three-phase flow functions used in the simulation cases were described in the previous chapter.

4.2 EFFECT OF MATRIX PERMEABILITY HETEROGENEITY

Three cases are considered in this section to quantify the impact of permeability heterogeneity on matrix-fracture transfer in the intermediate scale model. These are: (1) a case with a uniform permeability distribution, (2) a case with heterogeneous and randomly distributed permeability and (3) a matrix with heterogeneous permeability which increases upwards. The two heterogeneous matrix permeability cases have similar permeability distributions (Fig. 4.2). The homogeneous permeability is equal to the arithmetic average of the matrix permeability in the two heterogeneous cases. All other properties, including porosity, remain the same in the three cases. The selection of permeability ranges and order were inspired by data from an outcrop of the San Andreas Formation. The data are shown in a later section.

Fig. 4.3 shows the resulting recovery profiles for the WAG simulations using the three different matrix permeabilities. The speed of oil recovery during water and gas cycles is slower for heterogeneous matrix permeability. The permeability arrangement, randomly distributed versus an upwards increasing permeability, also impacts the recovery factor during water imbibition. The random perme-

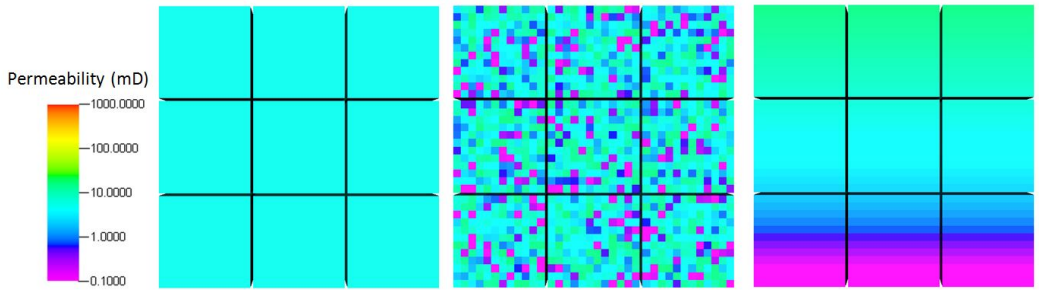

(a)

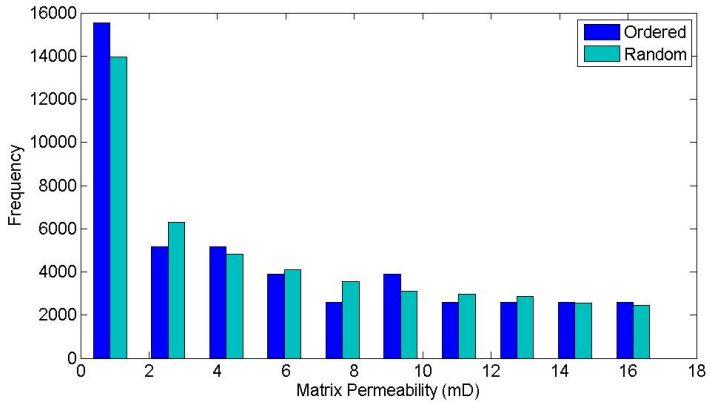

(b)

Figure 4.2: X-Z cross-sectional view of the three cases considered to study the effect of permeability heterogeneity. (a) Matrix permeability for the homogeneous, randomly heterogeneous and ordered heterogeneous porous cases, (from left to right). (b) Histogram showing the distribution of the two heterogeneous matrix permeability distributions.

ability distribution produces more oil towards the end of the first WAG injection cycle. However, both heterogeneous permeability models have approximately the same cumulative oil recovery at the end of the gas injection (second WAG injection cycle). Both models also lead to lower final oil recoveries compared to the homogeneous matrix permeability. This observation is notable because all three cases have the same average permeability.

Although the heterogeneous cases have regions with higher permeability compared to those in the homogeneous case, their recovery is more sensitive to the low permeability regions. Fluid displacement by spontaneous imbibition and gravity drainage occurs at slower rates in the low-permeability regions of the heterogeneous matrix. Hence the speed of recovery is faster in the homogeneous case compared to both heterogeneous cases. As noted above, the randomly distributed permeability yields higher recovery factors compared to the ordered

matrix permeability at the end of the first WAG cycle. This is due to the high correlation length of low permeability regions in the ordered permeability model whereas in the random permeability distribution, the low permeability regions have very short correlation lengths and are surrounded by higher permeability regions. During water imbibition, the displacement becomes increasingly slower in the ordered heterogeneous case. The vertical permeability arrangement in the ordered permeability model (highest permeability at the top) facilitated a faster recovery compared to the other two cases early during the second cycle (gas injection). Hence, the incremental recovery was higher in the ordered heterogeneous model and therefore the cumulative recovery after two WAG cycles is similar for the two heterogeneous models.

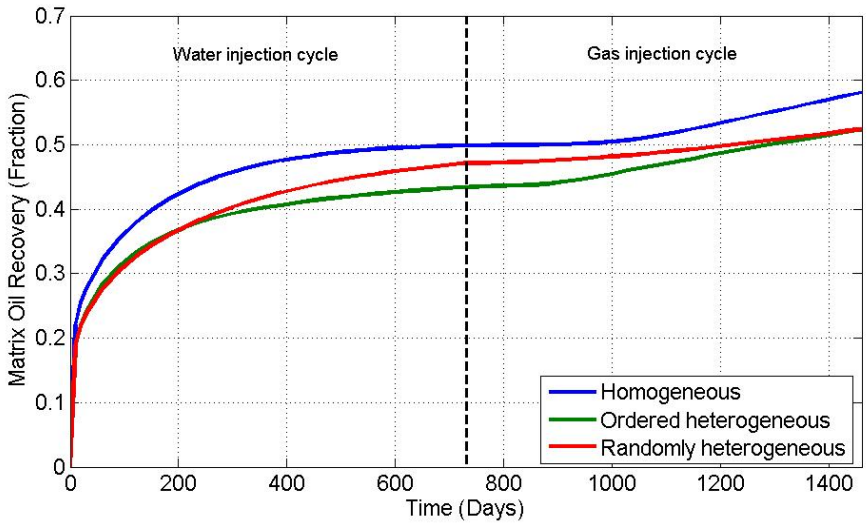

Figure 4.3: Comparison of recovery profiles in three different permeability distributions.

4.3 WATER-WET VS. OIL-WET UNIFORM WETTABILITY

In this section, a simple comparison is performed to quantify the effect of wettability on recovery from the intermediate-scale model. All simulation parameters are maintained the same except that flow functions were different for the water- and oil-wet cases. Fig. 4.4 shows the resulting recovery profiles for the oil-wet case. It is well known that the wettability of the rock matrix impacts the recovery of oil from matrix blocks, particularly during capillary-driven imbibition (e.g. Behbahani and Blunt, 2005; Fernø et al., 2011; Schmid and Geiger, 2013) and

our simulations show the same: only 14% of the oil phase is recovered in the oil-wet case compared to 42% in the water-wet case during the first WAG cycle, i.e. during imbibition of water (Fig. 4.4).

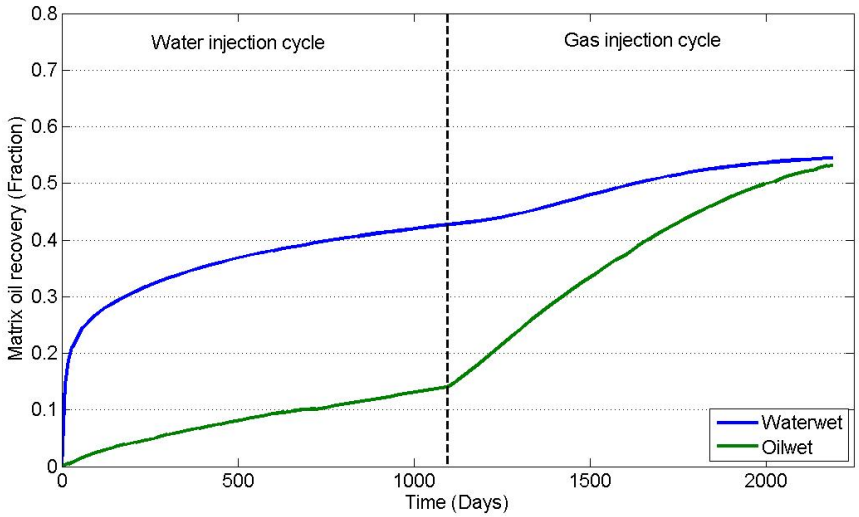

Figure 4.4: Comparison of oil recovery from water-wet and oil-wet matrix blocks in the intermediate scale model predicted using three-phase flow functions of the Berea sandstone.

In general, for capillary-dominated recovery, an increase in oil wetness decreases the rate of recovery from the matrix and the recovery factor (Behbahani and Blunt, 2005, Haugen et al., 2008). This is because water-oil capillary pressure values are negative in oil-wet pores and hence capillary forces prevent water from entering the matrix blocks. Subsequently, the water phase can only enter the matrix to displace the oil phase when the gravity potential is higher than capillary forces.

Fig. 4.4 also shows that gas injection is more effective in the oil-wet case compared to the water-wet case. The incremental recovery during the second WAG cycle was 39% in the oil-wet matrix compared to 13% in the water-wet matrix. The reason is twofold: Firstly, the initial oil saturation is higher when the matrix is oil-wet as a result of poor recovery after the water injection cycle. Secondly, because the recovery is gravity dominated when the matrix is oil-wet, water accumulates at the bottom of matrix blocks (Fig. 4.5) while gas displaces oil starting from the top. In contrast, gas interacts with the previously injected water in the water-wet case because water imbibed from all directions during the first water injection cycle (Fig. 4.5).

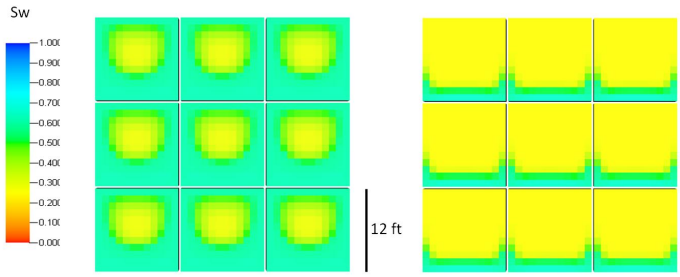

Figure 4.5: X-Z cross-sectional view of the distribution of water saturation (Sw) after the water injection cycle, i.e. the first WAG cycle, in a water-wet (left) and an oil-wet (right) rock matrix. Subsequent gas injected has to displace the previously injected water before it displaces the oil in the water-wet case.

4.4 EFFECT OF NON-UNIFORM WETTABILITY

As mentioned above, field evidence exists that demonstrates that the matrix wettability can also be heterogeneous in nature 4.1. It is hence likely that non-uniform wettability exists at a scale less than the size of the intermediate scale model, i.e. the scale that is comparable to a single reservoir simulation cell size. To study the impact of non-uniform wettability on matrix-fracture exchange, three-phase flow simulations for three cases were considered: (1) A water-wet rock matrix, (2) a rock matrix where wettability is randomly distributed with cells being either oil- or water-wet, and (3) a rock matrix where the wettability is ordered and the upper part of the matrix block is oil-wet while the lower is water-wet (Fig. 4.6). In all three scenarios, the ordered heterogeneous permeability distribution (Case 3 in Fig. 4.2) was used. Hence, in the ordered wettability scenario, the high permeability porous media is oil-wet while the low permeability is water-wet. Data for the water-wet and oil-wet cases are taken from pore-network simulation of the Berea sandstone as described in Chapter 3. As with the previous sensitivity, all other simulation parameters are kept constant.

Fig. 4.7 shows the oil recovery results during two WAG injection cycles for the two non-uniform wettability cases and a uniformly water-wet case. After the first water injection cycle, the water-wet case has the highest recovery followed by the ordered then the random wettability cases. During the gas injection cycle, the incremental recoveries for the ordered and random wettability cases were similar: 17.5% and 17.6% respectively. The incremental recovery for the water-wet case

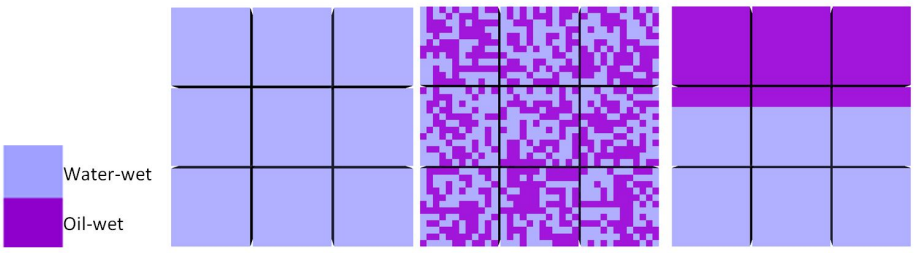

Figure 4.6: X-Z cross-sectional view of the models with three different wettability distributions: uniform, random and ordered wettability distributions in the matrix (left to right). These cases are used to investigate the effect of non-uniform wettability on recovery from matrix blocks.

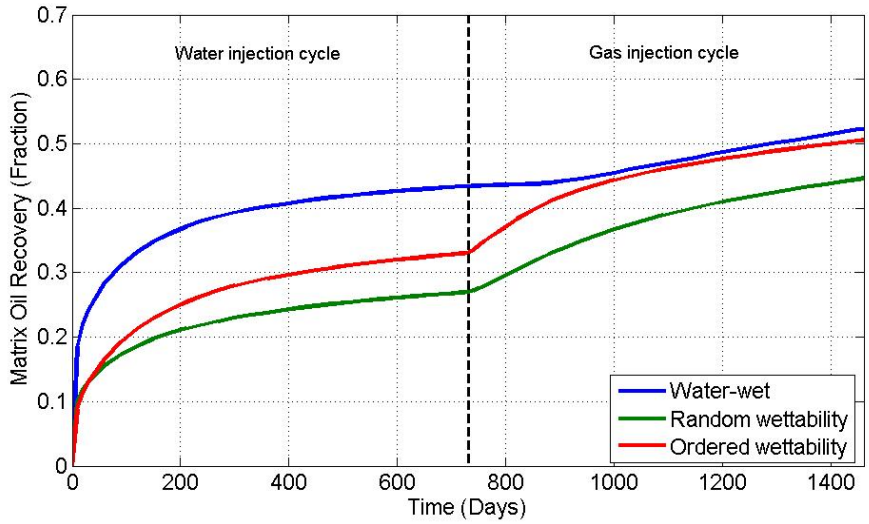

Figure 4.7: The effect of non-uniform wettability on oil recovery from matrix blocks.

is 8.9%. The final recovery of ordered wettability case (50.5%) is close to that of the water-wet case (52.3%). It should be noted that, overall, the distribution of wettability has a much greater impact on recovery compared to the distribution of permeability (Fig. 4.3).

As noted before, oil-water capillary pressures are positive in the strongly water-wet case and negative in the strongly oil-wet case. Therefore capillary forces support recovery during water injection through spontaneous imbibition in the water-wet cases and work against recovery in the oil-wet cases. During the water injection cycle, the water-wet rock matrix yields the highest recovery due to the rapid spontaneous imbibition. Furthermore, the capillary pressure curve remains positive; hence the ultimate recovery is determined by the residual oil saturation and not the oil saturation when the capillary pressure becomes nega-

tive, i.e. when spontaneous imbibition stops. This oil saturation value increases with increasing oil wetness (Behabahani and Blunt, 2005; Schmid and Geiger, 2013)

The ordered wettability model was set up such that the high-permeability region is oil-wet. Water hence does not spontaneously imbibe into the high-permeability region during water injection due to negative capillary pressures but the high permeability facilitates gas oil gravity drainage during gas injection in the second WAG cycle. The low permeability region is water-wet and therefore oil can be produced from this region when water is injected during the first WAG cycle. The combination of capillary forces in the low permeability regions and gravity forces in the high permeability regions leads to higher recoveries in the ordered wettability case compared to the random wettability case. In the random wettability case, the low permeability regions can be oil-wet and vice-versa, the high permeability region can be water-wet (see Figures 4.2 and 4.6).

4.5 EFFECT OF GEOMETRICAL HETEROGENEITIES

Four different matrix block geometries and shapes were investigated here to study the impact of geometrical heterogeneity on matrix-fracture transfer. These are shown in Fig. 4.8. In all simulations we assume that the rock is uniformly water-wet and the rock matrix permeability is also uniform.

The simulation results are shown in Fig. 4.9. During the water injection cycle, the sugar cube model gave the highest matrix recovery (39.5%), followed by the non-uniform matrix blocks model (36.0%), then the match sticks model (34.0%), and the single block model (20.2%). During the gas injection cycle, the incremental recovery was highest in the single block model (16.0%), followed by the non-uniform matrix blocks model (13.3%), the sugar cube model (12.8%) and the match sticks model (9.7%).

Also shown on Fig. 4.9b is the correlation between matrix-fracture interface areas and recovery factor after water injection for the four models. There is a proportional relationship between the recovery factor and the surface area. During the gas injection cycle, gravity forces prevail because of the density difference.

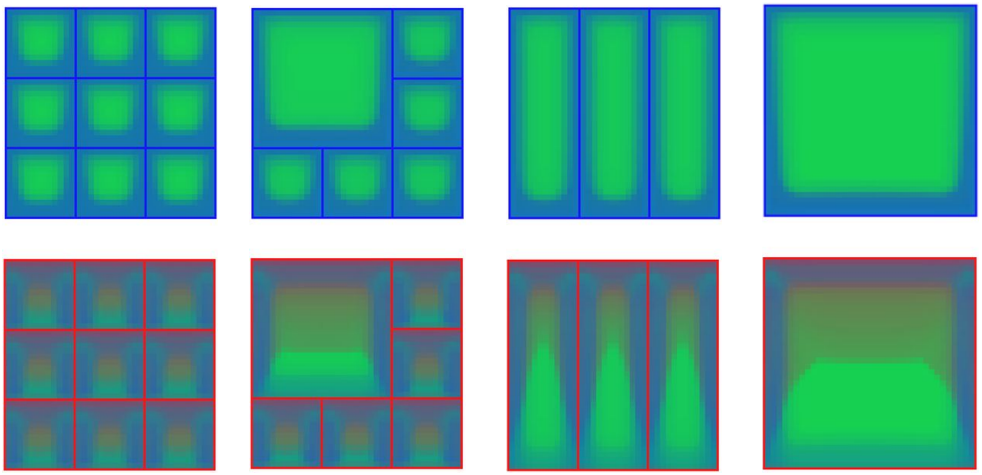

Figure 4.8: Side views of an idealized matrix-fracture arrangement in models with different matrix block sizes, showing the saturation distribution after a water injection (top) and subsequent gas injection (bottom). Matrix block geometries are (a) a sugar cube distribution, (b) non-uniform matrix block sizes, (c) match sticks, and (d) single block matrix shapes. Colours indicate fluid phases (green = oil, blue = water, red = gas).

However, the incremental recoveries due to gas injection are influenced by the oil saturation after water injection. Fig. 4.9c shows the results for a continuous gas injection without prior water flooding for comparison. Again, the sugar cube model recovery is the highest (42.4%), followed by non-uniform matrix blocks (40.5%). The match sticks and single block models have similar recovery factors, (28.3% and 29.0%, respectively). This time, the recovery factors do not correlate well with the total matrix-fracture surface areas. Rather, there is an inversely proportional relationship between recovery factor and the average vertical fracture spacing shown in Fig. 4.9d.

4.6 A CASE STUDY

It is intractable to apply the fine grid model with explicit fracture and matrix discretisation on full field simulations due to CPU time limitations. Therefore, dual porosity models are usually employed to simulate NFR. As shown in the previous sections, the intermediate-scale heterogeneities can impact recovery behaviour significantly. A key question then is: how accurate is the classical dual porosity model when these heterogeneities exist? To answer this question, a com-

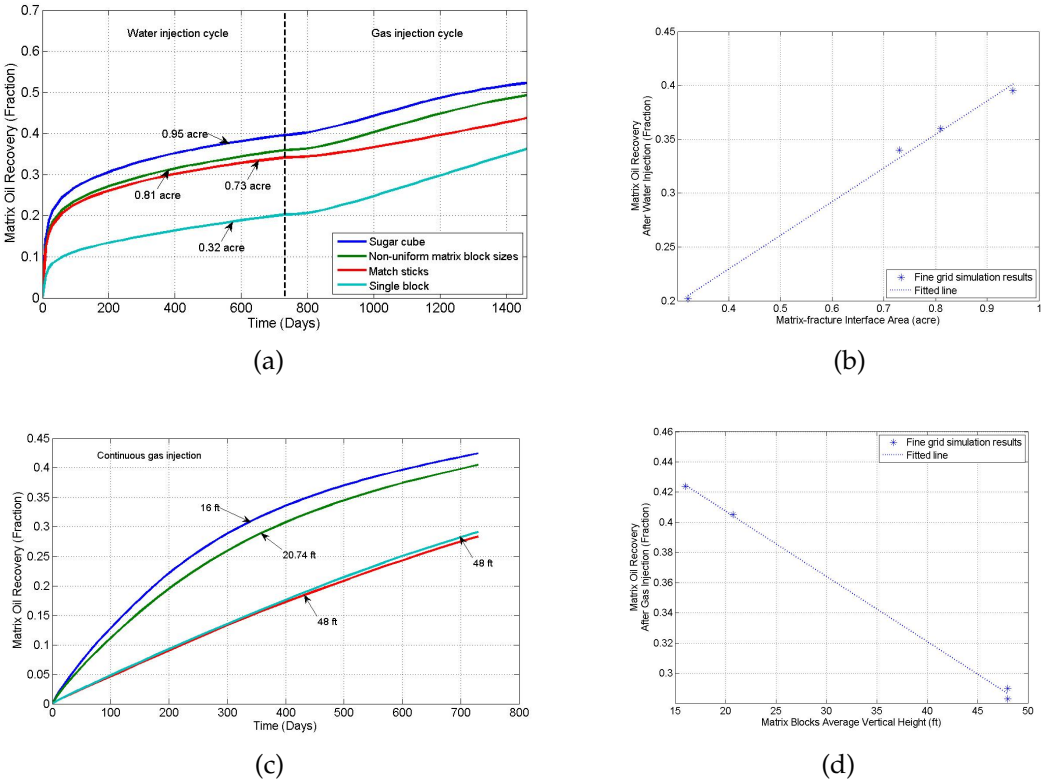

Figure 4.9: Sensitivity of matrix-fracture transfer to heterogeneity in matrix block geometries. (a) Comparison of oil recovery profiles for models with variable matrix block sizes and shapes (see Fig. 4.8). The numbers show the matrix-fracture interface area for each model. (b) The correlation between recovery after the water injection cycle and matrix-fracture interface areas. (c) Comparison of oil recovery due to continuous gas injection from the same models as in (a). The numbers give the average matrix block vertical height for each model. (d)). The correlation between recovery after continuous gas injection and average matrix block vertical height

parison of fine grid detailed models and equivalent dual porosity models is presented here. The data come from a heterogeneous carbonate formation outcrop which is well described in the literature. A simple fracture network is superimposed on the outcrop model to simulate matrix-fracture transfer. All simulations are 2D since the outcrop analogue was also mapped in 2D.

4.6.1 *Description of the outcrop*

The outcrop is part of San Andreas Formation that crops out along the Algerita Escarpment in New Mexico (Senger et al., 1991, Kerans et al., 1994, Jennings and Ward, 2000). It consists of nine cycles of a carbonate ramp deposit. Kerans et al.

(1994) described six rock types for these nine cycles, including their petrophysical properties and poro-perm relationships (Fig. 4.10b). The spatial distribution of these facies was provided in cross-sectional maps. Senger et al. (1991) and Jenning et al. (2000) reported variograms, which we used for petrophysical properties modelling. The available outcrop description allows for building independent geological and reservoir simulation models (e.g. Kazemi et al., 2012). Table 4.1 lists the facies and the corresponding petrophysical properties. A highly idealised fracture network (Fig. 4.11) is considered here comprising matrix blocks with average size of 100×10 m. As in the intermediate-scale model simulations, a water injection cycle is simulated followed by a gas injection cycle. The fracture properties, and fluid properties are the same as in intermediate-scale model (Table. 3.2).

Table 4.1: Petrophysical properties of the Lawyer canyon window simulated using Sequential Gaussian Simulation. The facies also includes a tight mudstone type that has very low porosity and permeability. Petrophysical properties are from (Lucia et al., 1992, Kerans et al., 1994). Note that we use the Berea sandstone network as a proxy to compute three-phase flow functions for the relatively uniform Grainstone facies. The flow functions are described in Chapter 3. The assumed fracture geometry is shown in Fig. 4.11

Facies	Reported porosity (fraction)	Simulated porosity (fraction)	Reported permeability average(mD)	Simulated permeability average (mD)	Representative flow functions
Highly Moldic	0.23	0.23	2.5	2.4	Carbonate 2
Moldic	0.16	0.16	2.2	2.3	Carbonate 2
Grainstone	0.12	0.13	17	18	Berea sst.
Grain dominated packstone	0.14	0.14	2.5	2.6	Carbonate 1
Mud dominated packstone	0.11	0.10	0.4	0.4	Carbonate 1

4.6.2 *Detailed fine grid simulation*

Fig. 4.10 shows the degree of lateral and vertical heterogeneity of a typical carbonate reservoir. The poro-perm relationship shows permeability values vary

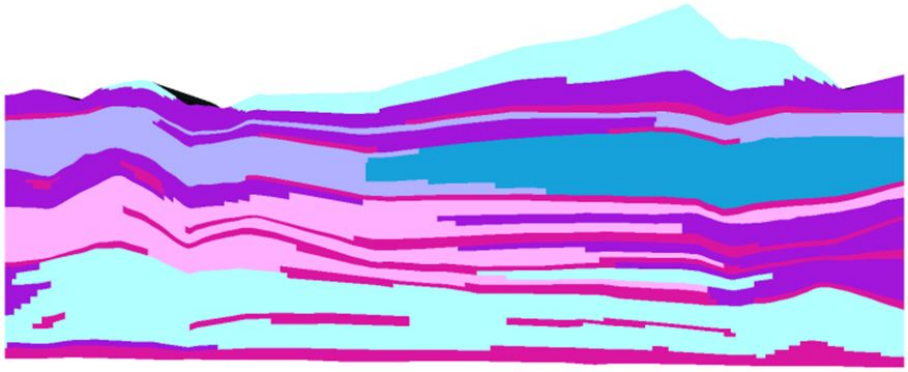

(a) Lateral variation of reservoir facies as described by Kerans et al. (1994)

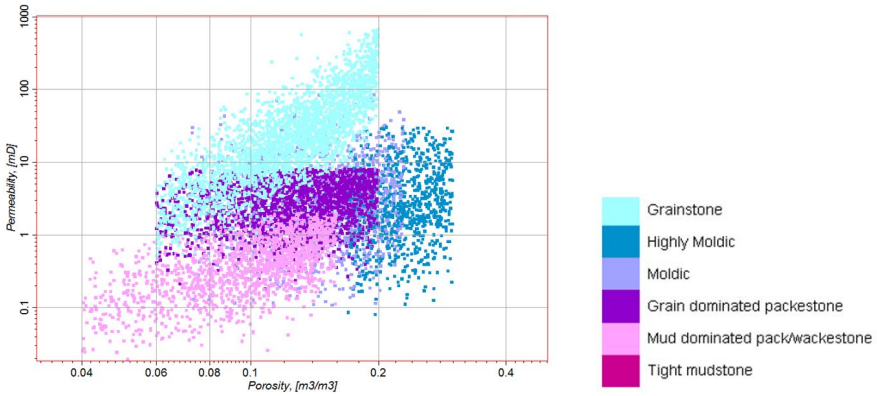

(b) Simulated permeability against porosity

Figure 4.10: Facies distribution and property heterogeneity in the Lawyer Canyon window outcrop of the San Andres Formation.

around four orders of magnitude at the same porosity value. Two WAG injection cylces are simulated using a fine grid model. This will be referred to as the single porosity model in the following analyses. It noted that the rock type and permeability heterogeneities affect water imbibition and gas gravity drainage performances (Fig. 4.11). For example, thin layers of tight mudstone prohibit the advance of water and/or gas into the matrix. Gas injection recovers oil faster in matrix blocks with high permeability rock type, mainly where the grainstone rock type is located (compare Fig. 4.10 and 4.11). Also, water imbibition is not uniform in the rock matrix, even in matrix blocks that consist of only one rock type because petrophysical properties can vary within a rock type.

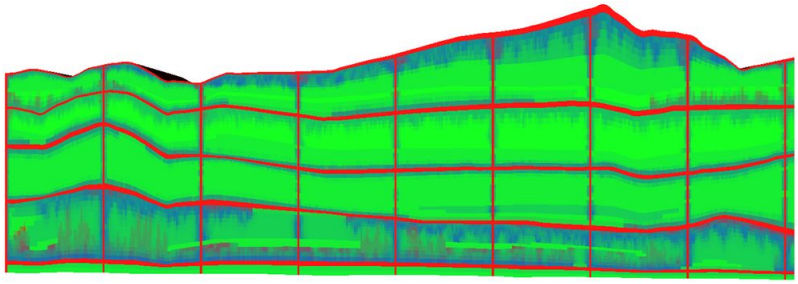

Figure 4.11: Distribution of phase saturation after two WAG flooding cycles starting in the Lawyer Canyon window outcrop. Water injection continued for 90 days, followed by gas injection for 90 days. Colours denote the different phases (green=oil, blue=water, red=gas). Note that the idealized fractures can be easily identified as they are gas-filled. The fracture permeability is 1000 mD and they have fixed fluid saturation (100% water during water injection and 100% gas during gas injection)

4.6.3 *Equivalent dual porosity representation*

In a conventional workflow, the small-scale heterogeneities observed in the outcrop model are difficult to capture even though they impact recovery. This is particularly true with respect to the limitation of the conventional dual porosity models: they only permit one rock type to be present in each matrix block in a simulation grid block and further assume that this matrix block has uniform permeability and porosity. Such property is usually upscaled using the "most of" methodology in which the simulation grid-block inherits the flow functions of the dominant rock type irrespective of other rock types that may be present. Permeability is averaged, using flow-based upscaling methods, over a simulation grid-block.

To quantify the effect of these heterogeneities and how upscaling them affects recovery, we considered three matrix blocks for comparison with dual porosity models (Fig. 4.12). The dual porosity model porosity and permeability values were upscaled from the matrix block properties using weighted arithmetic averaging and geometric averaging, respectively. The initial water saturation was upscaled using pore-volume weighted arithmetic averaging. The flow functions were taken for the dominant rock type using the "most of" method. The shape factor was calculated from the geometry of the matrix block using Eq. 2.19. The bulk volume and matrix-fracture exchange areas are estimated from the geome-

try of the matrix blocks. The results clearly show dual porosity models overestimating recovery in all three matrix blocks (Fig. 4.12).

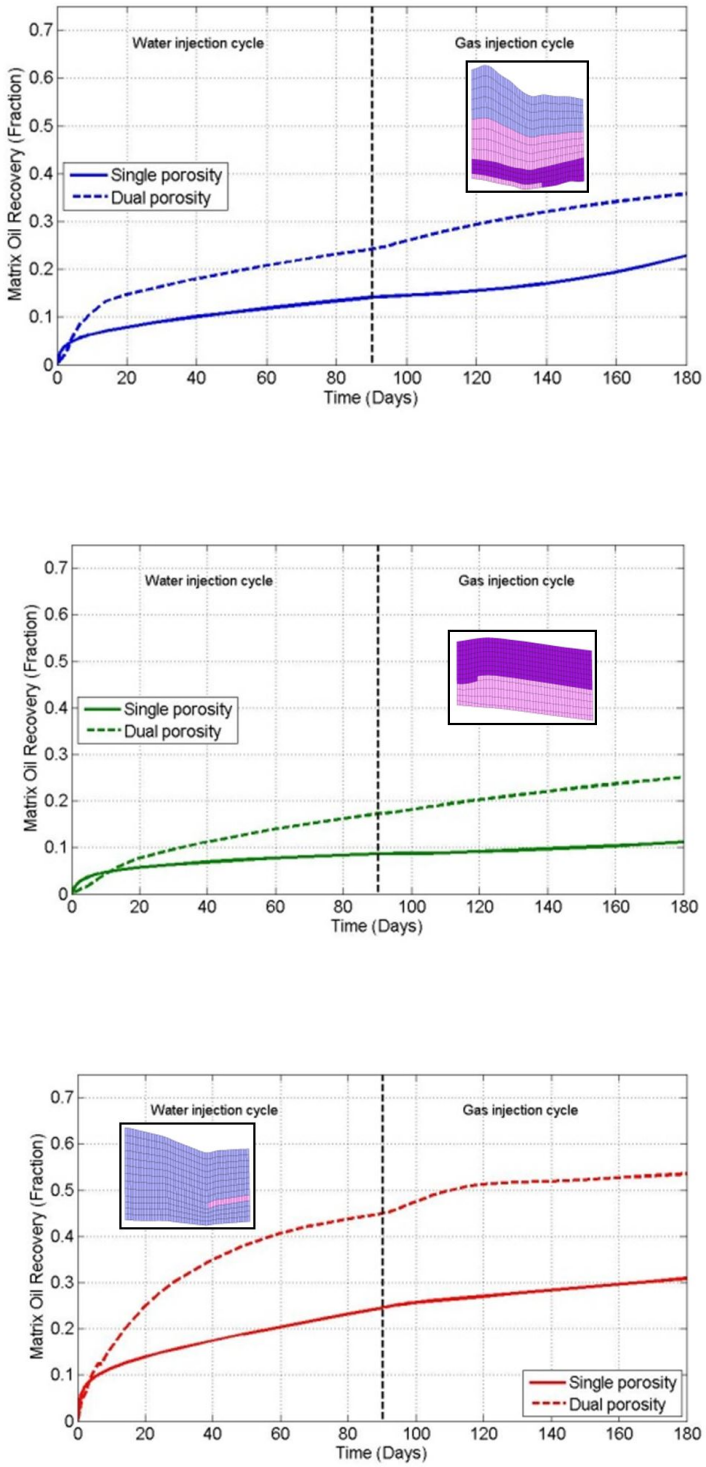

Figure 4.12: Comparison of recovery profiles in three sub-regions of the outcrop model and their dual porosity models. The matrix blocks are shown on each chart with various rock types (colour coded as per Fig. 4.10). For dual porosity models, only the dominant rock type is taken as representative.

4.7 DISCUSSION

4.7.1 *Fluid interactions*

The fine grid simulations gave insights on matrix-fracture transfer under three-phase flow. For the parameters considered in this study, the recovery was most sensitive to the wettability of the matrix. It is well known that wettability controls recovery during water injection cycles. We also found that the three-phase fluid interaction depends on wettability.

Fig. 4.13 schematically shows how the fluids interact and displace each other when water and gas enter the matrix block at water-wet and oil-wet conditions. In the water-wet case and during the water injection cycle, we observe that oil recovery follows two distinct behaviours. The first occurs over very short time-scales (few days) and is characterized by fast recovery as water imbibes into the matrix. The second occurs over longer time-scales: slow recovery after water injection establishes a ring-like region that surrounds the oil in the matrix centre (e.g. Fig. 4.5). This region has low oil saturation and therefore low oil mobility. These two distinct behaviours can be observed in recovery profiles in Figs. 4.3, 4.4, 4.7 and 4.9a. During the gas injection, a three-phase interface region develops at the top of the matrix block as soon as gas injection starts. This is indicated by the purple colour in Fig. 4.13.

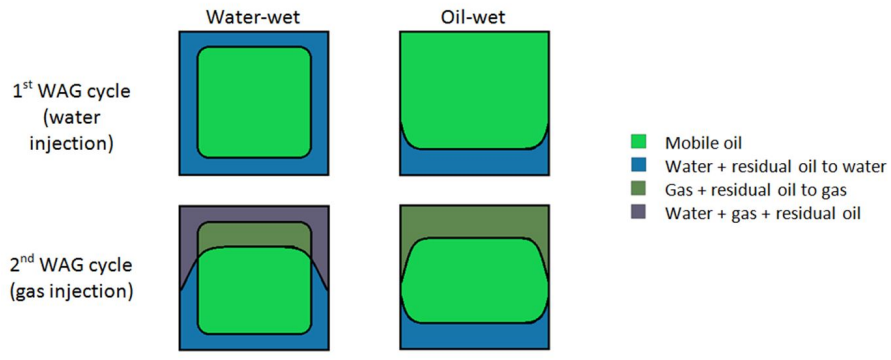

Figure 4.13: An idealised sketch showing the fluid interactions during WAG injection in a rock matrix with different wettability states.

In the oil-wet case, each phase accumulates at a different location (top for gas, bottom for water) due to gravity forces. Hence a three-phase interface region

develops only when the two injected fluids meet inside the matrix blocks. Before they meet, two-phase relative permeability data may give reasonable estimates of recovery. Hysteresis effects are envisaged to have minimal effect on the predicted oil recovery in the oil-wet case. This is because only when the injected fluids meet, a three-phase interface region will form and hysteresis will become important.

A second observation is that gas injection in the water-wet matrix is not immediately effective. This is shown in Figs. 4.3, 4.4, 4.7 and 4.9a. Here, the incremental oil recovery during the early stages of the gas injection cycle is insignificant for the water-wet cases. This can be explained as follows: After the water injection cycle in a water-wet matrix, imbibed water surrounds the high saturation oil in the block centres (Fig. 4.5). During the early stages of gas injection in the second WAG cycle, gas first displaces water before it reaches regions with high oil saturation in the centre of the matrix. This also implies that when gas is injected after a water flood, it is to be expected that gas displaces water that was injected in the previous WAG cycle. Similarly, when water is injected after the gas injection, some of the water first displaces gas when it imbibes into the matrix blocks. This further implies that if WAG injection cycles are short compared to the size of the matrix block, water and gas are likely to displace each other instead of recovering additional oil. This might be one of the reasons why gas injection in some reservoirs did not contribute to oil recovery (e.g. Jackobsson and Christian, 1994).

4.7.2 *Upscaling to dual porosity models*

The classical dual porosity model employs transfer functions to model the matrix-fracture interactions. Hence, the move from explicit models to dual porosity models resembles fundamentally an upscaling process. The fluid interaction observation discussed above highlight the important factors that must be captured in this upscaling process. The fluid configurations shown in Fig. 4.13 cannot be represented in a classical dual porosity model without sub-domain discretisation because the fluid saturations have no spatial arrangement inside the matrix

cell. It is therefore expected that a transfer function with a single matrix cell will fail to reproduce the fine grid simulations.

An equivalent dual porosity model to the water-wet intermediate scale model was created. All geometrical parameters in the dual porosity model are known from the intermediate-scale model and listed in Table. 4.2. In the dual porosity model, the transfer function of Quandalle and Sabathier (1989) is used because it models the interplay of gravity and capillary forces during two-phase flow more accurately compared to other transfer functions (Abushaikha and Gosselin, 2008). In Fig. 4.14a, the saturation profiles computed using the dual porosity model are compared to the single porosity model at three different times (10, 200 and 730 days). As discussed previously in Chapter 2, the dual porosity model overestimates recovery (Fig. 4.14b)because it fails to honour the saturation gradient in the matrix blocks (Eq. 2.22).

Table 4.2: Geometrical parameters used in the dual porosity model

Imbibition shape factor	0.0469	ft^{-2}
Gravity drainage shape factor	0.0195	ft^{-2}
Vertical matrix block height	16	ft

4.7.3 *Effect of sub-cell heterogeneity*

The reason for miscalculation of recovery by the dual porosity models is attributed to the pseudo steady-state assumption. Another source for miscalculation is the simplification of heterogeneous matrix blocks by assuming uniform matrix properties.

The fracture geometry with non-uniform matrix block sizes (Fig. 4.8b) provides an example of sub-cell heterogeneity. It contains one large matrix block of the size 32×32×32 ft and 19 smaller matrix blocks of the size 16×16×16 ft. A volumetric average for the fracture spacing yields 20.74 ft compared to 16.0 ft in the intermediate-scale model. The imbibition and gravity drainage shape factors for the equivalent dual porosity model will be based on the average fracture spacing. Fig. 4.15 shows that the miscalculation of recovery can be even poorer when matrix block geometry is not uniform.

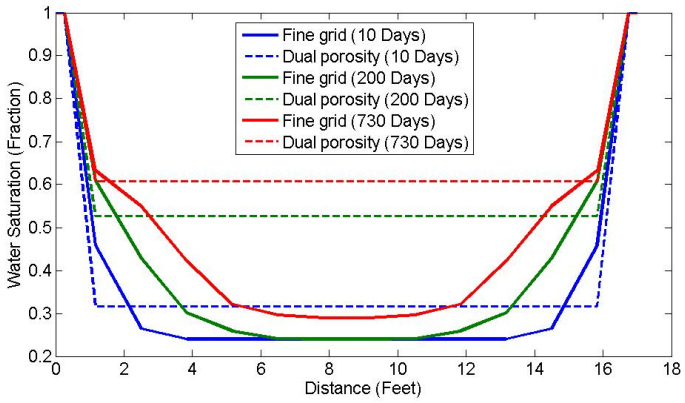

(a) Evolution of saturation profiles inside a single matrix block in the fine grid and an equivalent dual porosity models during water injection. The matrix block is surrounded by fractures where the water saturation is 100% and constant.

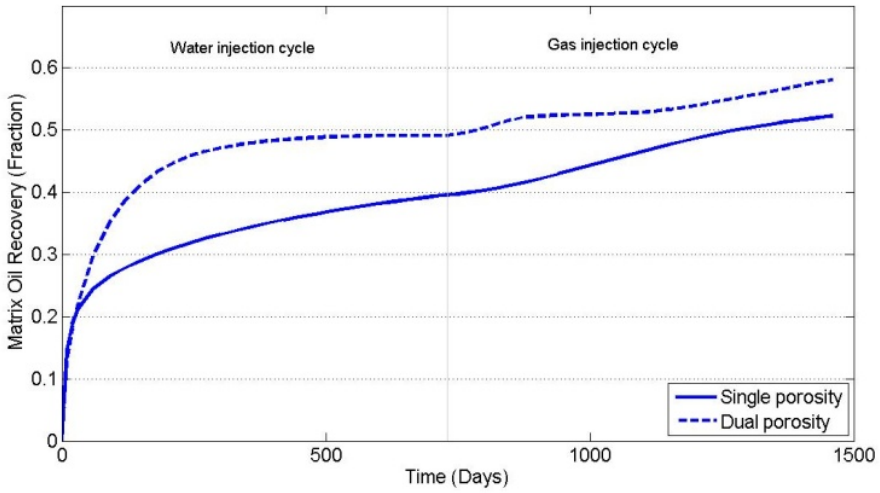

(b) Comparison of oil recovery in the intermediate scale model between the single porosity and the equivalent dual porosity models.

Figure 4.14: Comparison of simulation results of the single porosity and the dual porosity representation of the intermediate-scale model.

Different transfer rates (e.g. due to differently shaped matrix blocks or permeability variations) in a single reservoir simulation grid block can be modelled through multi-rate dual porosity (MRDP) models. MRDP models comprise a distribution of transfer rates within each reservoir simulation grid block to account for the fact that a single reservoir simulation grid block is likely to contain different matrix blocks with different shapes, permeabilities, and wettabilities. Each of the matrix blocks has its own transfer rate. The MRDP model hence requires less averaging of the matrix properties (Di Donato et al., 2007; Maier et al., 2013; Maier and Geiger, 2013).

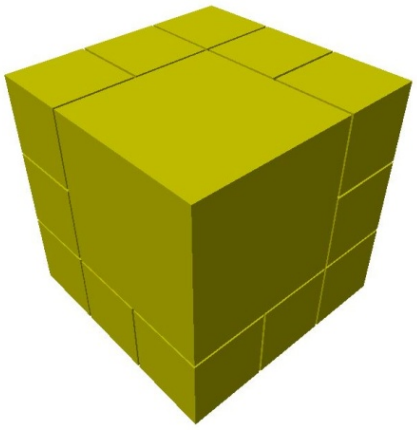

(a) Three-dimensional view of a model with variable matrix block sizes

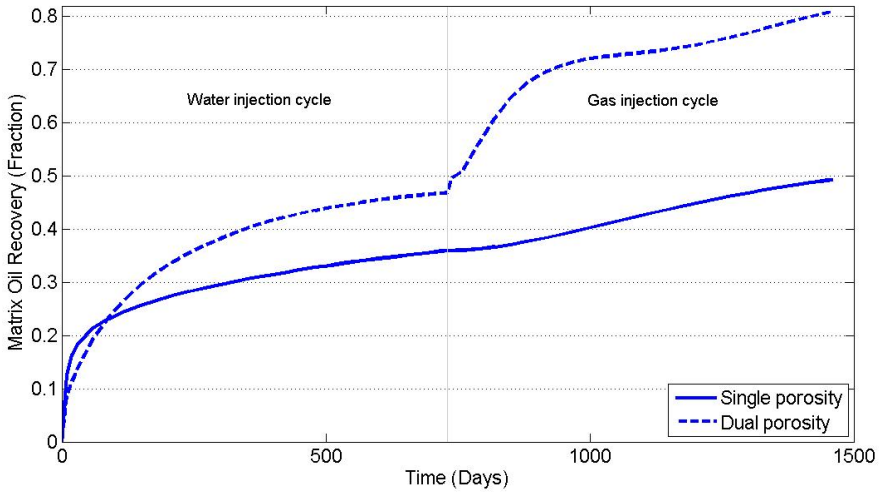

(b) Comparison of oil recovery using fine grid single porosity and dual porosity models of the geometry shown in (a)

Figure 4.15: Comparison of simulation results of the single porosity and the dual porosity models with matrix blocks of different sizes.

4.8 SUMMARY AND CONCLUSION

Capillary and gravity dominated fluid exchange between matrix blocks and fractures were examined during three-phase flow using detailed single porosity and equivalent dual porosity models. Three-phase relative permeability and capillary pressure data were derived from a state-of-the-art pore-network. The high-resolution fine grid simulation model enabled us to investigate the first-order parameters that control three-phase matrix-fracture transfer processes.

A sensitivity study showed that matrix heterogeneities in terms of wettability, block geometry and permeability affect matrix-fracture transfer rates signif-

icantly and that the different transfer rates arising from these heterogeneities cannot be averaged using classical dual porosity models. This was confirmed by a comparative study of single and dual porosity models in a real carbonate rock outcrop. The reasons for the miscalculation of recovery by the dual porosity models are (1) failure to honour the non-uniform saturation profiles noticed in the fine grid single porosity simulations; and (2) sub-cell heterogeneity of matrix properties and block geometries. To increase dual porosity models reliability, these two factors must be considered.

Multiple interacting continua (MINC) models and other sub-domain discretisation methods can be used to resolve the matrix saturation movement inside matrix blocks. However, it is not clear how the imbibition and gravity drainage shape factors can be calculated for each sub-domain. The sub-cell heterogeneity can be solved by using the multi-rate dual porosity model (MRDP) approach. The question here becomes, how can we combine the MINC and the multi-rate dual porosity models to capture both the non-uniform in water saturation and non-uniform property distribution?

The next chapter contains a suggested development in the classical dual porosity model to improve its reliability. It builds on the discussion and results of this chapter and aims to address the two assumptions in the classical dual porosity model that are responsible for the miscalculation of recovery.

5

AN IMPROVED DUAL POROSITY MODEL

5.1 INTRODUCTION

In all comparison cases presented in Chapter 4, the classical dual porosity model failed to match the detailed single porosity simulation of matrix-fracture transfer under three-phase flow. The assumptions of uniform state variables, e.g. fluid saturations; and matrix properties and block geometries were pointed out to be the two factors contributing to the mismatch. Two extensions of the dual porosity model exist that can overcome these assumptions. The first is the multiple interacting continua (MINC) model, one of the matrix sub-domain methods (e.g. Pruess and Narasimhan, 1985; Gilman, 1986; Beckner et al., 1991). This treats the first assumption as saturation fronts inside the matrix blocks can be resolved. The second extension is the multi-rate dual porosity (MRDP) model, which allow us to represent sub-cell heterogeneity (e.g. Haggerty and Gorelick, 1995; Haggerty et al., 2001; Geiger et al., 2013; Maier et al., 2013; Maier and Geiger, 2013).

Matrix-fracture transfer under three-phase flow involves capillary imbibition and gravity drainage recovery processes. The MINC sub-domains geometry is not suitable for the latter and therefore cannot be used directly without modifications. The sub-domain method of Bekner et al. (1991) can be used for imbibition and gravity drainage but it introduces a higher number of sub-domains (see Fig. 2.4). In this chapter, the simplest MINC geometry is used to calculate matrix-fracture transfer in the intermediate scale model. This is referred to as the *double-block* model. Modelling of imbibition and gravity drainage is separated by using different shape factors for each process. The double-block model is extended to represent sub-cell heterogeneities using the MRDP concept. These improvements are applied on two cases presented in Chapter 4 and compared against the detailed single porosity simulation results.

5.2 THE DOUBLE-BLOCK MODEL

The double-block model is essentially the simplest MINC model with two concentric matrix blocks (Fig. 5.1). The matrix block is partitioned to resolve fluid saturation fronts. In the original MINC model, the flow between M2 and M1, and M1 and F is governed by the geometry of the sub-domain such as cross-sectional area and nodal distances between the centres of the blocks. In this work, these geometrical factors will be appended as part of the shape factor calculations. However, before discussing the multi-phase transfer function in the double-block model, a single block transfer term is derived and its results are compared to commercial reservoir simulation results. This is done to make sure the derived transfer term is at least capable of matching the classical dual porosity transfer as implemented in the commercial reservoir simulators.

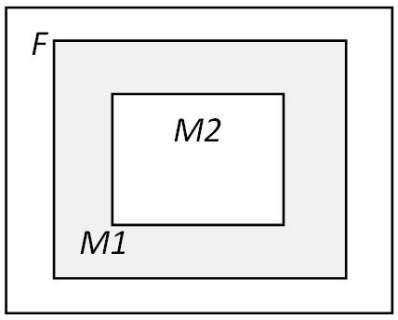

Figure 5.1: A schematic figure of the double-block model. fractures (F) communicate directly with the outer matrix (M1) and indirectly with the inner matrix (M2). Oil recovery from M2 is controlled by the oil mobility in M1.

5.2.1 *A transfer term for immiscible three-phase flow in a single matrix block*

As in the intermediate-scale model, the fractures are assumed to be constantly filled with water or gas. The capillary pressure in the fractures are also assumed to be negligible. Hence, the following expression applies:

$$p_{wf} = p_{of} = p_{gf} = p_f. \tag{5.1}$$

Eq. 2.18 can now be rewritten for the three phases in the following form

$$-\lambda_w(p_{wm} - p_f + G_{wg} + G_{wo}) = \frac{V_b}{\Delta t}\delta(\phi b_w S_w), \tag{5.2}$$

$$-\lambda_o(p_{om} - p_f + G_{og} + G_{ow}) = \frac{V_b}{\Delta t}\delta(\phi b_o S_o), \tag{5.3}$$

and

$$-\lambda_g(p_{gm} - p_f + G_{go} + G_{gw}) = \frac{V_b}{\Delta t}\delta(\phi b_g S_g). \tag{5.4}$$

Here, b_α is the shrinkage factor that is defined as $b_\alpha = 1/B_\alpha$. Therefore, the mobilities are updated as follows

$$\lambda_\alpha = \sigma k_{r\alpha}\left(\frac{kV_b b_\alpha}{\mu_\alpha}\right). \tag{5.5}$$

The multi-phase gravity terms are defined as

$$G_{\alpha\beta} = \frac{\sigma_z}{\sigma}(\rho_\alpha - \rho_\beta)\frac{gL_z}{2}(h_{\alpha m} - h_{\alpha f}), \tag{5.6}$$

where the subscripts α and β denote two different phases and h_α is a dimensionless variable that depends on the saturation of α as in the following relationship

$$h_\alpha = \frac{S_\alpha - \min(S_\alpha)}{1 - \min(S_\alpha) - S_{or\alpha}}. \tag{5.7}$$

Eqs. 5.2–5.4 are three equations to solve for six unknowns: p_{wm}, p_{om}, p_{gm}, S_{wm}, S_{om}, and S_{gm}. The closing equations are:

$$S_{wm} + S_{gm} + S_{om} = 1, \tag{5.8}$$

$$p_{wm} = p_{om} - p_{cwm} \tag{5.9}$$

and

$$p_{gm} = p_{om} + p_{cgm}. \tag{5.10}$$

The following operators are introduced to solve the flow equations in a coupled manner:

$$\zeta_o = \frac{b_w}{b_o} \tag{5.11}$$

and

$$\zeta_g = \frac{b_w}{b_g}. \tag{5.12}$$

Summing up Eq. 5.3 $\times$ Eq. 5.11 and Eq. 5.4 $\times$ Eq. 5.12 gives the following

$$\begin{aligned} &- \lambda_w(p_{om} - p_f - p_{cwm} + G_{wg} + G_{wo}) \\ &- \zeta_o\lambda_o(p_{om} - p_f + G_{og} + G_{ow}) \\ &- \zeta_g\lambda_g(p_{om} - p_f + p_{cgm} + G_{go} + G_{gw}) \\ &\qquad = \frac{V_b}{\Delta t} b_w \phi \delta (S_{wm} + S_{om} + S_{gm}) \end{aligned} \tag{5.13}$$

The RHS of the above equation collapses because $(S_{wm} + S_{om} + S_{gm})$ is always constant (Eq. 5.8). A potential difference, p_{diff} is introduced such that

$$p_{diff} = p_{om} - p_f. \tag{5.14}$$

Solving for p_{diff} in Eq. 5.13, one gets the following

$$p_{diff} = \frac{\lambda_w(-p_{cwm} + G_{wg} + G_{wo}) - \zeta_o\lambda_o(G_{og} + G_{ow}) - \zeta_g\lambda_g(p_{cgm} + G_{go} + G_{gw})}{-(\lambda_w + \zeta_o\lambda_o + \zeta_g\lambda_g)}. \tag{5.15}$$

Finally, S_{wm} and S_{gm} are calculated by substituting the value of p_{diff} in Eq. 5.2 and 5.4, respectively.

$$S_{wm}^{n+1} = S_{wm}^{n} - \frac{\Delta t\lambda_w}{\phi b_w V_b}(p_{diff} - p_{cwm} + G_{wg} + G_{wo}), \tag{5.16}$$

and

$$S_{gm}^{n+1} = S_{gm}^{n} - \frac{\Delta t\lambda_g}{\phi b_g V_b}(p_{diff} + p_{cgm} + G_{gw} + G_{go}). \tag{5.17}$$

The saturation is solved for explicitly in Eqs. 5.16 and 5.17. Hence the timestep Δt sizes could affect the accuracy of the results. For the chosen Δt values, a comparison is shown in Fig. 5.2 of the transfer term developed here, using implicit pressure explicit saturation (IMPES) solution, against a fully implicit commercial reservoir simulator. The reasonable match confirms that the numerical solution is acceptable and that the term gives similar results to those from commercial reservoir simultors.

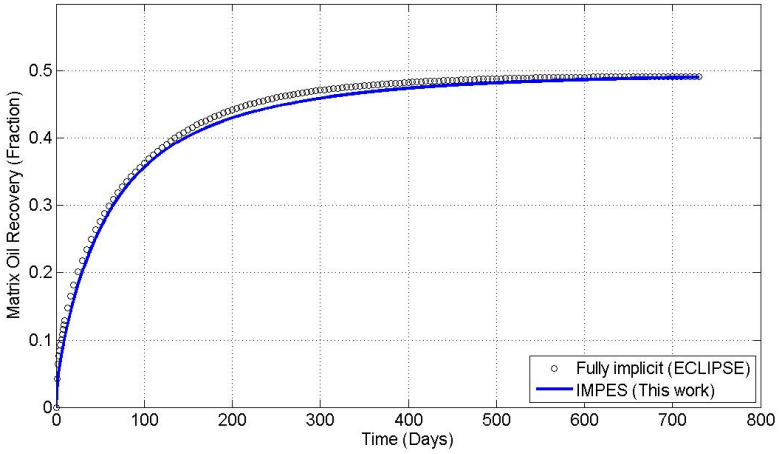

Figure 5.2: Comparison of matrix-fracture transfer calculation in *ECLIPSE* and the double block transfer term. The shape factors used in the transfer term are listed in Table. 4.2

5.2.2 *Matrix-fracture transfer in the double-block model*

The single block transfer term developed above can be applied twice to calculate the transfer between M2 and M1, and M1 and F. Hence, the number of unknown variables doubles. The solution for each matrix block follows the same order as in the above subsection. However, the transfer function for M2 is controlled by the conditions in M1. For example, the gravity terms for M2 will take the following form:

$$G_{\alpha\beta} = \frac{\sigma_{zM2}}{\sigma_{M2}}(\rho_\alpha - \rho_\beta)\frac{gL_z}{2}(h_{\alpha M1} - h_{\alpha M2}). \tag{5.18}$$

The shape factors σ_{M1}, σ_{zM1}, σ_{M2} and σ_{zM2} are determined based on the average fracture spacing in the three principal directions: L_x , L_y and L_z in addition to the outer block thickness $\Delta/2$ as shown in Fig. 5.3.

The surface area over which spontaneous imbibition occurs at the outer matrix block is the sum of the areas of the matrix block sides,$2L_xL_y + 2L_xL_z + 2L_yL_z$. The potential distance of the imbibition front is the same as the outer block thickness $\Delta/2$ and the volume is given by $(L_xL_yL_z) - ((L_x - \Delta)(L_y - \Delta)(L_z - \Delta))$. The imbibition and gravity drainage shape factors are calculated using the relationship in Eq. 2.19. Due to the large area and a relatively short front movement

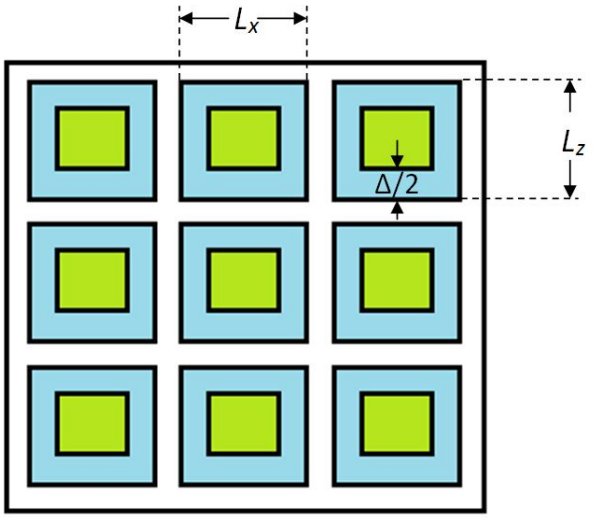

Figure 5.3: The geometrical arrangement in the double block model. All matrix subdomains have the same pressure and saturation values at a given time during matrix-fracture transfer.

distance, the shape factor for M1 is relatively large compared to that of M2 (see below) and is given by:

$$\sigma_{M1} = \frac{2L_xL_y + 2L_xL_z + 2L_yL_z}{\frac{\Delta}{2}[(L_xL_yL_z) - ((L_x - \Delta)(L_y - \Delta)(L_z - \Delta))]}. \tag{5.19}$$

Similarly, the area and volume are computed geometrically for the inner matrix block, M2. The imbibition front can advance from the matrix faces to the centre of M2. This can be approximated by $\sqrt[3]{(L_x - \Delta)(L_y - \Delta)(L_z - \Delta)}/2$ The imbibition shape factor for M2, hence, is calculated as

$$\sigma_{M1} = \frac{2(L_x - \Delta)(L_y - \Delta) + 2(L_x - \Delta)(L_z - \Delta) + 2(L_y - \Delta)(L_z - \Delta)}{\frac{\sqrt[3]{(L_x-\Delta)(L_y-\Delta)(L_z-\Delta)}}{2}[(L_x - \Delta)(L_y - \Delta)(L_z - \Delta)]}. \tag{5.20}$$

Unlike the spontaneous imbibition, gravity drainage displacement is unidirectional. This is straightforward for M2. The acting cross-sectional area for such a displacement for M2 is approximated by $(L_x - \Delta)(L_y - \Delta) + 2(L_x - \Delta)(L_z - \Delta) + 2(L_y - \Delta)(L_z - \Delta)$. This is equivalent to the area of the top matrix blocks in addition to the sides. The potential distance of the gravity drainage front is equal to

M2's vertical height, $L_z - \Delta$. Consequently, the gravity drainage shape factor for M2 is

$$\sigma_{zM2} = \frac{(L_x - \Delta)(L_y - \Delta) + 2(L_x - \Delta)(L_z - \Delta) + 2(L_y - \Delta)(L_z - \Delta)}{(L_z - \Delta)[(L_x - \Delta)(L_y - \Delta)(L_z - \Delta)]} \tag{5.21}$$

The gravity drainage cross-sectional area for M1 is computed through weighted averaging as follows

$$\begin{aligned} A_{zM1} = {} & \frac{\Delta}{L_z}(L_x L_y) + \frac{L_z - \Delta}{L_z}(L_x L_y - (L_x - \Delta)(L_y - \Delta)) \\ & + 2\left[\frac{\Delta}{L_x}(L_y L_z) + \frac{L_x - \Delta}{L_x}(L_y L_z - (L_y - \Delta)(L_z - \Delta))\right] \\ & + 2\left[\frac{\Delta}{L_y}(L_x L_z) + \frac{L_y - \Delta}{L_y}(L_x L_z - (L_x - \Delta)(L_z - \Delta))\right]. \end{aligned} \tag{5.22}$$

Similarly, the front vertical displacement distance is calculated using weighted averaging:

$$d_{zM1} = \frac{\Delta}{\sqrt{L_x L_y}}(L_z) + \frac{\sqrt{L_x L_y} - \Delta}{\sqrt{L_x L_y}}(\Delta). \tag{5.23}$$

Hence, the gravity drainage shape factor for M1 is given by

$$\sigma_{zM1} = \frac{A_{zM1}}{d_{zM1}[(L_x L_y L_z) - ((L_x - \Delta)(L_y - \Delta)(L_z - \Delta))]}. \tag{5.24}$$

The vertical height for M1 is $h_{M1} = L_z$, while for M2 it is $h_{M2} = L_z - \Delta$. The bulk volume of the matrix sub-domains is calculated based on the volume of a simulation cell as follows:

$$V_{bM1} = \frac{V_m}{L_x L_y L_z}(L_x L_y L_z - (L_x - \Delta)(L_y - \Delta)(L_z - \Delta)), \tag{5.25}$$

and

$$V_{bM2} = \frac{V_m}{L_x L_y L_z}(L_x - \Delta)(L_y - \Delta)(L_z - \Delta). \tag{5.26}$$

where V_m is the total matrix volume in the simulation cell. Note that if $\Delta = 0$, then $V_{bM1} = 0$; while if $\Delta = L$ then $V_{bM2} = 0$. In both cases, the double block model behaves as the classical dual porosity model.

5.2.3 *Application on the intermediate-scale model*

The double-block shape factors calculated for the intermediate-scale model are summarised in Table 5.1. Fig. 5.4 compares the observed recovery from fine grid simulations of the intermediate-scale model, the recovery estimate of a classical dual porosity model and the double-block model. In the double block model, the outer matrix block enables fast imbibition into the matrix (Compare the shape factors of the two blocks in Table 5.1). Hence, early time recovery can be matched. The outer matrix block also controls the exchange with the inner matrix block. For example, imbibition into the inner matrix occurs only after the water saturation in the outer matrix is sufficiently large. The two effects combined lead to a markedly improved match of the fine grid simulation.

Table 5.1: The double-block geometrical parameters for the intermediate-scale model

Fracture spacing, L_x	16.0	ft
Fracture spacing, L_y	16.0	ft
Fracture spacing, L_z	16.0	ft
Outer block width, $\Delta/2$	2.5	ft
Outer block imbibition shape factor σ_{M1}	0.7513	ft^{-2}
Inner block imbibition shape factor σ_{M2}	0.0658	ft^{-2}
Outer block gravity drainage shape factor σ_{zM1}	0.1600	ft^{-2}
Inner block gravity drainage shape factor σ_{zM2}	0.0330	ft^{-2}

In Fig. 5.4, there is a slight mismatch between the fine-grid simulations and the double-block early during the gas injection cycle. As will be discussed below, this is a grid effect caused by the geometry of the outer matrix block. Nevertheless,

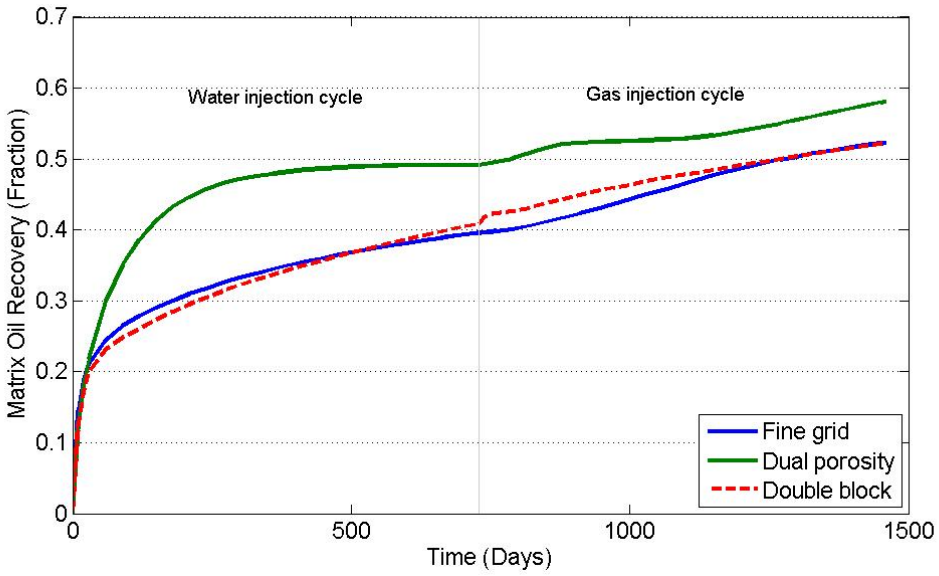

Figure 5.4: Comparison of oil recovery in the intermediate scale model using single porosity, an equivalent dual porosity model and the double block model. All cases use pore-network derived three-phase flow functions.

the results are closer to the fine grid simulation than the classical dual porosity model. The double-block model does not require pseudoisation of flow functions or transient shape factors.

The original MINC model is best suited for capillary dominated multi-phase flow because of the geometry of the sub-domains. The mass flux between the sub-domains is calculated using their volumes, interface areas and nodal distances. These geometrical parameters are computed once for a given matrix block size; changes in matrix block sizes, e.g. as part of reservoir history matching, can be implemented by changing matrix permeability (Wu and Pruess, 1988).

The double-block model builds on the MINC model, but accounts for both imbibition and gravity drainage processes. It allows using two-dimensional tables for flow functions to incorporate pore-network modelling derived three-phase flow functions. Note that the double-block model uses shape factors to calculate transfer rates from the two sub-domains. Using a shape factor to quantify the exchange between the inner and outer matrix block has two advantages: First, we can account for gravity drainage and imbibition by using different shape factor for each process. Secondly, the shape factor can be adjusted for different matrix block sizes without changing the matrix permeability.

The matrix-fracture transfer could also be estimated utilising recent extensions of the MINC model. (Karimi-Fard et al., 2006, Gong et al., 2008, Tatomir et al., 2011) have demonstrated that the shape of each MINC sub-region can be estimated accurately for more complex fracture geometries than those discussed in our work. The sub-region shapes can be computed using local unstructured-grid simulations that explicitly account for both, fractures and matrix, for each reservoir simulation grid block. This MINC extension also leads to very accurate full-field predictions but comes at the extra cost of the computing the shape of the sub-regions locally for each reservoir simulation grid block before the reservoir simulation commences. In contrast, our proposed double block model requires less computational effort and uses the same input parameters as the standard dual porosity model, i.e. fracture spacing, in addition to one geometrical factor. Hence, can be implemented straightforwardly into commercial and research grade reservoir simulators (e.g. Lie et al., 2012) as part of standard reservoir characterisation workflows that employ Discrete Fracture Network models to compute the effective properties of the fracture network (Dershowitz et al., 2000). Finally, the double block model can be extended straightforwardly to account for matrix heterogeneities using a multi-rate dual porosity formulation, as will be discussed below.

5.3 THE MULTI-RATE DOUBLE-BLOCK MODEL

5.3.1 *The multi-rate concept*

The classical dual porosity estimation of matrix-fracture transfer was inaccurate for the real carbonate outcrop window (Fig. 4.12) or the intermediate-scale model with non-uniform matrix block distributions (Fig. 4.15b). One of the reasons for this inaccuracy is the assumption that all matrix blocks have uniform properties, geometries and sizes. The multi-rate dual porosity concept allows using a distribution of transfer rates depending on matrix block properties and geome-

tries. For example, based on Eq. 2.16, the transfer rate for a two-phase oil-water problem in a single matrix block can be rewritten as:

$$\tau_w = \sigma V_b k_m \frac{k_{rw}}{\mu_w} \left[(p_{wf} - p_{wm}) - \frac{\sigma_z}{\sigma} (\gamma_w - \gamma_o)(h_{wf} - h_{wm}) \right], \tag{5.27}$$

where τ is the transfer rate. Multi-rate dual porosity models (MRDP) accommodate a distribution of matrix block rates due to heterogeneity. The heterogeneity can be due to geometrical heterogeneity or porosity and permeability heterogeneity. If the permeability of the matrix blocks is assumed to be constant, a multi-rate transfer rate due to geometrical heterogeneity can be written as follows:

$$\tau_w = \sum_{i=1}^{N} \sigma_i V_{bi} k_m \frac{k_{rw}}{\mu_w} \left[(p_{wf} - p_{wmi}) - \frac{\sigma_{zi}}{\sigma_i} (\gamma_w - \gamma_o)(h_{wf} - h_{wmi}) \right], \tag{5.28}$$

where N is the number of rates. The characterisation factors needed for each rate are σ, σ_z and V_b. Hence, the double block model can be extended to a multi-rate double block model by adding extra terms as in Eq. 5.28.

5.3.2 *Application on the intermediate-scale model*

Fig. 5.5 compares results from the fine grid simulation with a classical single block, a double block, and a multi-rate double block dual porosity model. The classical single block dual porosity model fails to match both, early and late time recovery. The double block model predicts low recovery compared to the fine grid during the gas injection cycle but still yields a much improved match compared to the classical single block dual porosity model. The best result is obtained with the multi-rate double block dual porosity model. However, this model did not completely match fine grid simulation results during gravity drainage because of the outer matrix blocks geometry as discussed previously. Nevertheless, the multi-rate double block model is capable to match recovery significantly more accurately compared to the other dual porosity models.

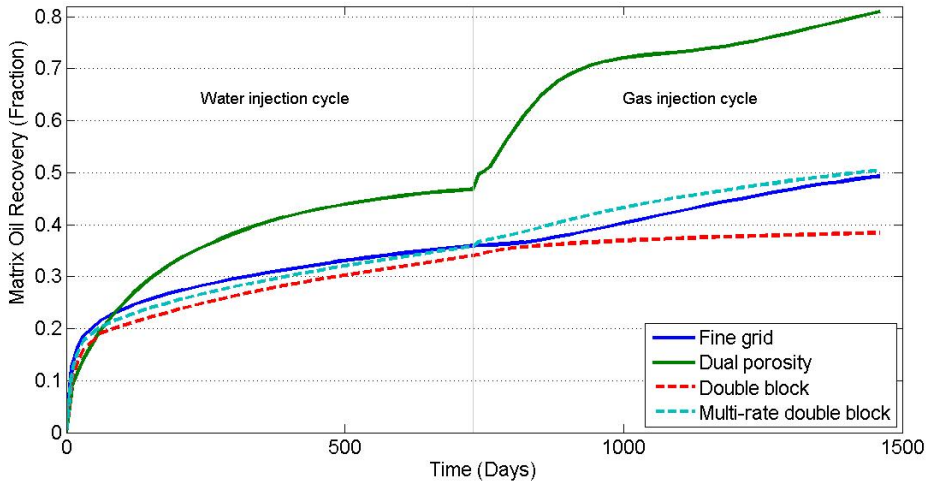

Figure 5.5: Comparison of oil recovery using fine grid simulation, single block and the double block model.

The reason for this poorer match by the single-rate double block model is the averaging of fracture spacing. The size and geometry of the matrix block controls the speed of recovery and hence the variably sized blocks will have different phase saturations. Consequently, their individual flow function parameters are affecting mobilities and fluid interaction regions in each matrix block, which leads to a more complex and ultimately higher recovery. A single average of geometrical factors is not able to capture these effects.

5.4 SUMMARY AND CONCLUSIONS

In this chapter, we presented two extensions to existing dual porosity models to better approximate matrix-fracture transfer during three-phase flow. To facilitate the extensions, a transfer term was derived and solved using the IMPES method. The transfer term closely matched predictions made by a fully implicit commercial reservoir simulator. The two extensions are (1) the double-block model that allows capturing transient effects due to fluid saturation gradients inside matrix blocks. (2) Multi-rate double-block model which enables multiple transfer rates within a single simulation cell. The two extensions were applied on the intermediate-scale model and their results were matching the fine grid single porosity simulation.

The extensions were based on the classical dual porosity transfer approach and can be implemented in reservoir simulators straightforwardly. Hence, these two extensions serve the objectives of this thesis on both accuracy and efficiency. This chapter concludes the first part of the thesis, in which the emphasis was on matrix-fracture transfer under three-phase flow through a step-wise upscaling approach (Fig. 5.6). The pore-scale heterogeneities and multi-phase effects are included in the detailed single porosity simulation of matrix-fracture transfer. The dual porosity models were extended to estimate the transfer more accurately. The aim was to represent the effect of heterogeneity at each level using appropriate upscaling methods so that reservoir-scale simulations are more accurate.

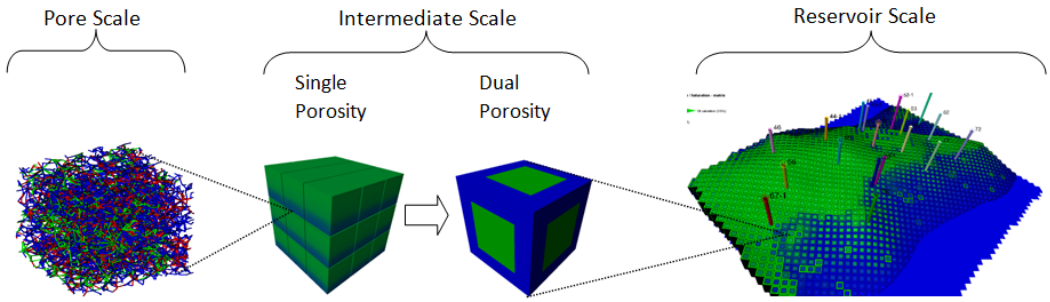

Figure 5.6: A step-wise upscaling procedure of recovery processes in naturally fractured reservoirs. Colours represent different phases (red = gas, green = oil, blue = water).

The question that arises then is whether we can actually characterize a multi-rate dual porosity medium from the data that are typically collected for a fractured reservoir. Clustering analysis and spatial organization of wellbore intersecting fractures can be used in approximating matrix block size distribution. Outcrop analogues provide information on fracture spacing and matrix block sizes. This information can be used in combination with discrete fracture network (DFN) modelling to obtain different likelihoods of block sizes and shape factor. Classical geomodelling of the rock matrix already provides information on permeability and wettability distributions in the rock matrix. In the second part of the thesis, we focus on DFN upscaling accuracy and develop new upscaling methods that provide input parameters for the extensions presented in this part.

Part II

DFN UPSCALING AND IMPROVEMENT

In this part, the discrete fracture network (DFN) upscaling methods are assessed using a number of case studies. A workflow for quantification of DFN upscaling errors is presented. This workflow revealed the dependency of the DFN upscaling results on selections related to the DFN upscaling method, the boundary conditions used and the simulation cell size. The effect of DFN upscaling on history matching results is examined for a real fractured reservoir. The results showed that the effect of the DFN upscaling should be considered as an uncertainty in NFR models. Finally, a new shape factor upscaling method is presented. The method allows us to characterise MRDP models from DFN geometries.

6

ASSESSMENT OF DFN UPSCALING ERRORS

6.1 INTRODUCTION

The discrete fracture network (DFN) approach is an efficient and accurate way to model fractures in fractured reservoirs. DFNs can capture the connectivity and scale-dependent heterogeneity of fractured reservoirs (Dershowitz et al., 2000). DFN upscaling is a process where the fracture networks are converted to cell properties suitable for single- or dual porosity models. The objective is to retain the DFN dynamic behaviour in the continuum models.

The individual cells sizes in continuum models must be equivalent to or above the scale of a representative elementary volume (REV) of a porous medium (Hubbert, 1956, Bear, 1972, Caers, 2005). For fractured media, this condition is true only when fractures are dense and well connected (Long et al., 1982, Berkowitz, 2002). For example, Müller et al. (2010) found a REV of 10 meters in a fractured geothermal reservoir. While this scale is relatively massive compared to a REV of a porous medium, it is less than the size of a typical simulation cell. Jackson et al. (2000) and Botros et al. (2008) also showed that continuum models can reliably represent fracture connectivity without scaling issues. However, their DFN models were very connected and hence this may not apply to all DFNs.

In fact, it is widely accepted that fracture lengths and properties show a scaling behaviour such that a REV may not exist. Scale dependency of fracture equivalent permeability is experienced not only in upscaling of fractured media properties (e.g. Long et al., 1982; Dershowitz et al., 2000) but also in laboratory and field observations (Margolin et al., 1998, Berkowitz, 2002, Neuman and Di Federico, 2003, Neuman, 2005, Katsuaki and Yuichi, 2006, Bonnet et al., 2001, Odling, 1997). In fractured porous media, the simulation cell size is often designed based on the measurement scale of porous media properties such as porosity and absolute permeability. The simulation cell size is more often limited by the available CPU time. This poses a limitation generally on the use of the continuum mod-

elling approach for simulation of flow in fractured formations. DFN upscaling results are hence expected to depend on the size of the simulation cell.

DFN upscaling follows analytical or flow-based methods. It was shown that Oda's method (Oda, 1985) overestimate equivalent fracture permeability while the flow-based method is computationally expensive and is intractable to apply on full field simulations (Chapter 2). Furthermore, the flow-based upscaling results are subject to the boundary conditions used during the upscaling. Hence, the DFN upscaling method and boundary conditions are additional factors that influence the DFN upscaling results.

The quality of the an upscaled matrix properties model in unfractured reservoirs is normally assessed to ensure that the coarse model captures effective flow properties of the detailed fine model. As such, the ultimate comparison is achieved when the two models are subjected to flow simulation under the same boundary conditions. Such a comparison may not be possible due to computational limitations associated with simulating flow in the fine model (normally contains a few million cells). Streamline simulation, however, can be used for qualitative comparisons due to its efficiency in assessing the quality of upscaling results (Fig. 6.1). Here, the reciprocal of the time of flight (TOF), a property of the streamlines, provided a qualitative measure of how good the coarse model captures the slowness/fastness of fluid flow in the fine model (Samier et al., 2002, King et al., 2006). However, in scale-dependent problems such as upscaling of fractured reservoirs, it is not known which coarse scale is the most accurate because the fine model is a discrete fracture network. For example, the comparative assessment of upscaling may not be helpful unless the streamline properties exist on the DFN itself.

In this chapter, the DFN upscaling errors are explored and the impact of the upscaling error is quantified in two case studies. More quantitative analysis of the DFN upscaling is attempted and suggested DFN upscaling assessment workflow is provided. The three factors affecting DFN upscaling that are considered here are (1) the simulation cell size, (2) the upscaling method and (3) the boundary conditions used for flow-based DFN upscaling. As noted above, DFN upscaling errors depend on the fracture connectivity and the existence of a REV.

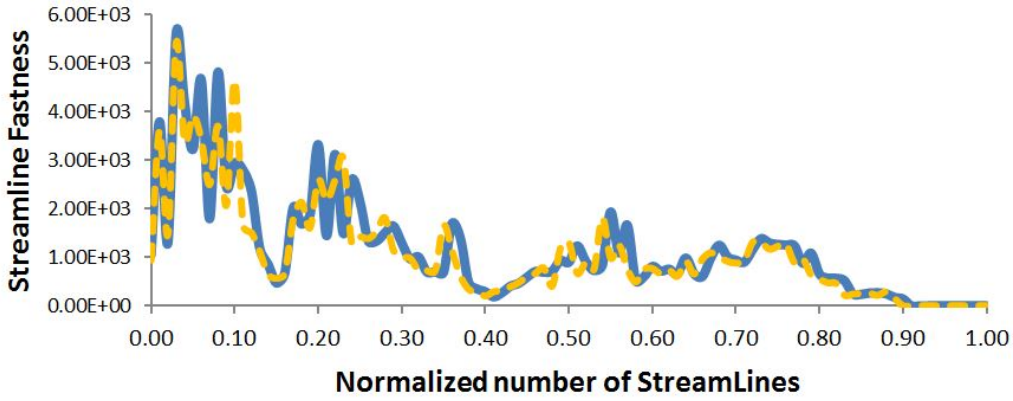

Figure 6.1: The reciprocal of the time of flight (TOF), a character of streamlines, plotted against the normalized number of streamlines. This plot represents the closeness of one model to the other. The two models represent one DFN upscaled to different two different simulation cell sizes.

The relationship between connectivity and upscaling errors is examined first in a case study using fracture data from the Teapot Dome Field in Wyoming. Then, a quantitative assessment workflow is presented and applied on a sector-scale DFN model representing a real fractured reservoir from the San Andreas formation in California.

6.2 DFN CONNECTIVITY AND UPSCALING ERRORS

To investigate the relationship between DFN connectivity and upscaling errors, a realistic dataset from four wells drilled in the Teapot Dome structure, Wyoming. The data are publically available from the Rocky Mountain Oilfield Testing Center (RMOTC) an affiliate of the U.S. Department of Energy. Previous works (Smith, 2008, Schwartz, 2006) provided detailed description and image log interpretations of the Tensleep Formation. Fig. 6.2 shows the fracture orientation data obtained from the four wells. Fracture orientation and dip angle based on this dataset has informed the DFN, which was generated in a sector model.

DFN connectivity increases with fracture length and intensity. The objective of this section is to study the effect of fracture connectivity on DFN upscaling errors. Hence, the fracture length (FL) and intensity (P_{32}) were varied significantly and the impact on DFN upscaling is investigated. The DFN upscaling was per-

formed for the same DFNs with two different simulation cell sizes. The DFN upscaling methods used here are Oda's method and a flow-based method with open boundary conditions. As noted before, flow-based upscaling methods are intensive computationally. Hence, the size of the model was reduced to a sector model to manage all the DFN upscaling required for the comparison. More description of the Tensleep Formation in the Teapot Dome Field is available in Chapter 7 where the full field model is used to study the effects of DFN upscaling on the history matching results.

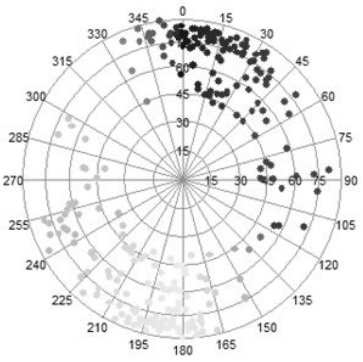

Figure 6.2: Stereonet diagram representing fracture dip angle and dip azimuth from four wells at Teapot Dome, Wyoming.

Fracture lengths considered in this study were chosen to cover a wide range of short to long fractures such that they impact fracture connectivity. The fracture lengths are based on outcrop measurements (Olson et al., 2001) are: 50, 100 and 450 m. Similarly, intensity of fractures considered were chosen to reflect different fracture connectivities from poor to well connected fractures. Fracture intensities represented by (P_{32}) were 0.01, 0.04 and 0.2 m^2/m^3. DFN upscaling and reservoir simulations were run for two simulation cell sizes: small cells of 30×30 m and large cells of 120×120 m.

6.2.1 *Static comparison of DFN upscaling results*

Here, we discuss the similarity and differences of the upscaled effective permeability for the different FL and P_{32} values, different upscaling methods and different simulation cell sizes. The similarity increases if the upscaled permeability values for Oda's method and the flow-based method lie close to the diagonal

line (which represents the equation: $y = x$). The first set of plots (Fig. 6.3) represents the large simulation cell size of 120×120 m. The similarity between the two methods enhances as the intensity P_{32} and fracture length FL increase. Both P_{32} and FL increase DFN connectivity leading to equal upscaling results even though different upscaling methods are used. The impact of P_{32} on fracture connectivity is more apparent than that of FL: Even for the largest FL value of 450 m (i.e. when the fractures are well connected), the upscaling results from Oda's and flow-based methods are different for low P_{32} values of 0.01 and 0.04 m^2/m^3. On the other hand, upscaling results of Oda's and flow based methods are more similar for the largest P_{32}, even when FL is only 100 m.

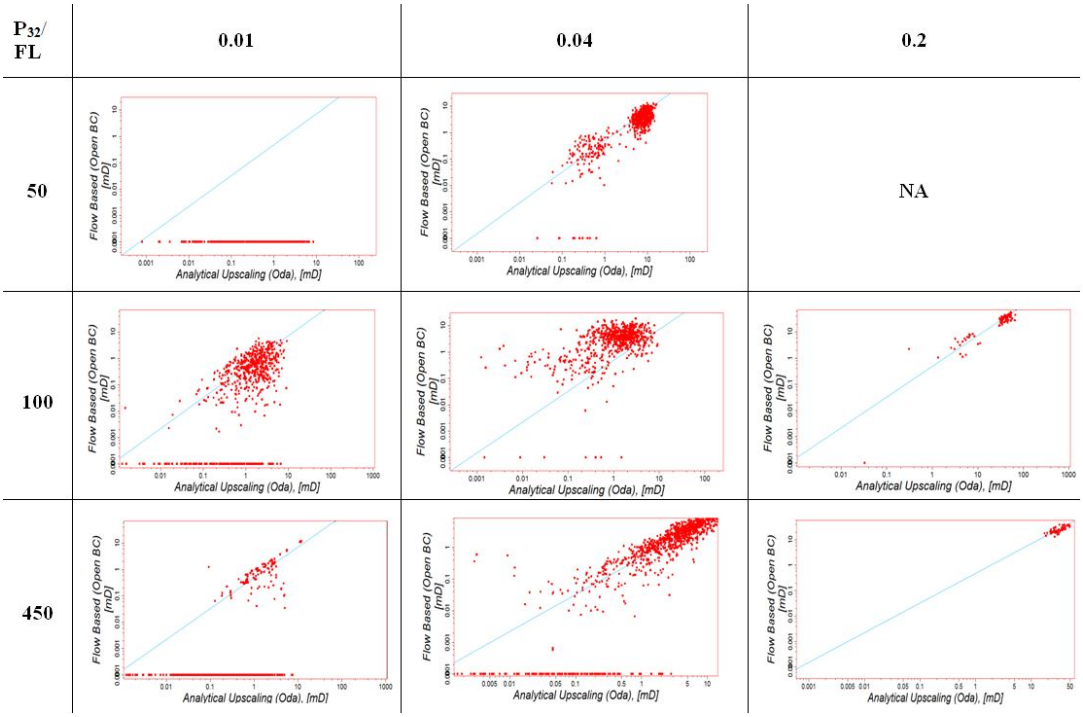

Figure 6.3: Cross-plots comparing flow-based DFN upscaling method results and Oda's method for different fracture lengths and fracture intensities. The simulation cell size is 120×120 m. When P32 is high and FL is short, the number of fracture objects becomes too large for DFN upscaling.

The second set of plots (Fig. 6.4) represents the small grid-block size of 30×30 m. The similarity between the two methods increases as with increasing P_{32} and FL. There is generally better agreement compared to (Fig. 6.3) where the simulation cell size was four times larger. The reason is that Oda's method tends to overestimate fracture connectivity. The larger the simulation cell, the larger the overestimation.

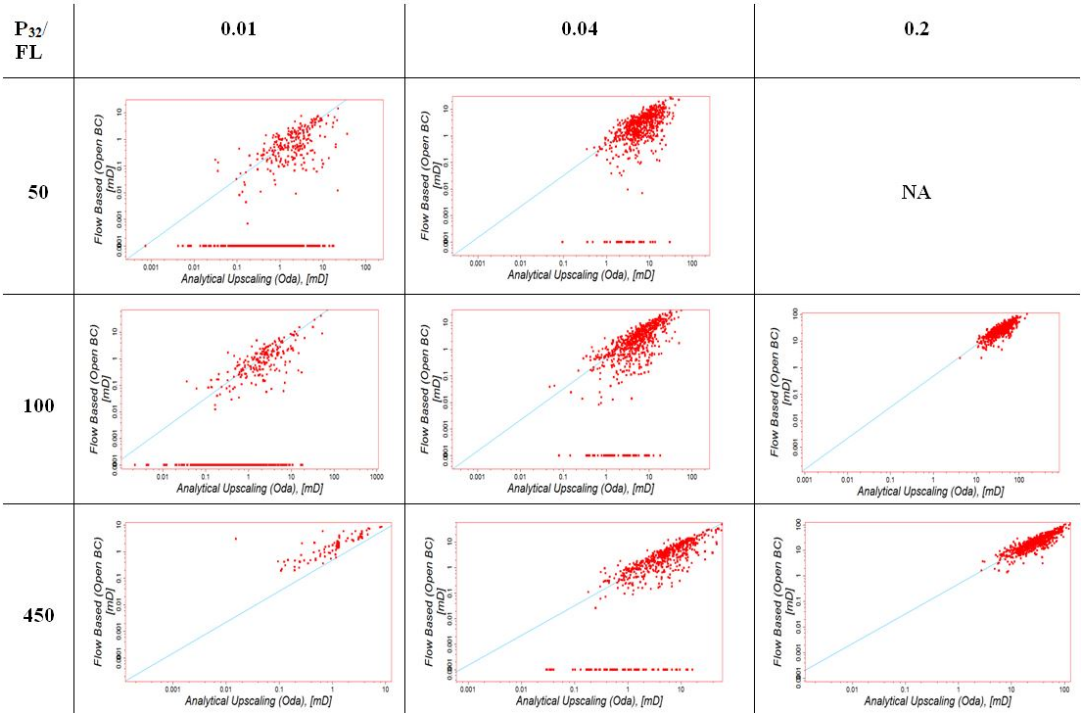

Figure 6.4: Cross-plots comparing flow-based DFN upscaling method results and Oda's method for different fracture lengths and fracture intensities. The simulation cell size is 30×30 m.

6.2.2 *Dynamic comparison of DFN upscaling results*

To quantify the effect of DFN upscaling error on the prediction of oil production at the sector scale, we used two DFN models and simulated oil production in the sector model. The two DFN models are:

(a) High intensity and medium fracture length ($P_{32} = 0.2 m^2/m^3, FL = 100 m$)

(b) High intensity and long fractures ($P_{32} = 0.2 m^2/m^3, FL = 450 m$)

Note that these DFN models show high similarities between Oda's and the flow-based method as shown in Fig. 6.3 and 6.4. The DFN models were the highest fracture intensity such that Oda's method is likely to be applicable. For each DFN model [e.g. (a) and (b)], four upscaling scenarios are investigated

1. Oda's method, simulation cell size of $30 \times 30 m$
2. Flow-based method (open boundary conditions), simulation cell size of $30 \times 30 m$

3. Oda's method, simulation cell size of $120 \times 120\text{m}$

4. Flow-based method (open boundary conditions), simulation cell size of $120 \times 120\text{m}$

The sector-scale model is shown in Fig. 6.5. Flow simulation is performed in a single-porosity model. The fracture permeability was taken as the result of DFN upscaling for the above four cases. All other model properties are kept constant during the flow simulation and are summarised in Table 6.1.

Table 6.1: Description of parameters used in the sector model from the Teapot Dome Field

Type of simulation model	Single porosity
Rock properties	
Porosity	0.2
Permeability	*Upscaled from DFN*
Fluid properties (oil)	
Density	$56\text{lb}/\text{ft}^3$
Average formation volume factor	1.2RB/STB
Average viscosity	1.4cp
Initial and boundary conditions	
Initial pressure and datum depth	3000psia at 590ft
Oil water contact depth	500ft
Types of boundary conditions around well sector	*flux*
Well Production control	
Well bottom-hole pressure	14.7psia *"open flow"*

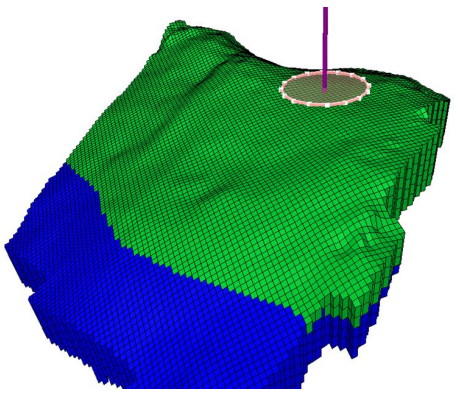

Figure 6.5: Initial fluid distribution in the Teapot Dome model (blue = water, green = oil). Sector Model around the production well is shown. Sector model diameter is 620 m

Fig. 6.6a shows the well production rate against time for Model (a). Although the upscaled permeabilities for Oda's and flow-based methods are very similar (Fig. 6.3 and 6.4), there is a significant variation in the simulated flow rates. Well flow rates for models computed with Oda's method are significantly higher than flow rates computed for models that use flow-based upscaling. This holds when we compare results of the same simulation cell sizes. Fig. 6.6b shows the well production rates against time for Model (b). In all cases we observe less sensitivity to changes in upscaling method and changes in size of the grid-block compared to Model (a). This can be explained by the increased connectivity of the DFN in Model (b).

The ranges of simulated cumulative oil recovery for Model (a) vary from 6.8% to 19.1% during the time of production. For model (b) the range is between 13.4% and 14.7%. Clearly, the choice of DFN upscaling method and grid-block size has a strong impact on oil recovery estimates and therefore should be done with utmost care because it can easily mask the uncertainty in the underlying geological model. The degree of the impact, however, depends on the connectivity of the DFN. Fig. 6.6b shows that flow-based and Oda's methods gave more similar production profiles because of the high connectivity of the DFN, especially with the smaller simulation cell size. In such a case, Oda's method is superior to flow-based methods because of its efficiency. However, it appears to be difficult to assess a priori which upscaling method is more accurate or, indeed, if all upscaling methods and simulation cell sizes yield similar results.

6.3 QUANTITATIVE EVALUATION OF DFN UPSCALING ERRORS

The previous case study clearly shows the need for selecting an adequate upscaling method and simulation cell size before performing reservoir simulation runs, otherwise it will be difficult to distinguish how the results are affected by geological uncertainty and how by DFN upscaling errors. Calibrating the dynamic model against field data (production data, transient well testing data) may hence be challenging because the simulation results is likely affected by both, geological uncertainty and DFN upscaling errors. A first step towards deciphering

(a) Well Production Rate for Model (a) with fracture length 100 m.

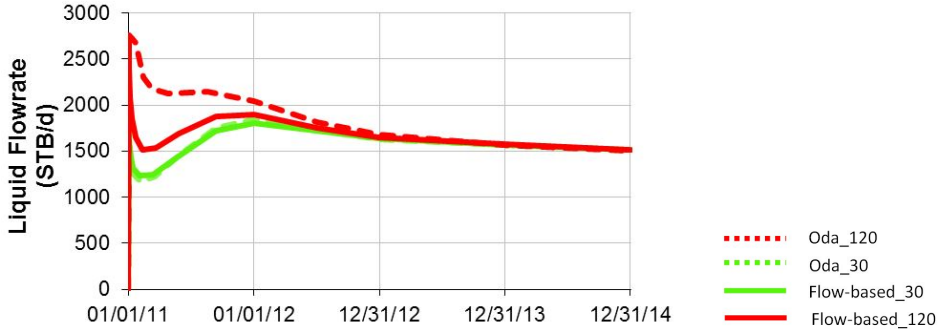

(b) Well Production Rate for Model (b) with fracture length 450 m.

Figure 6.6: Simulation results of the sector scale model

these effects is to quantify the DFN upscaling errors separately prior to full field simulations. Here, a method is presented to quantify the DFN upscaling errors for a sector scale model.

The method is explained in Fig. 6.7. There are two upscaling steps involved: The first is the upscaling of DFN which marks the change from the scale-dependent DFN model to a simulation cell of fixed size. The second upscaling step occurs at the scale of the sector model and computes the average permeability of the entire sector model. This is performed using flow-based upscaling from the simulation cell size at which the DFN upscaling was performed to the sector scale. The second step is necessary in this quantitative evaluation workflow to allow comparison of DFN upscaling with different simulation cell sizes, different upscaling methods and different boundary conditions. The sector scale average permeability is also equivalent to the well test permeability. Well testing represents an important element to understand the behaviour of naturally fractured reservoirs and considered one of strong indicators that fractures exist or do not

exist (e.g. Narr et al., 2006). This links the quantitative evaluation workflow to the actual scale of measurement at which a reference permeability observation may exist. In the reminder of this section, the quantitative evaluation workflow is applied on a realization of the FRACS2000 model, a sector scale model of a fractured onshore reservoir in California (Matthäi et al., 2007).

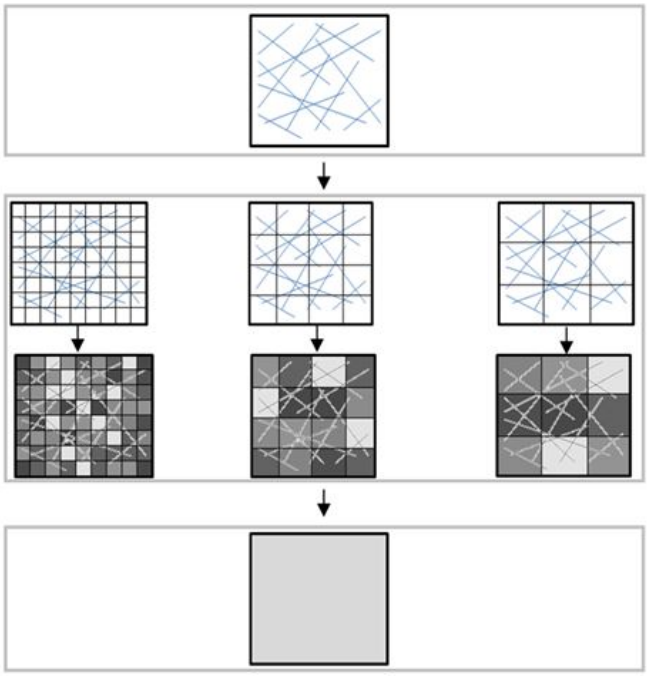

Figure 6.7: A workflow for assessment of DFN upscaling results. Generated DFN models are upscaled to various dynamic models with different grid-block cell sizes using different DFN upscaling methods. The various models are then compared to each other by upscaling to a final target grid block size of the full sector scale.

6.3.1 *Application of the assessment workflow on FRACS2000*

The FRACS2000 model has been used in previous upscaling studies (Matthai et al., 2007, Matthai and Nick, 2009). FRACS2000 is a representation of the San Andreas Formation in an onshore field in California. It comprises a DFN generated based on borehole images and core data. The field exhibits early water breakthrough, a typical production challenge in fractured reservoirs. FRACS2000 is a layer confined DFN comprising two conjugate fracture sets which have similar size distributions (Table. 6.2). The various input parameters used to generate the DFN are given in Fig. 6.8 and Table 6.2. In contrast to models built based on the

Teapot Dome discussed above, the fractures of the FRACS2000 model are just above the percolation threshold and hence less well connected. This may cause additional upscaling challenges to those discussed above. As in the previous example, the Teapot Dome, all simulations are also run in single-porosity model to avoid additional complications that may occur in a dual-porosity model.

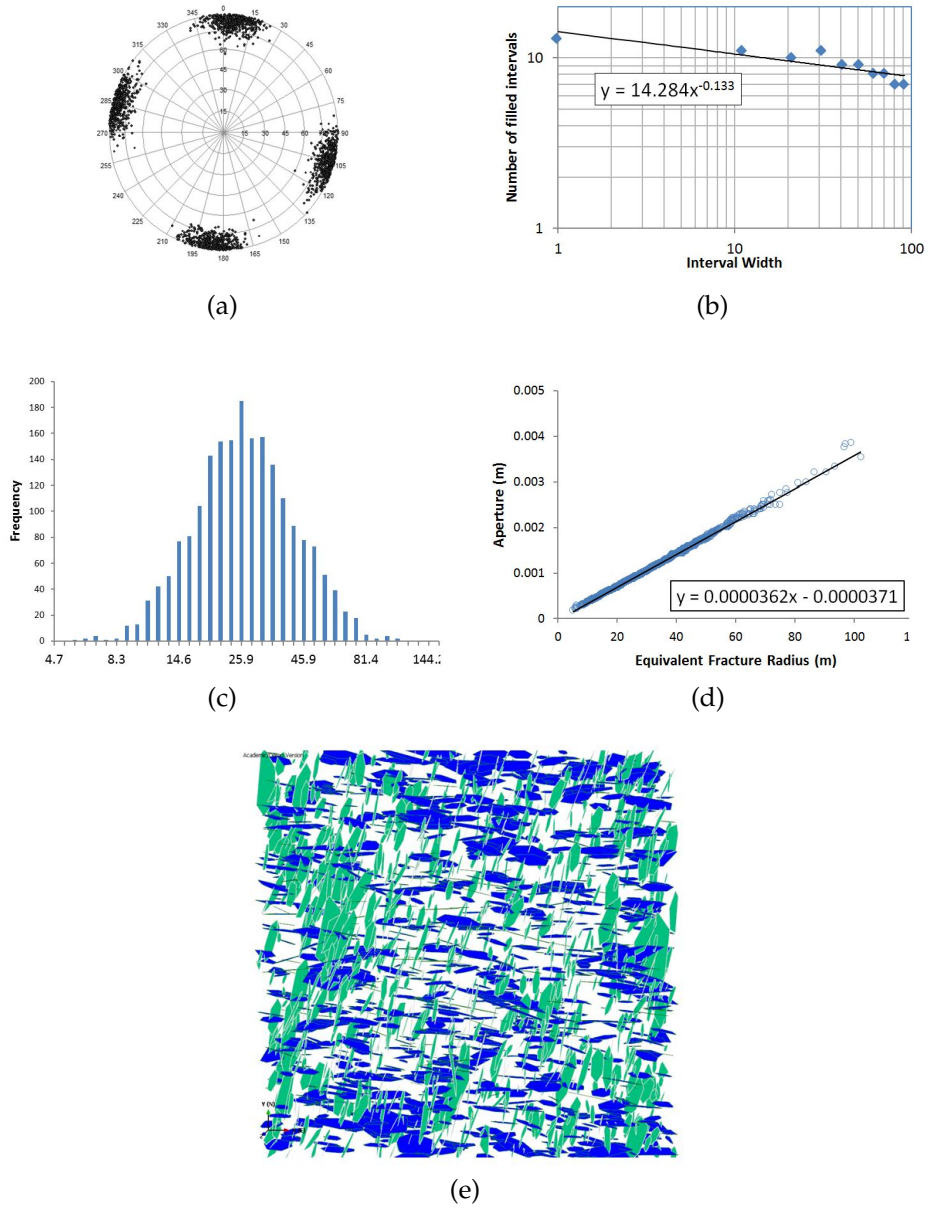

Figure 6.8: Input parameters used to generate the FRACS2000 model. (a) Fracture pole orientation represented by a Schmid diagram (b) Spatial analysis using the box counting technique (carried out with *FRACMAN*); The absolute exponent value is less than 1.0. (c) Fracture size log normal distribution. (d) Fracture aperture is linked to fracture sizes through the relationship shown in the plot. Consequently, fracture aperture must follow a log-normal distribution. (e) Top view of the layer confined FRACS2000 model with fractures represented by hexagonal surfaces. Dimensions are $1000 \times 1000 \times 200$m.

Table 6.2: Fracture statistics of FRACS2000

Fracture set 1	
Number of fractures	1,000
Fracture area/volume (m^2/m^3)	0.0155085
Fracture volume/model volume (fraction)	2.329×10^{-5}
Mean fracture orientation (trend)	285
Mean equivalent radius (m)	28.3
Mean fracture area (m^2)	3202
Fracture set 2	
Number of fractures	1,000
Fracture area/volume (m^2/m^3)	0.015156
Fracture volume/model volume (fraction)	2.19143×10^{-5}
Mean fracture orientation (trend)	182
Mean equivalent radius (m)	28.3
Mean fracture area (m^2)	3031

6.3.2 *Effects of upscaling method and boundary conditions*

The DFN upscaling was evaluated for the following simulation cell sizes: 50×50, 100×100, 200×200, 500×500 and 1000×1000. The latter is the full sector scale. The upscaling methods tested are: Oda's method, a flow-based method with open boundary conditions and a flow-based method with closed boundary conditions. The second upscaling step to calculate the average sector-scale permeability is performed using the flow-based upscaling. The results are shown in Fig. 6.9. They show that Oda's method gives the highest permeability. Except for the flow-based method with closed boundary conditions, the average permeability at the sector scale is dependent on the simulation cell on which the DFN upscaling was evaluated (increasing permeability with cell size). The reason why closed boundary conditions might underestimate overall fracture connectivity was discussed in Chapter 2, Figure 2.8. Overall, the DFN upscaling results vary over approximately three orders of magnitude. This is a significant effect that explains the effect of DFN upscaling on production flow rates estimation in the Teapot Dome Field (Fig. 6.6).

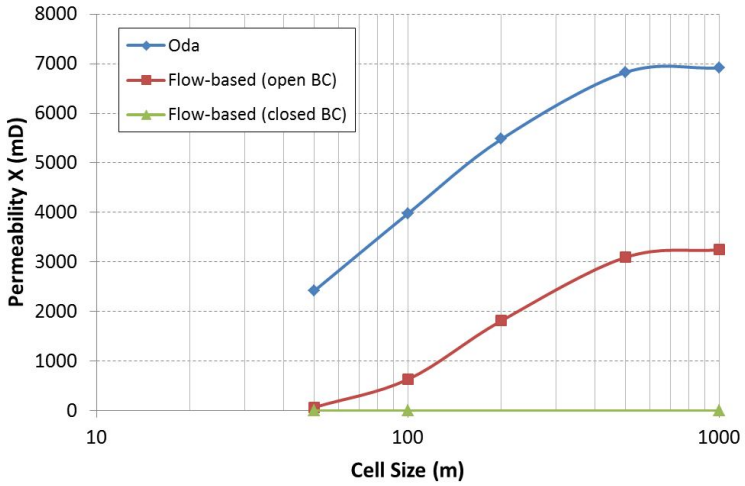

Figure 6.9: Assessment of DFN upscaling results in FRACS2000. Sector-scale permeability in the x-direction is shown to be sensitive to the DFN upscaling method, the boundary condition used and the simulation cell size

To generalise the findings in this work, two equiprobable realisations having the same statistics as FRACS2000 (Fig. 6.8, Table. 6.2) were generated. These are denoted REAL1 and REAL2 in Fig. 6.10. The results show that the scale dependency trend exists for the realisations as for FRACS2000. The figure also draws attention the level of uncertainty associating DFN generation.

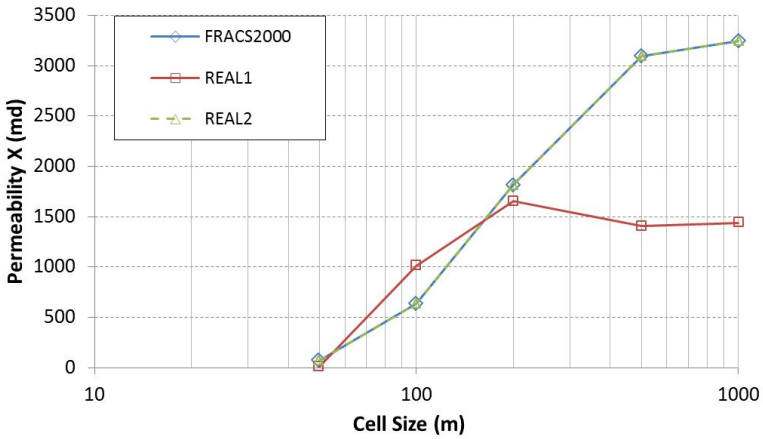

Figure 6.10: Assessment of DFN upscaling results in equi-probable realisation of FRACS2000

6.3.3 *Comparison with DFM upscaling*

It was noted before that DFM models are sometimes used to investigate well testing in fractured porous media. Since DFM models are perceived more accu-

rate than other model types, they may provide a reference solution to use in the workflow to quantify DFN upscaling errors and to improve the reliability of the DFN upscaling process. As we require steady-state single porosity simulation at the sector scale to compute the effective permeability, the CPU time of the DFM flow-based upscaling in this case can be comparable to that of Oda's method.

In the DFM model considered here, fractures are modelled as two-dimensional ellipses, approximating the hexagonal fracture shapes in the original FRACS2000. The upscaling is performed using open boundary conditions and is done for the sector-scale. The results are listed in Table 6.3. If the results are compared with DFN upscaling results in Fig. 6.9, they show that DFN flow-based upscaling with open boundary conditions for a cell size of 70×70 m gives the closest match to the DFM upscaling results. Furthermore, the DFM model can be used to study the sensitivity of the ensemble sector-scale permeability and anisotropy to the permeability of the matrix. The results displayed in Table. 3 show a significant change; especially with vertical-horizontal permeability anisotropy although matrix porosity and permeability are uniform.

Table 6.3: DFM-based sector-scale permeability of FRACS2000

Matrix properties		DFM upscaling results				
$\phi[-]$	$k[mD]$	$k_x[mD]$	$k_y[mD]$	$k_z[mD]$	$k_y/k_x[-]$	$k_z/k_x[-]$
1×10^{-5}	1×10^{-3}	238	57	904	0.23	3.8
0.20	100	1167	222	1428	0.19	1.2

6.4 SUMMARY AND CONCLUSIONS

In this chapter, the DFN upscaling errors were investigated and its impact on reservoir simulation results was evaluated. Generally, DFN upscaling errors were small for well connected fracture networks. In some cases, the DFN upscaling errors can vary over three orders of magnitude depending on the fracture geometry and properties and therefore poses a significant uncertainty that easily masks the geological uncertainty. The results also confirm that Oda's method overestimate equivalent fracture permeability. This overestimation increases with the

simulation cell size. Flow-based upscaling is less sensitive to changes in simulation cell sizes, but it is highly dependent on the boundary conditions.

A quantitative evaluation workflow for DFN upscaling was presented. This workflow satisfies two objectives: (1) it allows studying the sensitivity to simulation cell sizes, DFN upscaling method and the types of boundary conditions on the average sector-scale permeability. By quantifying the upscaling error, we assign ranges to any simulation results obtained. Hence, the workflow allows for uncertainty evaluation due to DFN upscaling errors. (2) In the presence of well test data, the average permeability at the sector scale can be linked to the well test permeability because the well test measurement scale and the reference sector scale are comparable. Therefore, the quantitative evaluation workflow can be used with a reference solution to help in deciding which simulation cell size, upscaling method or boundary conditions are suitable for the area around the well. DFM simulations can be used as reference solutions, especially in reservoirs where matrix permeability can be high (Fig. 6.11).

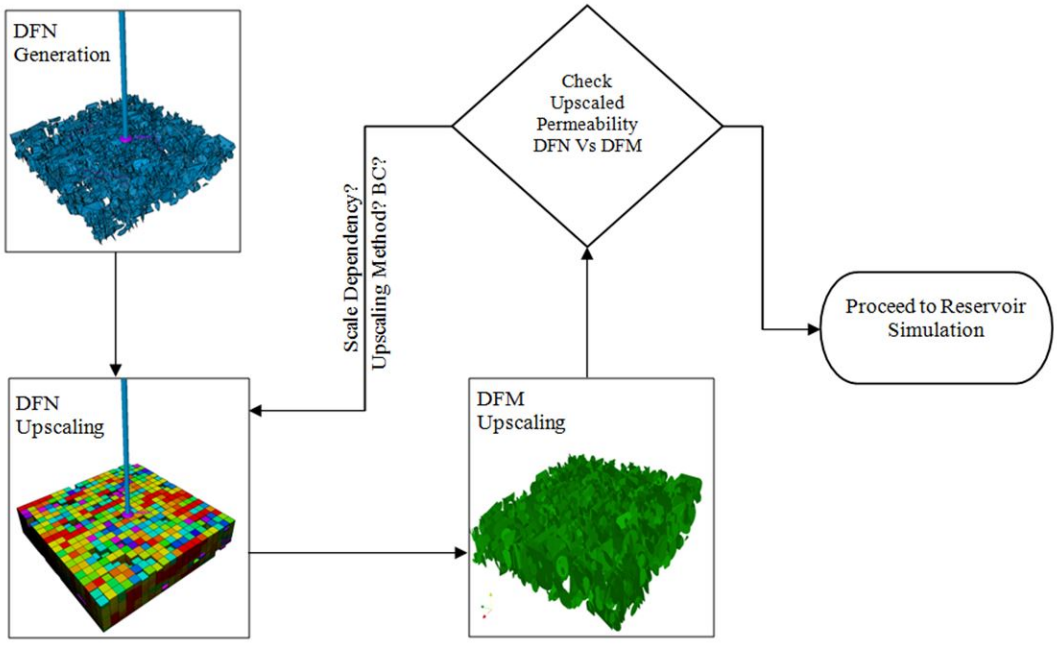

Figure 6.11: DFM-assisted DFN upscaling workflow to minimize upscaling error for fractured reservoirs due to the choice of upscaling method and/or simulation cell size.

In the next chapter, the impact of DFN upscaling errors on the results of history matching real production data is examined for the fractured Tensleep Formation in the Teapot Dome Field.

7

THE EFFECT OF DFN UPSCALING ON HISTORY MATCHING NATURALLY FRACTURED RESERVOIRS

7.1 INTRODUCTION

History matching is recognized as an important step in validation of a reservoir model, and the quality of a history match affects the validity of its future forecast. Since high impact business decisions are usually based on such forecasts, reservoir engineers face two challenges to manage the associated risk. These challenges are: the non-uniqueness of a history-matched model and numerical and/or conceptual modelling errors. The first challenge necessitates the need for a computer assisted history matching that efficiently explores the uncertain parameters space. The second challenge necessitates the need for integrated studies to minimize modelling errors.

Modelling errors include numerical solution errors such as convergence errors and truncation errors (both in space and time). Perhaps more important are the mathematical model errors arising from sub-grid scale phenomena, which have been ignored or modelled improperly at the field scale (Christie et al., 2006, Christie et al., 2005). These are likely to be more pronounced in fractured reservoirs, because the dual porosity model has the simplifying assumptions such as the pseudo steady-state and uniform matrix blocks geometries, sizes and properties (Chapter 2). Both are assumptions that can lead to significant errors in recovery prediction (Chapter 4). Another error source is matrix upscaling, which can already lead to significant errors in unfractured reservoirs (Sablok and Aziz, 2008). Even more concerning are DFN upscaling errors, which can account for more than 12% absolute change in oil recovery and mask geological uncertainty (Chapter 6). One risk of history matching is that the history matching algorithms find a model that yield a good history match but only because the errors discussed above cancel each other. This can be exacerbated by measurement errors,

leading to flawed history matched models with limited value to forecast production (Christie et al., 2005).

In NFR reservoir simulation practice, assisted history matching is often detached from the DFN upscaling process. This is because it is easier to implement assisted history matching using the end-product of the DFN upscaling, i.e. the effective fracture properties. While this can accelerate the assisted history matching workflow, it can lead to increased modelling errors as fracture properties can easily become inconsistent with the original DFN input parameters (e.g. fracture intensity, length, height, and hydraulic aperture) and hence the geological understanding of the NFR. Another problem in this approach is that the DFN upscaling error may lead to a geological prior with the wrong flow properties, which masks the real dynamic behaviour, causing the history matching algorithms to converge to a geologically inconsistent solution.

Previous research on history matching NFR showed the importance of linking the history matching process with the original fracture model properties rather than effective fracture properties. For example, Cui and Kelkar (2005) preserved the consistency between fracture permeability and matrix shape factors i.e. the DFN upscaling outputs by history matching on fracture intensity. Suzuki et al., (2007) approached history matching of NFR by varying elastic stress simulation parameters rather than effective fracture permeabilities to preserve geological and geomechanical consistencies.

In this chapter, the aim is to resolve the history matching challenges described above in an integrated framework for a fractured reservoir. This is achieved through (1) establishing a link between DFN modelling and history matching to preserve geological consistency and (2) reducing modelling errors that occur as a result of DFN upscaling. The chapter starts by an introduction of the Bayesian framework in a computer-assisted history matching workflow to update reservoir models with DFN upscaling results. This is followed by a case study of history matching in a real fractured reservoir. The reservoir model is described in terms of matrix and fracture domains. A comparison is carried out for three DFN upscaling cases for the same DFN. A history match is attempted

for each upscaling case. A comparison of the history matched models is given in the end followed by concluding remarks.

7.2 HISTORY MATCHING OF NFR UNDER THE BAYESIAN FRAMEWORK

Perturbing uncertain reservoir parameters to obtain an automatic history match has been attempted since the 1960s, see Dougherty (1972) or Oliver and Chen (2011) for reviews. In parallel, the notion to constrain parameter range over which values are perturbed, such that they are geologically realistic, exists since then. Gavalas et al., (1976) discussed that additional geological information should be utilized as prior knowledge in a Bayesian framework to achieve geologically consistent history matched models. Recently, in multipoint geostatistics, prior geological knowledge is preserved through training images to arrive at models that not only match the production data, but also the geological architecture of the reservoir (Caers, 2003, Rojas et al., 2012). Similarly, DFN modelling generates fracture models honouring geological data and hence can provide a mean to constrain history matching of reservoir models if properly upscaled.

The Bayesian framework is well used in various uncertainty quantification algorithms (e.g. (Zhang et al., 2005, Christie et al., 2006). It provides an efficient tool to update the probability of a model given some new information, e.g. a mismatch of a given parameter samples.

$$p(m|O) = \frac{p(m)p(O|m)}{p(O)}, \tag{7.1}$$

where $p(m|O)$ represents the posterior probability that is updated once we have obtained more information. The model prior probability, $p(m)$, is represented by individual parameter distributions and the correlation between the distributions. This approach allows us to constrain the model to DFN upscaled properties. $p(O|m)$ is the likelihood of the observation given the model is correct. It is linked to the misfit value between calculated and observed data. The least square method is normally used to evaluate the misfit.

An actual DFN property can impact more than one DFN upscaled property. For example, fracture intensity affects fracture permeability and the matrix block size. The second model of the 6th SPE Comparative Solution project (Firoozabadi and Thomas, 1990) can be used to illustrate how poorly defined prior probabilities can produce history matched models that are geologically inconsistent. A water injection case is considered in a simple cross-sectional dual porosity model (Fig. 7.1) (Model 2 in the original SPE 6th paper). The model comprises three layers, corresponding to three reservoir zones of different fracture properties.

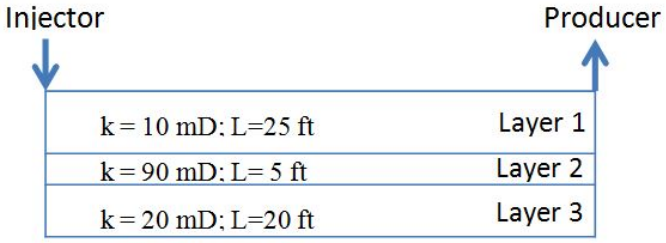

Figure 7.1: A simple cross-sectional model from the 6th SPE Comparative Solution project, described in (Firoozabadi and Thomas, 1990). Each layer represents a fracture zone with different fracture properties. Matrix shape factors are calculated using Kazemi's formula (Kazemi et al., 1976) for identical fracture spacing.

Table 7.1: Fracture properties considered uncertain with corresponding min-max range. The properties are varied to automatically history match SPE 6th Model 2 (Fig. 7.1)

Parameter	Range	Truth case
Fracture permeability (mD), Layer 1	5 – 200	10
Fracture permeability (mD), Layer 2	5 – 200	90
Fracture permeability (mD), Layer 3	5 – 200	20
Matrix block size (ft), Layer 1	1 – 50	25
Matrix block size (ft), Layer 2	1 – 50	5
Matrix block size (ft), Layer 3	1 – 50	10

The uncertain parameters and their min-max ranges that can be altered in the history matching process are shown in Table. 7.1. 500 cases are run to automatically history match the observed data using the Particle Swarm Optimization algorithm (Mohamed et al., 2010, Hajizadeh et al., 2011). Results from the history matching show that sampled parameter values cover a wide range of the initial parameter space (Fig. 7.2). Some clustering can be observed where parameter

combinations give minimal misfit values. The history match quality is reasonable (Fig. 7.3). However, parameter match is poor, particularly for layer 2 and layer 3 parameters. This is not only due to history matching errors as discussed in Tavassoli et al. (2004), but also due to the fact that prior information on the correlation between the parameters is missing, resulting in non-realistic parameter combinations. As can be seen Fig. 7.3, in the future forecast the oil production was overestimated.

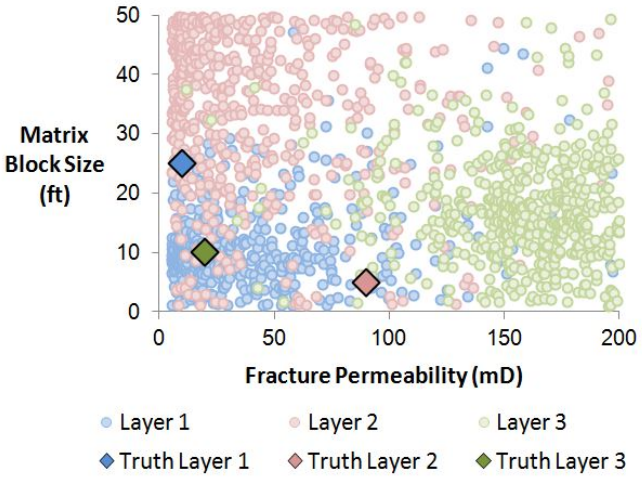

Figure 7.2: Parameter match for SPE 6th Model 2. 500 parameter values were sampled by an automatic history matching algorithm. The coloured circles represent the various layers. The coloured diamonds represent the truth case for the three layers of the second model in 6th SPE Comparative Solution project.

Geological information on cross-correlation between the fracture properties can be available from outcrop data, or image logs. DFN models are normally generated based on these observation data. Hence, in principle DFN upscaling will produce geologically consistent properties to use for reservoir simulation. This is superior to an approach where fracture properties are changed heuristically to history match the production data. If more information is available from a representative DFN model of the SPE 6th model, the fracture properties can be cross-correlated as shown in Fig. 7.4a and the prior probability can be updated accordingly. The result is an improved parameter match (Fig. 7.4b) and an improved history match (Fig. 7.5).

The results for this idealized example show that a wide range of parameter combinations, which all yield a reasonable history match, are possible but they do lead to different forecasts. It is hence important to avoid the non-realistic

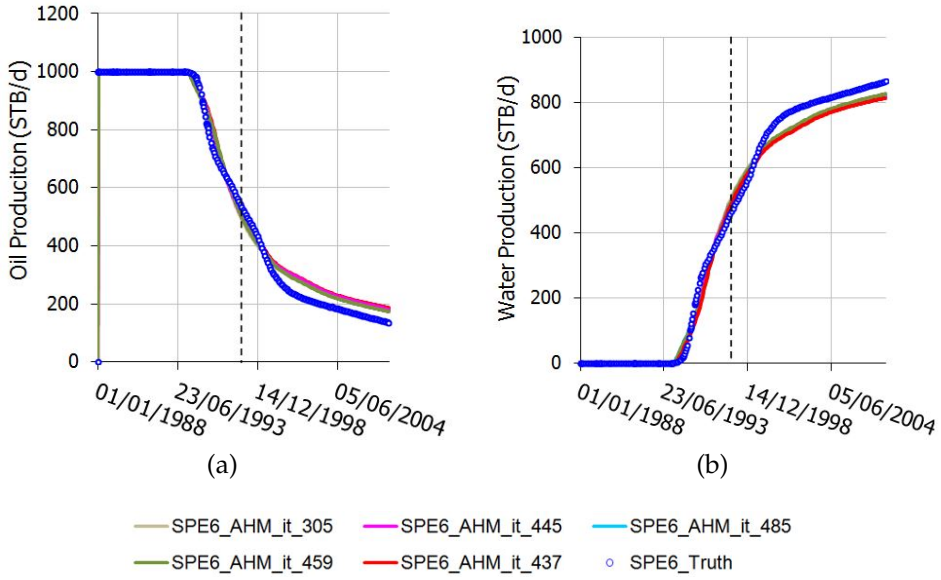

Figure 7.3: History matching results of the SPE 6th Model 2. Results are shown for the best five automatically history matched cases. The dashed vertical line separates between history matching and forecasting

combinations of sampled parameter values by manipulating the original DFN properties, e.g. fracture intensity, and calculate fracture block properties, e.g. permeability and matrix shape factors, rather than modifying the upscaled properties of the DFN directly. However, there may be distinct trends which allow us to link fracture properties with fracture block properties such that when an effective parameter is changed, one can ensure that the geological model is not violated. In other words, history matching can only change parameters such that geological trends/correlations are honoured and if parameter combinations are found outside this trend/correlation they are automatically rejected.

7.3 A HISTORY MATCHING CASE STUDY

The Tensleep Formation in the Teapot Dome Field provides an excellent example to study NFRs. Most of the field dataset is now in the public domain and is facilitated by the Rocky Mountain Oilfield Testing Center (RMOTC). The field is located in Wyoming (Fig. 7.6), U.S.A. It is an elongated North-South trending anticline located in the Southwest edge of the Powder River Basin (Cooper et al., 2006, Chiaramonte et al., 2008, Schwartz, 2006, Smith, 2008). Fracture data are

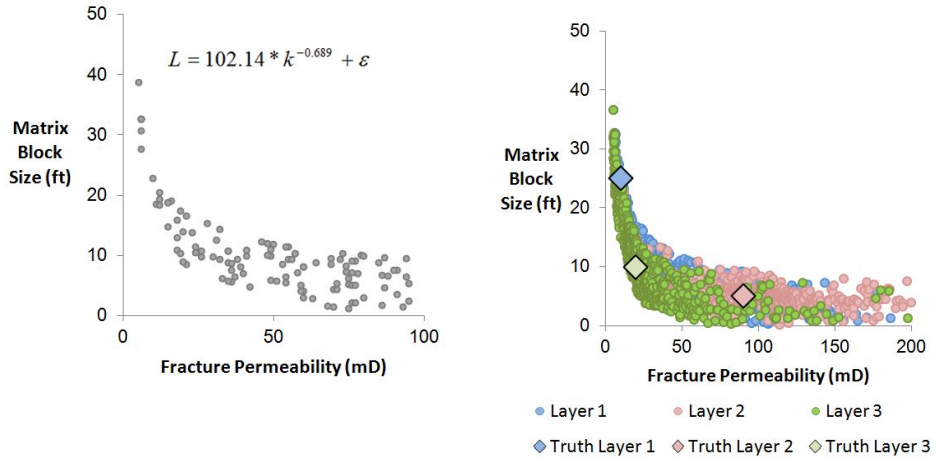

(a) (b)

Figure 7.4: Parameter match of the SPE 6th Model 2 after adding a geological prior. (a) A correlation between matrix block size, L, and fracture permeability, k, is constructed. ε is a dispersion parameter added for more flexibility in the correlation. This is assumed to have come from outcrop data or a representative DFN model. (b) 500 parameter values sampled by an automatic history matching algorithm incorporating the new correlation.

reasonably abundant ranging from outcrop and seismic data to borehole images. The production data show very steep water-breakthrough profiles, which is one characteristic for NFR comprising a well-connected fracture network. The field is supported by a strong artesian aquifer and despite the fact that oil production started in 1959, the formation pressure is maintained and has not declined. This is another indication of the connectivity of fractures in the Tensleep Formation.

The Tensleep Formation is one of several producing intervals in the Teapot Dome Field. It consists of Aeolian sandstone interbedded with tight, and relatively thin, dolomite layers. The average total thickness of the formation is 200 feet. The main members of the Tensleep formation are (from top to bottom): A Sandstone, B Dolomite, B Sandstone, C Dolomite and C Sandstone layers. The Tensleep Formation contains oil in Section 10 of the Field (Fig. 7.6) and hence is the focus of this work. Seismic interpretation provided the structural framework of the field which has been confirmed by well-tops from 18 wells. 15 well logs were used to correlate the sandstone and dolomite units across the area of interest, and were interpreted to evaluate the matrix rock properties: porosity and initial water saturation. Five petrophysical rock types were identified in cored intervals using the concept of hydraulic units (Amaefule et al., 1993). Core data

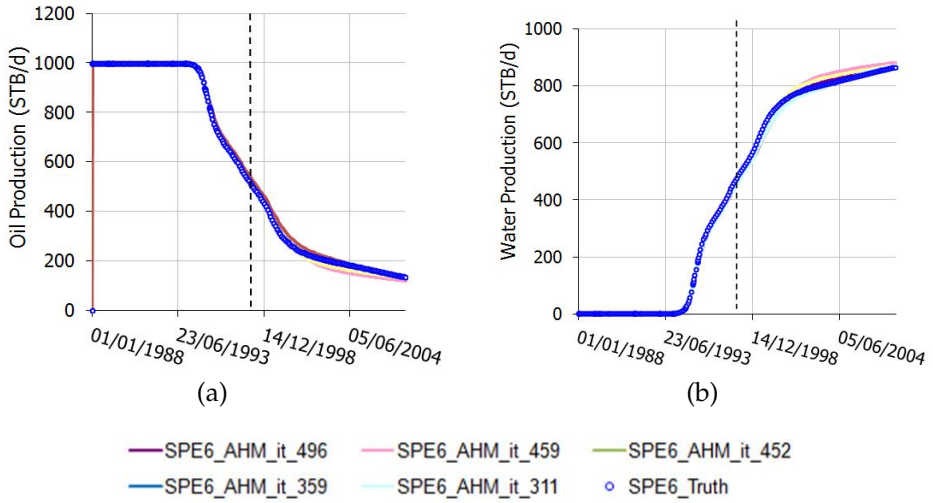

Figure 7.5: History matching results of the SPE 6th Model 2 after adding a geological prior. Results are shown for the best five automatically history matched cases. The dashed vertical line separates between history matching and forecasting

also provided plug measurements of the matrix permeability (Fig. 7.7a). Neural networks were trained in the core intervals and used to predict rock facies from well logs in uncored intervals. Fluid properties and relative permeability data are taken from (Garcia, 2005).

A fine grid (static) model was constructed with cell size of $50\times50\times1$ ft. Following analysis of well log data (Fig. 7.7b), the static model was populated with rock facies and porosity properties using the Sequential Indicator Simulation and Sequential Gaussian Simulation methods, respectively. Log-derived J-functions allowed reasonably accurate prediction of initial water saturation distribution (Fig. 7.7c). This increased the confidence in facies property predicted by the neural networks. The static model was then upscaled to a dynamic model with average cell size of $100\times100\times5$ ft. Streamline simulations were used for qualitative comparisons between static and dynamic models. The streamline shapes were very similar in the static and dynamic models.

Cooper et al. (2006) mapped fractures exposed in outcrops at the southern edges of the Teapot Dome. They found three fracture sets: parallel, perpendicular and oblique to the fold hinge. Schwartz (2006) analyzed image log interpretations and provided valuable subsurface information about the strike, dip and aperture of the open fractures of the Tensleep. The dominant fractures are per-

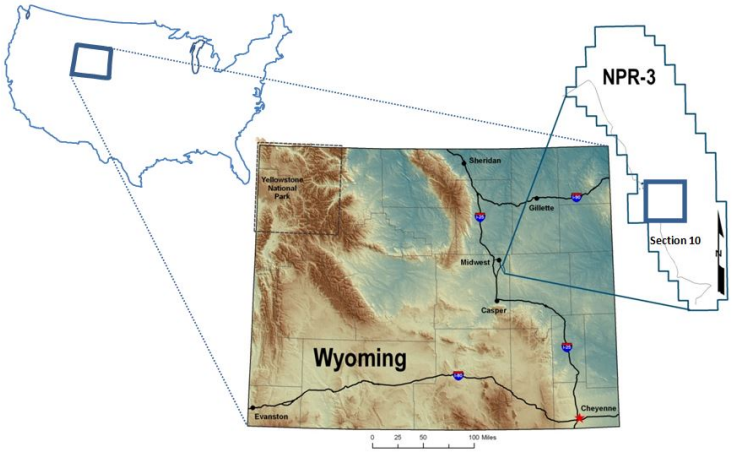

Figure 7.6: Location of the Teapot Dome field, formerly known as Naval Petroleum Reserve-3 (NPR-3). Map was modified from the Rocky Mountain Oilfield Testing Center.

pendicular to the hinge strike, which has a local NE trend in the study area (Fig. 7.8a). Two fracture drivers were considered in our model: proximity to faults and curvature of the fold surface. Cooper et al. (2006) noticed an increase in fracture intensity close to faults. Two faults are present in this model (Fig. 7.8b), a major NE striking fault and a minor NW striking fault. Fold controlled fracture intensity increases with curvature of layers.

Fracture length is not possible to be inferred from image logs. Hence, Schwartz estimated fracture lengths from aperture-length relationships. He reported fracture lengths in the range from 1.5 to 90 ft [0.47 to 27.42 m]. Cooper et al. (2006) however, reported much longer fractures of more than 330 ft [100 m]. In the present model, there are multiple layers with various thicknesses. Hence, a fixed aspect ratio derived from outcrop data is used here to model fracture length as a function of bed thickness (Smith 2008).

One of the uncertainties during DFN modelling is to convert the fracture count data from wells to fracture intensity property that can be used in 3D modelling. Fracture intensity and orientation are directly related to the DFN connectivity (Fig. 7.9). Hence this is a major uncertainty in DFN modelling. The following DFN drivers and parameters were considered when predicting fracture intensity: The damaged zone width, various combinations of fault and fold influences and intensity multipliers of the producing layers A, B and C sandstones along with

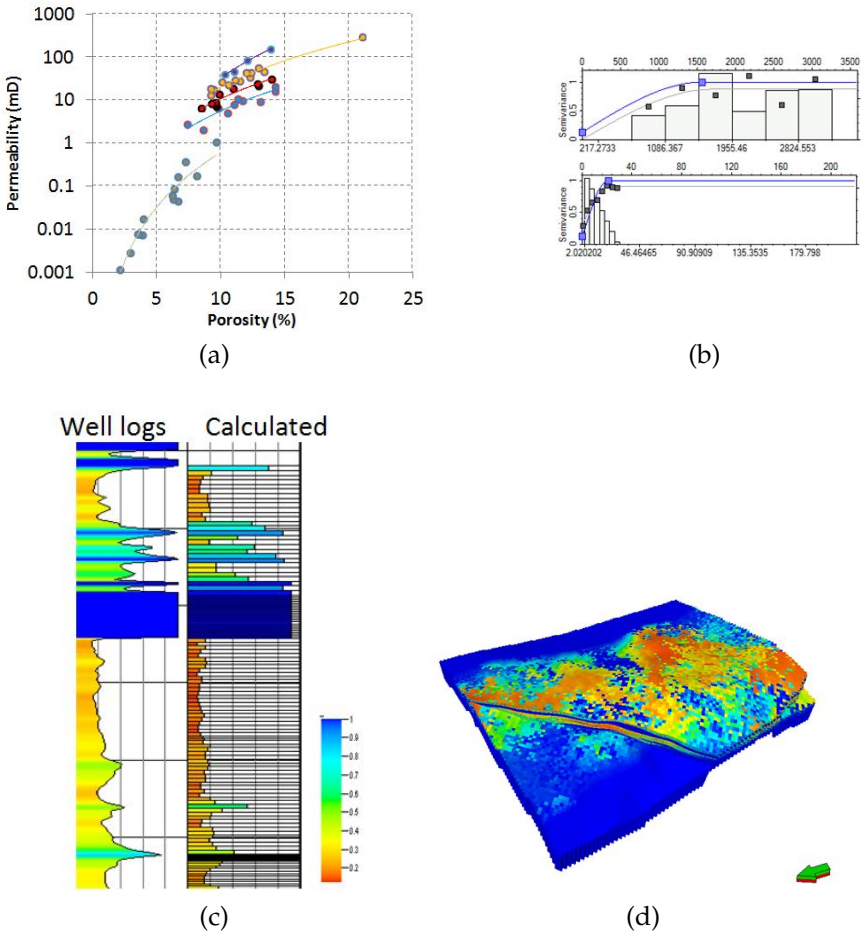

Figure 7.7: Characterisation of matrix properties of the Tensleep Formation, the Teapot Dome Field. (a) Permeability prediction from core data. Five petrophysical groups were identified. (b) Example of well log data analysis to generate horizontal (upper) and vertical (lower) variograms. (c) Comparison of calculated water saturation with well log interpretations of an uncored interval in well 56-TPX-10. (d) water saturation property populated in the static model.

the dolomite layers. All multipliers are derived from well fracture counts, i.e. corresponding to one dimensional fracture intensity (P_{10}).

As discussed in Chapter 6, three factors affect the DFN upscaling outcome. These are: (1) the simulation cell size, (2) the DFN upscaling method and (3) the boundary conditions used in the upscaling. A sector-scale model of 100×100 m was sampled from the DFN of the Tensleep Formation for the purpose of DFN upscaling errors quantification. The quantification workflow presented in Chapter 6 was used to investigate the effect of the three factors above. Results are shown in Fig. 7.10. The values cover a wide range, spanning over three orders of magnitude. Clearly, this is a first order uncertainty which will influence fluid flow and recovery prediction. The variability of the permeability value reflects

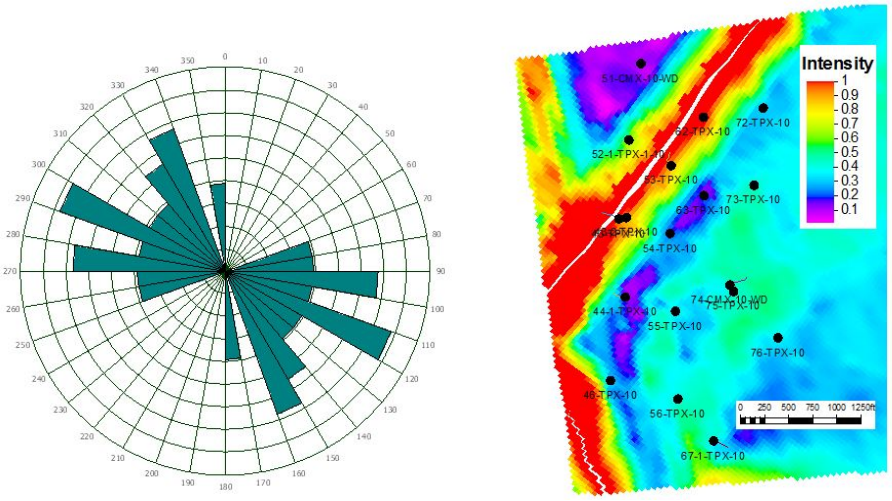

(a) (b)

Figure 7.8: Characterisation of fracture properties of the Tensleep Formation, the Teapot Dome Field. (a) Rose diagram showing the strike of fractures in sandstone layers based on image logs from well 67-1-TPX-10. (b) Combination of fault and fold related fracture intensity. The map also shows the location of the oil production wells targeting the Tensleep Formation.

the amount of modelling errors that can be introduced through DFN upscaling approach. To evaluate the effect of DFN upscaling errors on history matching of NFR, we consider three DFN upscaling cases:

1. Oda's method with a cell size of $100 \times 100\mathrm{ft}(33 \times 33\mathrm{m})$
2. Improved Oda's method with a cell size of $100 \times 100\mathrm{ft}(33 \times 33\mathrm{m})$
3. Improved Oda's method with a cell size of $200 \times 200\mathrm{ft}(33 \times 66\mathrm{m})$

Flow-based upscaling methods were intractable for the full field model. Hence, only analytical upscaling methods were tested. In all three cases, the vertical cell dimension was kept constant. The evaluation of different upscaling methods (cases 1 and 2) is straight forward, however to evaluate two cases with different cell sizes (cases 2 and 3) the results of higher resolution is downscaled to the smaller resolution to neuteralise numerical dispersion effects when comparing the history matching results (Fig. 7.11).

The field was divided into four regions based on the fracture intensity driver values (Fig. 7.12). Each region was assigned different multipliers for the properties shown in Table. 7.2. Hence, prior knowledge contains the hydraulic behaviour as determined by the DFN itself and the DFN upscaling process. In

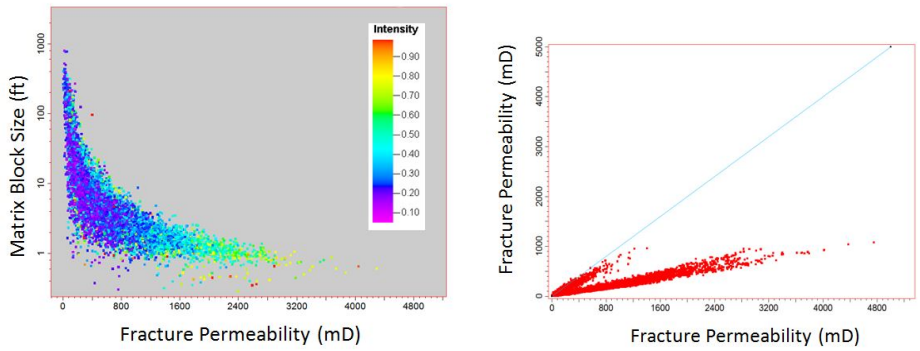

(a) (b)

Figure 7.9: Fracture properties estimated based on a DFN of the Tensleep Formation, the Teapot Dome Field. (a) Matrix block size versus fracture permeability and fracture intensity. (b) Fracture permeability tensor (Y=perpendicular to main fracture strike, X=parallel to main fracture strike)

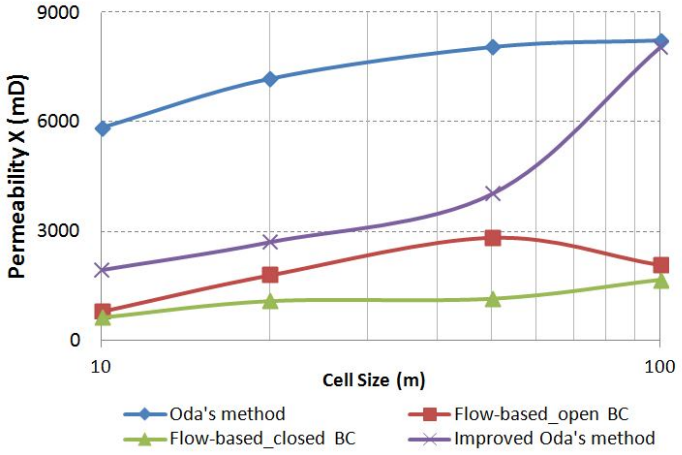

Figure 7.10: Equivalent fracture permeability in a sector of the Tensleep Formation as a function of simulation cell sizes, boundary conditions and the DFN upscaling method.

total, 16 parameters were considered uncertain. History matching is based on liquid production.

To compare the history matching results from the three DFN upscaling cases discussed above, the oil and water production rates for well with different history matching quality (Fig. 7.13 and 7.14). Wells that show good agreement for the oil production rate and simulated production rates do this for all DFN upscaling methods and cell sizes. Likewise, wells that show poor agreement for observed and simulated production do this regardless of the DFN upscaling and cell size (Fig. 7.13). The observed and calculated water production rates are in excellent agreement for all the wells (Fig. 7.14).

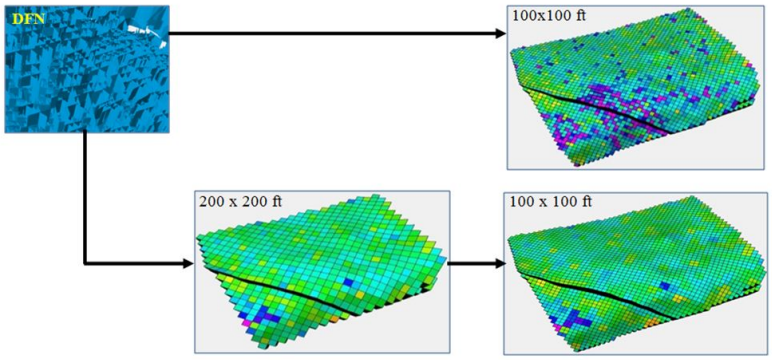

Figure 7.11: A workflow to compare DFN upscaling for various cell sizes

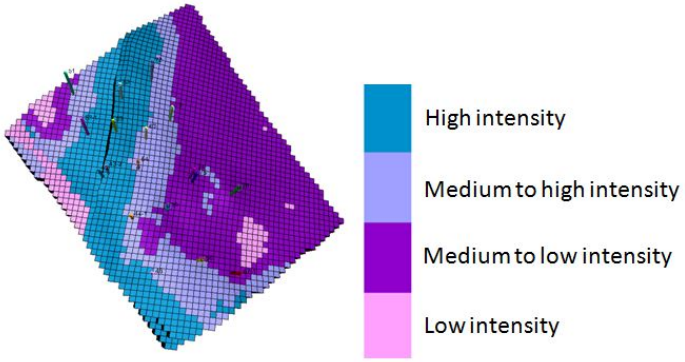

Figure 7.12: Prameterisation of fracture properties using areas of similar fracture intensity

Although there are slight differences in simulated oil production data for the three different DFN upscaling approaches (Fig. 7.13), the quality of the history match is comparable in the three DFN upscaling cases. The well with the worst history matching results, Well 44-1-TpX-10 shown in the last raw of Fig. 7.13, was close to the fault and lacked well logging data. It is suspected that with some additional work it is possible to obtain better matches for those wells that display poor agreement between simulated and observed oil production rates. This first round of history matching results may lead to refine the history matching parameters and ranges to improve the history matching quality. Hence, it is likely that in the end the three DFN upscaling cases will have very similar history matching qualities.

However, the resulting history matched fracture permeability fields vary tremendously depending on which of the three DFN upscaling methods was chosen (Fig. 7.15). This implies that although the DFN upscaling error can be "corrected"

Table 7.2: History matching parameters and their respective multiplier ranges used to history match the Tensleep Formation, the Teapot Dome Field

Property	Multiplier
Fracture permeability X	$0.01 - 100$
Fracture permeability Y	$0.01 - 100$
Fracture permeability Z	$0.01 - 100$
Matrix block size	$0.001 - 100$

during the history matching process and models with a reasonable quality for the history match can be obtained. However, these models vary fundamentally and it is doubtful which of the final models is closest to the truth. Hence it is doubtful which model should be taken forward to forecast future production, if any at all. This dramatically exemplifies how crucial proper DFN upscaling is. Not only can wrong upscaling mask any geological uncertainty (Chapter 6), it can also lead to history matched models with vastly different properties, all giving reasonably adequate history matches but likely being of little use for making reliable production forecast. Hence the common reservoir engineering notion that "a fractured reservoir model is adequate if a good history match can be achieved" should be followed with great caution.

7.4 DISCUSSION

As noted in the introductory chapters, DFN models integrate fracture related data from outcrop analogues, image logs, seismic interpretation and dynamic well testing. Hence, DFN modelling increases the accuracy of NFR simulation results by relating the fracture properties to the geological description of the fractures. An idealised history matching workflow is shown in Fig. 7.16, where the history matching parameters are not the fracture permeabilities used in reservoir simulation. Rather, the history matching parameters are geological parameters such as fracture orientation, apertures, intensity, etc. In this *"big loop"* history matching is it assumed that static model upscaling and DFN upscaling can be performed with high degree of accuracy. It is also assumed that modelling errors

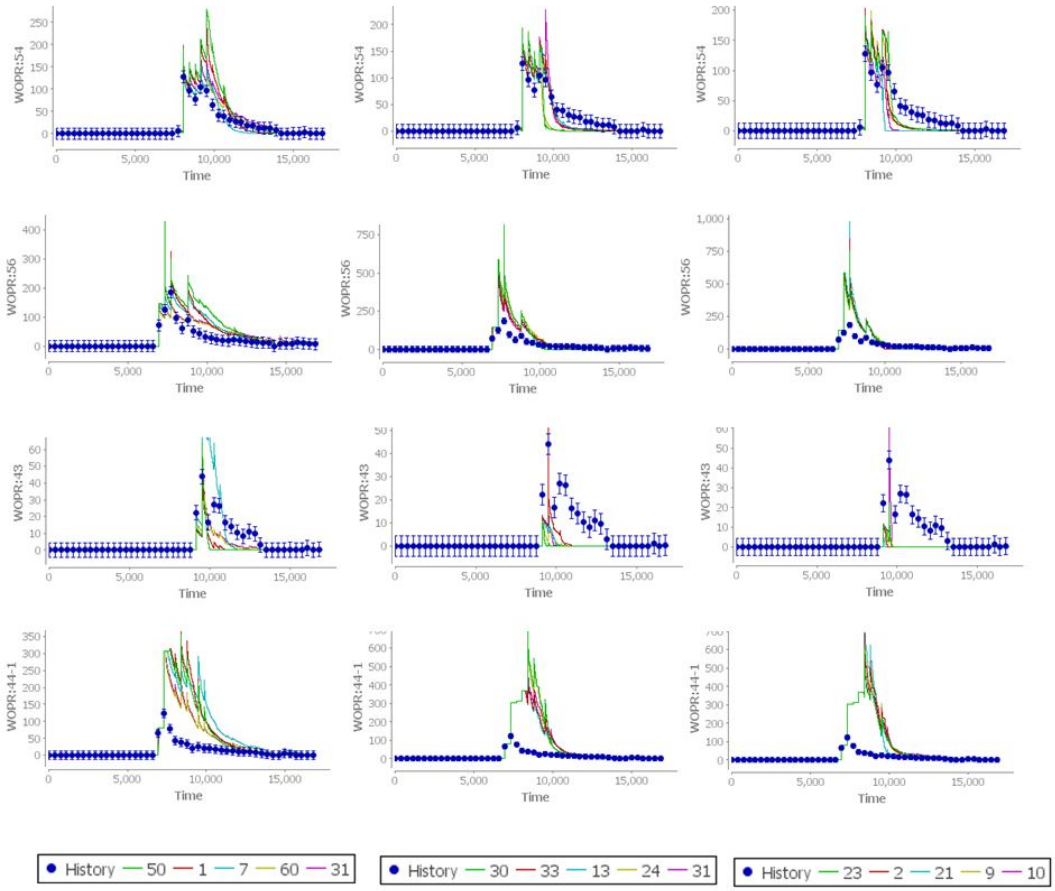

Figure 7.13: Comparison of history matching results: Well Oil Production Rate (WOPR), for the three different cases: Oda's method 100×100 ft, Improved Oda's method 100×100 ft and Improved Oda's method 200×200 ft (left to right)

are minimal. Such an idealised history matching workflow is exhaustive but its implementation is not realistic due to modelling and resources limitations.

On the other hand, given the high uncertainty that normally associates NFR, the DFN upscaling errors, and CPU time limitation; reservoir engineers may decide to apply history matching by simply perturbing the fracture properties in the dynamic model until the results fit the observed production data, represented by the dotted arrow in Fig. 7.16. This *"short loop"* history matching is computationally cheap but the prediction ability of the models is questionable. The challenge therefore is how to combine the advantages of both the big loop and the short loop approaches by focusing on geological realism, reduced upscaling errors and efficiency of the history matching workflow.

One approach that guarantees improved geological realism is by incorporating the geological modelling tool as part of the history matching process. For exam-

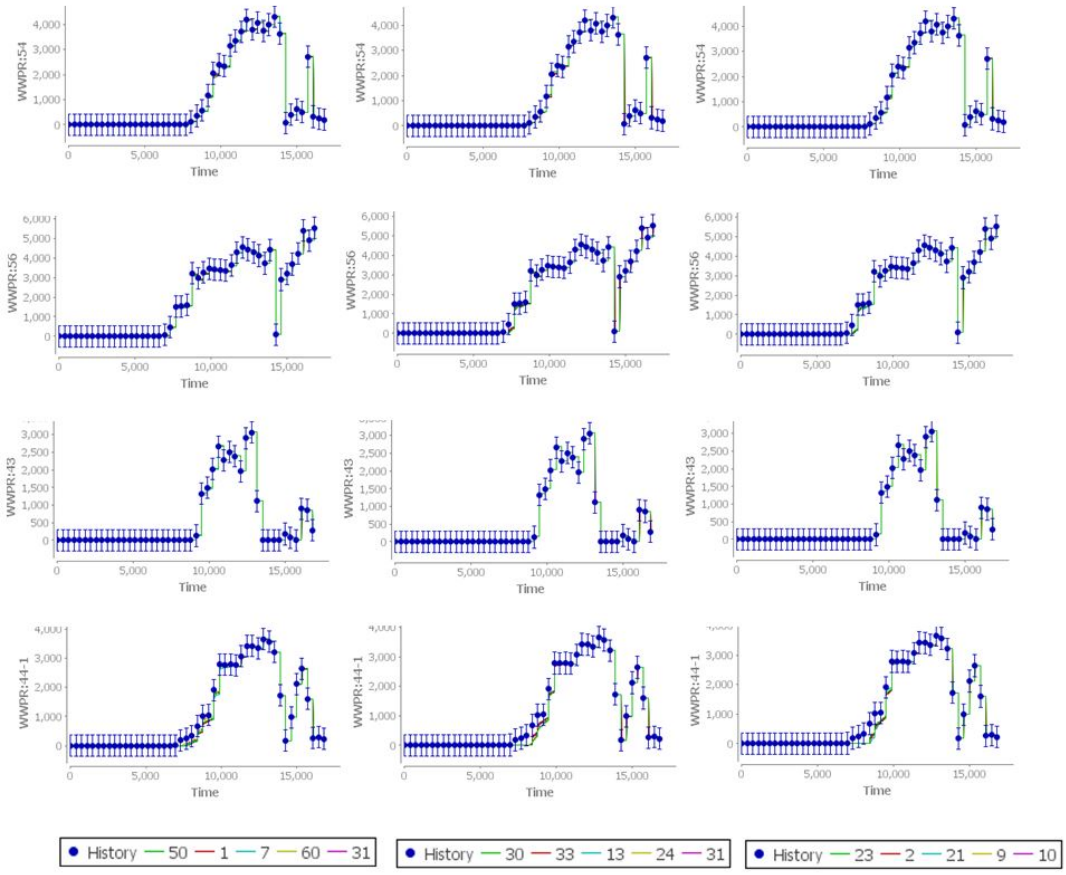

Figure 7.14: Comparison of history matching results: Well water Production Rate (WWPR), for the three different cases: Oda's method 100×100 ft, Improved Oda's method 100×100 ft and Improved Oda's method 200×200 ft (left to right)

ple, the incorporation of training images to update the model prior knowledge during history matching (Caers, 2003; Rojas et al, 2012) produces geologically consistent history matched models, similarly for fractured reservoirs, the work of Cui and Kelkar (2005) and Suzuki et al., (2007). The synthetic history matching case based on the SPE 6th comparative solution project showed that investing in geological consistency by introducing cross-correlations between the history matching parameters improved the quality of the history match.

DFN upscaling is usually performed once using the available method and to the simulation cell size that best suits the CPU capacity. The Tensleep Formation history matching results show that different DFN upscaling cases gave different permeability fields, even though the history matching quality was comparable. This exemplifies the need for more work to accurately quantify the upscaling errors of DFN and their impact on history matching and production forecasting

in NFR. The least that is possible to do is to study the sensitivity of the history matching results to the DFN upscaling method. This can be done simply by repeating the history matching workflow starting from fracture properties evaluated using different DFN upscaling methods and simulation cell sizes. Subsequently, even if it is not possible to quantify the upscaling errors accurately, this exercise gives a sense for the uncertainty arising as a result of the DFN upscaling errors.

7.5 SUMMARY AND CONCLUSION

In this chapter, the effect of DFN upscaling on history matching of a real fractured reservoir was tested. The evaluation of the DFN upscaling effect is performed by history matching three models which contained different fracture properties. The difference of fracture properties was due to the DFN upscaling method used only. It was shown that the history matching quality for the three models was comparable. However, the permeability distribution in the three models was different which means that the forecast of these models will be different as well. The results call for paying more attention to the DFN upscaling step and show the importance of quantifying the upscaling errors.

Due to the high uncertainty accompanying DFN modelling and upscaling, history matching is often mistakenly thought of as a way to correct for the lack of knowledge and upscaling errors. The results in this chapter show the non-uniqueness of the history matching results. To increase the confidence in the history matching workflow; the history matched models must be consistent with the geological concepts.

As the DFN upscaling results are dependent on the simulation cell size, the upscaling method and boundary conditions used, the next chapter presents a workflow to facilitate selecting these three factors for fracture permeability upscaling based the available reservoir engineering data. It also contains an improved shape factor upscaling methodology that feeds in the multi-rate dual porosity models and therefore enables capturing sub-cell geometrical heterogeneities.

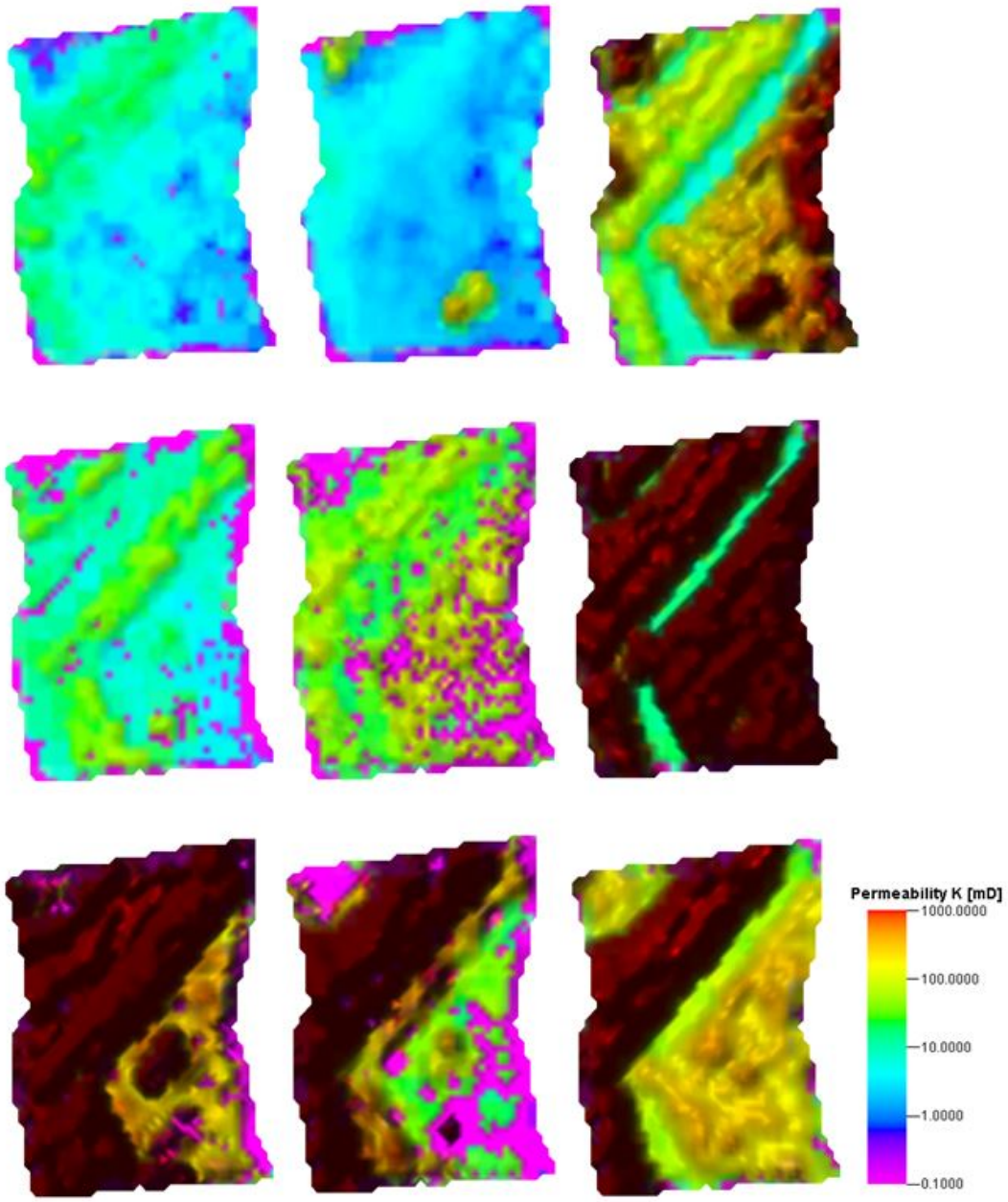

Figure 7.15: Comparison of fracture permeability distribution in the three history matched models. permeability distributions (in X, Y and Z direction from left to right) for the best three history matched cases for the three cases: Oda's method 100×100ft (top), Improved Oda's method 100×100 ft (mid) and Improved Oda's method 200×200 ft (bottom).

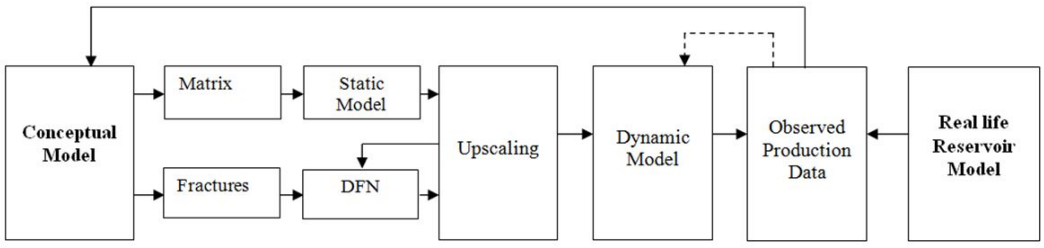

Figure 7.16: An idealised reservoir simulation and history matching workflow for NFR.

8

IMPROVED DFN UPSCALING

8.1 INTRODUCTION

In Chapter 6, the impact of DFN upscaling has been assessed for a number of case studies. The case studies showed that the effect of DFN upscaling on simulated recovery prediction may result in 12% absolute change in recovery. This difference is only due to the choices made when the DFN was upscaled. A workflow to quantify the DFN upscaling errors was presented. It was showen in Chapter 7 that the upscaling error cannot be corrected by history matching the field production data because of the non-uniqueness of the history matched models.

The reason for DFN upscaling errors is twofold. First, analytical DFN upscaling involves simplifying assumptions. Second, the DFN upscaling assumes a representative elementary volume (REV) such that fractures can be considered as an equivalent porous medium. Many formations follow scaling patterns and hence an REV is not present (Odling, 1997, Bonnet et al., 2001, Berkowitz, 2002, Neuman and Di Federico, 2003, Neuman, 2005).

It was discussed in Part I of this thesis that matrix block sizes are heterogeneous and seldom uniform at the scale of a typical simulation cell (Fig. 8.1). Therefore, only results from a multi-rate dual porosity (MRDP) model were able to match fine grid simulations of matrix-fracture transfer in a model that had non-uniform matrix block sizes 5.5. The characterisation of the MRDP model was possible because fracture geometry in the intermediate-scale model was ideal and the shape factors could be calculated easily. However, in reality, fractures are much more complex and shape factors cannot be calculated straightforwardly.

The aim of this chapter is to address two questions. (1) How should DFN upscaling be approached when there is no REV and the flow-based methods are intractable? (2) How would a MRDP model be characterised for realistic fracture

geometries? To answer the first question, a workflow is presented to facilitate the selection of the DFN upscaling method, boundary conditions and the simulation cell size based on the available reservoir engineering data. The workflow builds on the DFN upscaling assessment methodology presented in Chapter 6. As for the second question, an improved shape factor upscaling method is presented that allows us to characterise fracture spacings and shape factors for MRDP models based on DFN geometries. The utility of the new upscaling method is demonstrated based on the fracture distribution shown in Fig. 8.1.

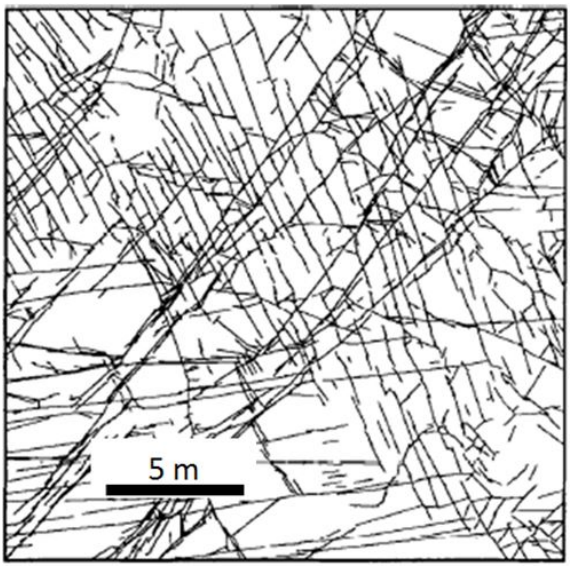

Figure 8.1: Top-view of fractures mapped from an outcrop of the Hornelen Basin in Norway. Note the variability of matrix block sizes at scales less than the size of a typical simulation cell.

8.2 IMPROVED DFN PERMEABILITY UPSCALING

As noted before, the factors that affect DFN upscaling results are (1) simulation cell size, (2) DFN upscaling method and (3) boundary conditions. Additionally, the options to select these factors are very limited. For example, the simulation cell size is usually limited by the CPU time. Flow-based DFN upscaling methods are intractable for full field DFN upscaling. Hence, analytical methods are widely used because of their efficiency. Sensitivity of the upscaling results to these factors is the first step towards improving the DFN permeability upscaling.

When fractures are well connected (e.g. Jackson et al., 2000; Botros et al., 2008; Müller et al., 2010), the DFN upscaling is not sensetive to the simulation cell size as long as it is higher than the REV. In the case study presented in Chapter 6, the DFN with higher connectivity was less sensitive to changes in the simulation cell size (compare Fig. 6.6a to 6.6b. Thus, it appreas that the sensitivity of the DFN upscaling results to the simulation cell size is mainly related to the absence or presence of the REV. Long et al. (1982) studied the factors that affect the fracture connectivity, and hence contribute to the presence of the REV. These factors can be summarised as follows:

1. Fracture density: Increased fracture density leads to increased connectivity.

2. Hydraulic aperture: When all the fractures contribute to fluid flow, the overall connectivity increases. However, aperture distribution often follow a log-normal distribution and some fractures have very high aperture values while others have low values. This increases the anisotropy of the permeability field and lead to reduced likelihood that fractures can be treated as a porous medium.

3. Fracture orientation: If the fracture orientation is variable, there is less anisotropy in the fracture network. Conversely, if the fractures are oriented in one direction, the fluid flow is concentrated in that direction and the anisotropy is high. Hence, the wide distribution of fracture orientation contribute to the existence of a REV.

4. Sample size: The sample size is analogous to the simulation cell size. It is the size at which the fracture conductivity is examined. It was found that the larger that size is, the more likely it is to represent fracture connectivity. In other words, it is more likely to capture a REV if the sample size is large.

The DFN upscaling results should at least match the connectivity observations from the well data. These observations usually come from well data including production/injection flow rates and bottom hole pressures. If the reservoir contains a number of wells, each well will drain and influence a region depending on its production/injection rate, the matrix properties and fracture properties. In

fields with multiple production/injection wells, the pressure perturbation distribution is such that it is numerically equivalent to closed boundaries between the wells (e.g. Lee, 1982). The boundaries between the drainage areas may be open to flow. The flow could be natural such as from an aquifer or gas cap. In the case of an injector-produce pair, the boundaries are also open. When the boundaries are not natural, they are referred to as imaginary. The closed boundaries could also be natural, such as in the case of a sealing fault or a stratigraphic barrier, or imaginary boundaries in the cases of producer-producer or injector-injector pairs. This is illustrated in Fig. 8.2 by using streamlines that define the flow paths.

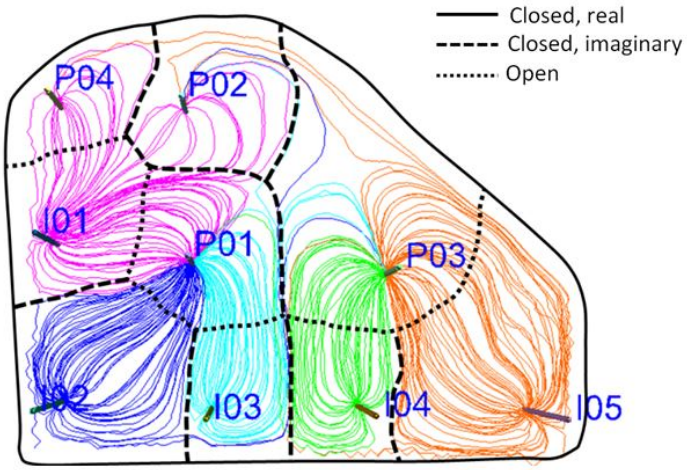

Figure 8.2: An example of establishing sector regions in a field with multiple injection and production wells. The colours of streamlines represent the source injection well.

The sector scale defined above is the most reasonable scale at which the DFN upscaling should be evaluated because of the following. First, the well drainage region represents the actual flow scale. Pressure perturbation as a result of production/injection starts at the well and is minimal at the boundaries of the sector. Furthermore, the sector scale is the most likely scale at which the REV condition will be met. Recall that lab and field measurement of equivalent fracture permeability showed scale dependency (Margolin et al., 1998, Berkowitz, 2002, Neuman and Di Federico, 2003, Katsuaki and Yuichi, 2006). This is attributed to increase fracture connectivity with sample size discussed by Long et al. (1982) and Berkowitz (2002). Hence, even if a REV may not exist, at least the DFN

upscaling results would match the measured fracture connectivity at the actual flow scale.

Second, DFN upscaling at the sector scale is less computationally demanding. During DFN upscaling, the DFN is clipped on a cell by cell basis to calculate the effective permeability. Where possible, the flow based upscaling method is preferred at this scale as the analytical upscaling error increases with cell sizes (Fig. 6.9 and 7.10). In fact, single phase DFM simulations are also viable at this scale (Chapter 6).

Third, it is easier to assign the boundary conditions at the sector scale. Information if sector boundaries are closed or open is readily available from a number of reservoir engineering data. For example, seismic interpretation and well testing delineates the structural boundaries which are normally closed boundaries or partially sealing (e.g. faults). Well logs and RFT/MDT measurement identify the WOC which is an open boundary. To define constant rate or pressure values on the open boundaries, material balance calculations can quantify the amount of water encroachment from an aquifer.

The calculated sector scale average permeability can be compared to the sensitivity plots as shown in Figs.6.9 and 7.10. The purpose is to identify the combination of upscaling method, boundary conditions and simulation cell sizes that are best matching the sector scale average permeability. If the simulation simulation cell sizes that match the sector scale average permeability are larger than those required to capture rock matrix heterogeneity, the fracture properties could be mapped across different simulation grids through the conventional upscaling methods. This workflow is summarised in Fig. 8.3.

8.3 IMPROVED SHAPE FACTOR UPSCALING

Next, a new method is proposed to characterise dual dual porosity models with multiple fracture spacing to inform the MRDP model calculations of fluid transfer between the fractures and the porous media. As discussed in Chapter 5, the additional parameters needed are σ, σ_z and V_b for each matrix block size considered in the MRDP model. The shape factors can be calcualted using Eq. 2.19.

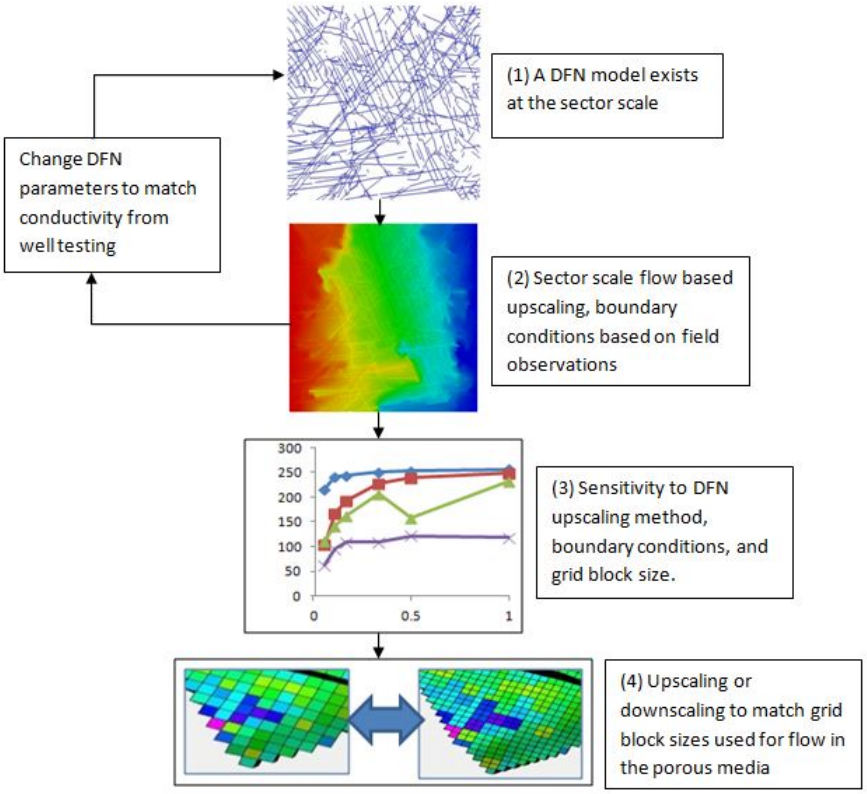

Figure 8.3: Summary of the workflow to improve permeability upscaling for DFNs. The first two steps concern the generation of DFN models and conditioning them to match static and dynamic observations. The third step compares the sector scale average permeability obtained in the second step with that of different DFN upscaling sensitivities. The final step is only necessary if the simulation cell size of the fracture domain does not match the size necessary to represent heterogeneity in rock properties.

Hence, the shape factors are linked to the fracture spacing using the following relationships (e.g. Eqs. 5.19–5.24):

$$\sigma = \frac{2L_xL_y + 2L_xL_z + 2L_yL_z}{\frac{\sqrt[3]{L_xL_yL_z}}{2}(L_xL_yL_z)}, \tag{8.1}$$

and

$$\sigma = \frac{L_xL_y + 2L_xL_z + 2L_yL_z}{L_z(L_xL_yL_z)}. \tag{8.2}$$

As noted in the discussion of the multi-directional spacing (MDS) shape factor upscaling method in (Fig. 2.9), the method already evaluates the distribution

of L_x, L_y and L_z. The method uses a statistical central tendency measure (e.g. arithmetic average, mode, etc) to find a representative fracture spacing value for each dimension. The approach suggested here is to quantify the distributions, for example by calculating the standard deviation, and represent the fracture spacing by more than one value. Subsequently, the matrix is represented by a number of components. Each component represent matrix blocks of a different size. For each matrix block size, we can obtain the shape factors σ and σ_z using Eqs. 8.1 and 8.2, respectively. The last geometrical parameter needed is the bulk volume for each matrix block size. The following methodology is proposed to calculate this parameter.

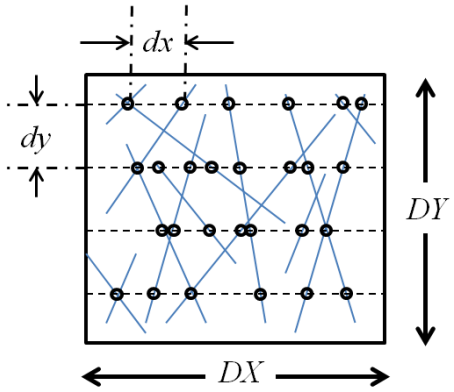

Figure 8.4: Variables used to calculate the fractional bulk volume for each transfer term in a multi-rate double porosity model. dx represents the spacing between intersection points (shown as circles) of fractures with the imaginary lines (dotted lines). dy represents the frequency of the imaginary lines. DX and DY represent the simulation cell dimensions in the two directions X and Y, respectively.

The bulk volume can be calculated as follows:

$$V_b = \sum_{j=1}^{J} \sum_{i=1}^{I} dx_{ij} \frac{DY}{dy} DZ - V_f. \tag{8.3}$$

In Eq. 8.3, J is the total number of imaginary lines (Fig. 8.4), I is total number of fracture spacings along each imaginary line and V_f is the fracture porosity. V_f is calculated as part of the DFN upscaling (Eq. 2.23). DX,DY and DZ are the dimensions of the simulation cell. dy represent the spacing between imaginary lines. Along each imaginary line in a given direction, the sum of the individual fracture spacing values (dx) is equal to the grid block size in the same direction

(DX). Eq. 8.3 suggests that the bulk volume is proportional to the total sum of all fracture spacing in one dimension. This implies that we can calculate the fraction of bulk volume occupied by matrix blocks that are higher, or lower, than a specific value. This cut-off value might come from geological observation in outcrop analogues or from image logs. The volume for each component of the transfer function is calculated by summing up all the fracture spacings that are higher, or lower, than the cut-off. We then divide the sum by the total sum of all fracture spacing values. This enables us to calculate a cumulative probability of the fractional bulk volume as a function of fracture spacing as shown in Fig. 8.6b

8.4 APPLICATION OF THE IMPROVED SHAPE FACTOR UPSCALING METHOD

The fracture outcrop map shown in Fig. 8.1 is used as an example to demonstrate the application of the improved shape factor upscaling method presented above. The map is digitised using a CAD software, and then a deterministic DFN was constructed based on the CAD model (Fig. 8.5). The geometry was also meshed with a very small cell size (0.02×0.02 m) to explicitly simulate matrix-fracture exchange under two-phase water and oil flow with a commercial reservoir simulator. Tho total number of cells is 810,000. The purpose is to compare MRDP model matrix-fracture transfer employing the shape factors and bulk volumes calculated with the improved method discussed above against fine grid simulation results.

For simplicity, a dual porosity model with two rates only is considered here. This means two groups of matrix blocks are defined based on the fracture spacing distributions: The first group consisting of small matrix blocks and the second group of large matrix blocks. The MDS method is employed to analyse the fracture spacing distribution (Fig. 8.6a). It is clear that the small matrix blocks have higher frequency than the large blocks. This observation is used as a criterion to distinguish between the small and large matrix blocks regions. Despite this high frequency, small matrix blocks only make up 40% of the bulk volume (Fig. 8.6b). The estimated geometrical parameters based on the improved shape

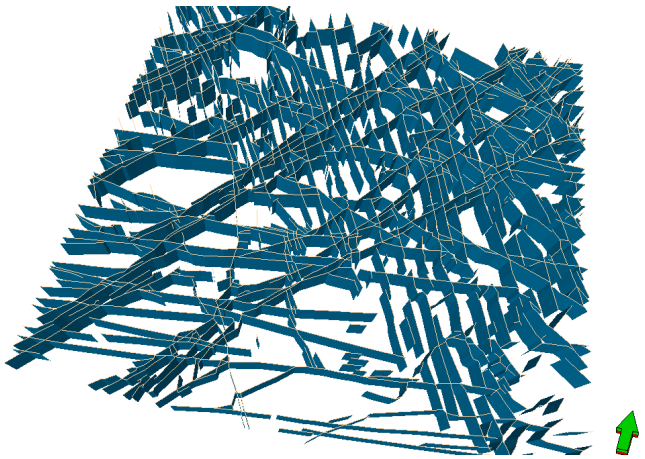

Figure 8.5: A deterministic discrete fracture network (DFN) representing the fracture geometry mapped by Odling (1997).

factor upscaling method are shown in Table 8.1 including the average shape factors for a classical single rate dual porosity model.

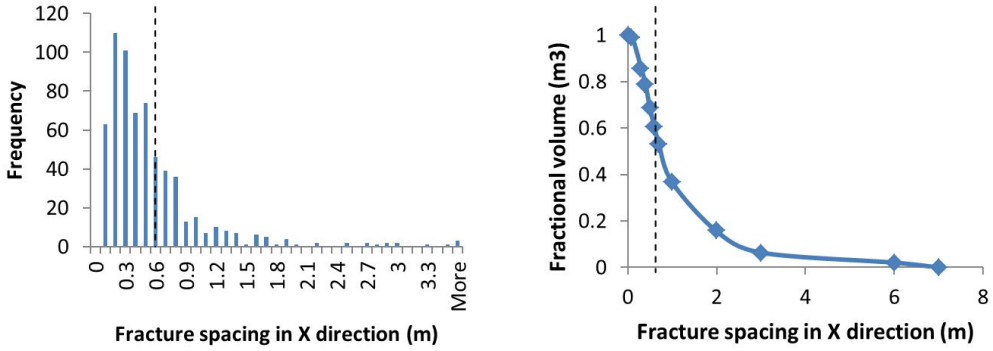

(a) Distribution of fracture spacing in X direction

(b) Fractional bulk volume as a function of fracture spacing in the X direction

Figure 8.6: Results of applying the improved shape factor upscaling method on a DFN model. The vertical dotted lines separate matrix blocks into two groups based on their sizes.

The properties of the matrix are the same as in the intermediate-scale model used in Chapters 3 and 4. These properties are detailed in Table 3.2. However, since this is a two-phase flow problem, only one-dimensional tables were used for relative permeability and capillary pressure (Fig. 8.7). In the fine grid model, capillary and gravity dominated matrix-fracture transfer is simulated for a period of two years while fractures were constantly filled with water (Fig. 8.8).

The calculation of matrix-fracture transfer functions for the classical and MRDP models was carried out using the transfer term developed in Chapter 5. Figure 8.9 shows the comparison of the fine grid solution, the dual porosity, and the

Table 8.1: Parameters used in double porosity models to compare with fine grid solution

Model		$L_x[m]$	$L_y[m]$	$\sigma[m^{-2}]$	$\sigma_z[m^{-2}]$	$V_b[-]$
Two-rate	Small blocks	0.576	0.492	2.65	0.703	0.40
	Large blocks	6.707	2.439	0.051	0.104	0.60
Single-rate (weighted average)		4.254	1.660	0.117	0.156	1.00

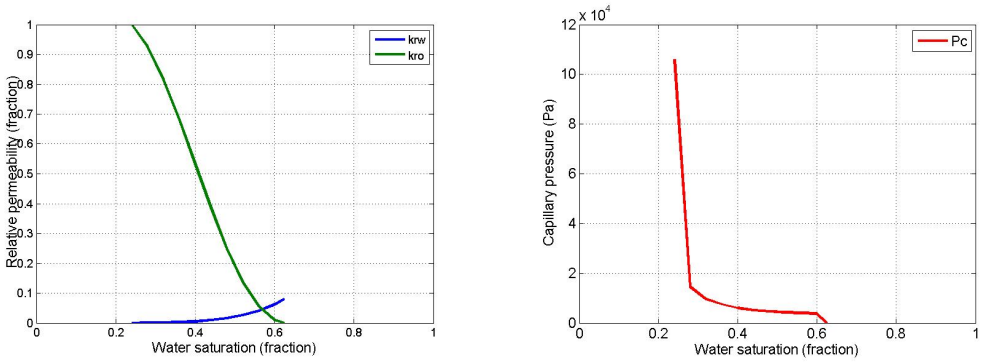

(a) (b)

Figure 8.7: Relative permeability and capillary pressure data used in the fine grid model of the fracture map from Odling (1997).

MRDP calculations. A single-rate double porosity model based on the small size blocks only matches the early recovery during the first hour, while the single rate model based on the large size blocks only matches the late recovery after 500 days. A third s single-rate dual porosity model was tested based on the volume weighted average of fracture spacing in the two dimensions. This model yielded results that were closer to the reference solution than the previous models, but the results miss both the early and late time recovery. The two-rate double porosity model reasonably matches the fine grid solution in early and late time recovery. The good match could be explained as follows: The small matrix blocks drain fast. The MRDP hence matches the early time rate. The large matrix blocks drain slower, enabling the MRDP to match the late time rate.

8.5 SUMMARY AND CONCLUDING REMARKS

The aim of this chapter was to improve the accuracy of DFN upscaling and its integration with reservoir simulation. First, a workflow has been suggested for DFN permeability upscaling based on the analysis of the case studies pre-

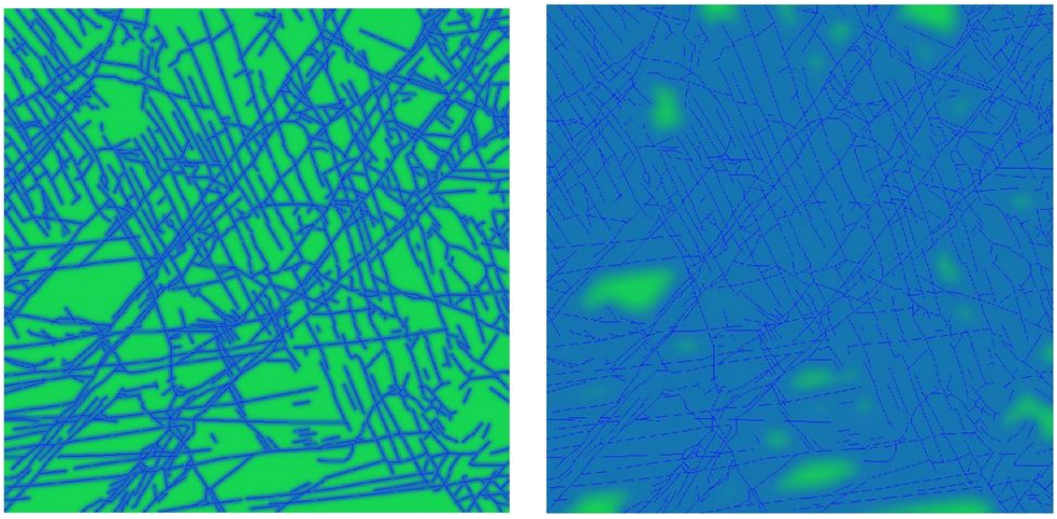

(a) (b)

Figure 8.8: The saturation distribution in the fine grid model after 18 days and 730 days. The colours denote the phases: blue is water, green is oil.

sented in Chapters 6 and 7. Second, an improved shape factor upscaling method has been presented. The method was applied to a realistic fracture geometry. The shape factor upscaling is based on the MDS method and was extended to characterise matrix blocks of different sizes to feed into multi-rate dual porosity models.

The improved permeability upscaling workflow for DFNs address two main reasons affecting the accuracy of the upscaling. These are the assumptions in the analytical DFN upscaling methods and the absence of a representative elementary volume (REV). Since the DFN upscaling results was sensitive to the selection of DFN upscaling method, boundary conditions and simulation cell size, the workflow attempts to base the decision on available reservoir engineering data. The DFN upscaling is evaluated at the sector scale, which is the actual flow scale. It is more likely that a REV exist at the sector scale. Furthermore, flow-based upscaling are applicable at the sector scale and boundary conditions are easy to assign at the sector scale.

The improved shape factor upscaling is a significant step towards more accurate dual porosity models. It allows us to capture the multi-rate characteristics related to matrix blocks of multiple sizes automatically from DFN models. It is based on the MDS upscaling which already evaluates the fracture spacing distribution (see Chapter 2). But this valuable information is typically disregarded by

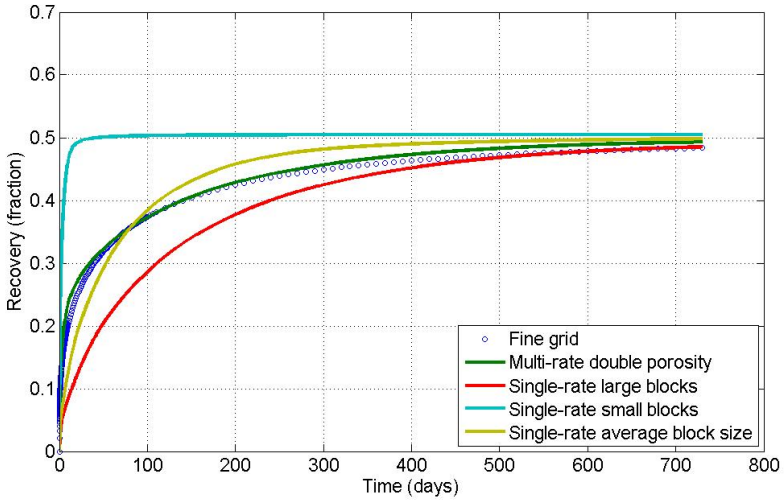

Figure 8.9: Comparisons of fine grid simulations with classical and multi-rate dual porosity models.

averaging the fracture spacing to calculate a single shape factor needed for the classical dual porosity model. The improved method considers the variability in fracture spacing and enables the calculation of multiple shape factors and the fractional bulk volumes needed for multi-rate dual porosity models. The MDS method is already implemented and is the standard in DFN modelling. Hence, the extension to the improved method suggested here can be implemented in current DFN software straightforwardly.

9

SUMMARY, CONCLUSION AND FUTURE WORK

9.1 SUMMARY AND CONCLUSION

Fractured carbonate reservoirs are important as they host a significant amount of the remaining petroleum reserves. To increase the ultimate recovery in these reservoirs, they are considered for enhanced oil recovery (EOR) methods, and here in particular water-alternating-gas (WAG) injection. However, fractured carbonate reservoirs are typically very heterogeneous across multiple scales which render their characterisation, upscaling and numerical simulation difficult. The dual porosity model, which is typically used for numerical simulation, contains a number of assumptions that are rarely applicable to natural fractures observed in outcrop analogues and subsurface reservoirs. The combination of geological heterogeneity and the underlying simplified assumptions of the dual porosity model affect the accuracy of reservoir simulation for fractured reservoirs. The objective of this work was to quantify and remove where possible upscaling and model errors so that reservoir engineers and geologists focus on quantifying the geological uncertainty of fractured reservoirs.

This thesis covered two main areas. The first concerned matrix-fracture transfer that is dominated by capillary and gravity forces. Hence, the multi-phase flow functions, relative permeability and capillary pressure curves, play a fundamental role. The second area concerned permeability upscaling in fracture networks. WAG injection establishes regions where the three phases coexist. To evaluate matrix-fracture transfer under three-phase flow, a multi-scale modelling workflow was adopted. The purpose was twofold. First, the workflow enables us to study the effect of heterogeneity at multiple levels on matrix-fracture transfer under three-phase flow. The second purpose is to improve the accuracy of commonly used upscaling methods.

The multi-scale modelling workflow started at the pore-scale. Three rock types were compared to investigate the effect of pore-level heterogeneity on three-

phase flow functions and the subsequent effect on matrix-fracture transfer at the scale of a typical reservoir simulation cell. A three-phase pore-network model was utilised to estimate the three-phase flow functions. These were then compared to three empirical models widely used for three-phase flow. Empirical models provided reasonable estimate for oil relative permeability when the oil saturation was high. When the oil saturation was low however, the empirical models estimation was in a disagreement with the pore-network model results. Hence the choice of the empirical model resulted in a 10% absolute change in oil recovery. The next step in the multi-scale modelling approach was to study the effect of heterogeneity at the intermediate scale on matrix-fracture transfer and the upscaling to dual porosity models (Chapter 4). It was found that wettability, matrix block sizes, and permeability heterogeneity affected the matrix-fracture transfer significantly. These heterogeneities must be taken into account for accurate fluid flow simulations. The upscaling to dual porosity models was examined using data from a real carbonate outcrop. It was found that dual porosity models generally overestimate recovery from matrix blocks due to two reasons, i.e. (1) the pseudo steady-state assumption of the classical dual porosity model and (2) the failure to resolve the intermediate scale heterogeneity.

An extended multiple interacting continua (MINC) model was therefore developed in Chapter 5 to improve the accuracy of three-phase flow using dual porosity models. This model is called the double block model. It was extended further to a multi-rate dual porosity (MRDP) model to account for the intermediate scale heterogeneities. The double block model was compared with detailed fine grid simulations and showed significantly more accurate results relative to the classical dual porosity model. This concluded the first part of the thesis. The focus of the second part of the thesis was on the upscaling of flow in fractures to an equivalent permeability. DFN upscaling is commonly used to evaluate the permeability values normally used for single or dual porosity models of NFR.

DFN upscaling was examined in two case studies to assess the accuracy of the results. The equivalent fracture permeability varied over three orders of magnitude. In a sector scale dynamic simulation, the DFN upscaling affected recovery by 12% absolute. A first step towards improved reservoir simulation results is to

study the sensitivity of DFN upscaling results to the upscaling method, boundary conditions and simulation cell sizes. Hence, a quantitative assessment workflow was presented and applied on a DFN model representing a real geological formation. The second step towards increased accuracy is to compare the DFN upscaling results against the DFM-based upscaling results.

The effect of DFN upscaling on history matching was examined for a real fractured reservoirs. The aim was to answer if history matching can correct for DFN upscaling errors. Three DFN upscaling scenarios were history matched separately. The quality of the history match in all these scenarios was comparable. However, the fracture permeability distributions in the three history-matched models were very different. It was recommended to study the sensitivity of the history matching results to different DFN upscaling choices before proceeding to predict future reservoir performance.

Finally, a workflow for improved fracture permeability upscaling was introduced. The workflow aims to base the DFN upscaling choices on the available reservoir engineering data. A new shape factor upscaling method was presented to characterise shape factors for multi-rate dual porosity models. The application of the improved shape factor upscaling method is demonstrated for a model with fracture geometries mapped from an outcrop. This improved method is a notable step towards more accurate but still efficient reservoir simulation of fractured reservoirs.

9.2 FUTURE WORK

The work to advance our numerical simulation of fractured reservoirs is far from complete and there are many areas for improvements. Based on the work presented in this thesis, the followings are recommendations for future work:

1. The improvements presented in Chapter 5 and Chapter 8 were applied on simple models such as the intermediate-scale model to test their accuracy. It is recommended to implement these improvements into research and open source reservoir simulators (e.g. Lie et al., 2012) for testing before the implementation into the commercial reservoir simulators and modelling

packages. Since the presented improvements are extensions of currently available methods, it is conjectured that their implementation is straightforward.

2. The Teapot Dome Field dataset gathered as part of this work was not fully utilised. This public domain data offer a great opportunity to test fracture simulation methods and compare the results with realistic production data. The field has been recommended for CO2 injection as EOR and CO2 sequestration purposes. The field is also considered for geothermal energy exploitation. These are important applications where the fractures are key to the successful design of a project. Also the DFN generated for the Tensleep Formation was not constrained by the available seismic data. A study of the effect of incorporation of seismic data on the quality of history matching is therefore recommended.

3. This work only considers simulation of immiscible WAG injection. However, nearly 80% of WAG injection cases were miscible (Christensen et al., 2001). Simulation of miscible WAG injection is more complex and requires a separate study to include the miscibility effects from the pore-scale, all the way to the reservoir scale.

4. The double block presented in this work was developed for a system where capillary forces are important. In gravity dominated matrix-fracture transfer the subdomain method of Gilman (1986) is more suitable. It is recommended to extend the double block model to a vertical stack geometry. The shape factors can be derived following the same methodology presented in this work

Part III

APPENDIX

A

TWO-DIMENSIONAL TABLES FOR FLOW FUNCTIONS

The common approach to model three-phase flow is to apply empirical models on two-phase flow functions. These are normally obtained through Special Core Analysis (SCAL) experiments. Three-phase flow functions can also be obtained by experiments or pore-network modelling. In three-phase flow functions, relative permeability and capillary pressure are tabulated as functions of two saturations (enough for three-phases as we have the closing relationship $S_3 = 1.0 - S_1 - S_2$). For example oil relative permeability, kro, can be treated as a function of water and gas saturations, S_w and S_g, as shown in Fig. A.1.

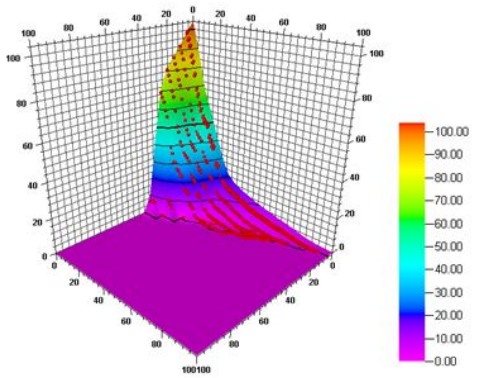

Figure A.1: A two-dimensional table showing Oil relative permeability values as a function of two saturations (All in percentage). The red dots represent the pore-network model results. For input to numerical simulators, a surface is fitted and smoothed and represented as two-dimensional table (Fig. A.2)

Sw

Sg \ Sw	0.0000	0.2000	0.4000	0.6000	0.8000	1.0000
0.0000	1.0000	0.8000	0.6000	0.4000	0.2000	0.0000
0.2000	0.8000	0.6000	0.4000	0.2000	0.0000	0.0000
0.4000	0.6000	0.4000	0.2000	0.0000	0.0000	0.0000
0.6000	0.4000	0.2000	0.0000	0.0000	0.0000	0.0000
0.8000	0.2000	0.0000	0.0000	0.0000	0.0000	0.0000
1.0000	0.0000	0.0000	0.0000	0.0000	0.0000	0.0000

kro

Figure A.2: A sample two-dimensional (2D) table to present oil relative permeability values (the blue box) as a function of two saturations: water, S_w, and gas, S_g (the red rectangles).

Two-phase flow functions represent one row in the 2D tables. For example, the three-phase oil relative permeability table shown in Figure A2 includes the two-phase oil-water displacement flow functions (at $S_g = 0$).

BIBLIOGRAPHY

AbuShaikha, A. S., and Gosselin, O. R., 2008, Matrix-Fracture Transfer Function in Dual-Medium Flow Simulation: Review, Comparison, and Validation - SPE-113890-MS, Europec/EAGE Conference and Exhibition: Rome, Italy, Society of Petroleum Engineers.

Agar, S. M., Geiger, S., Matthai, S. K., Alway, R., TomÃ¡s, S., Immenhauser, A., Shekhar, R., Paul, J., Benson, G., and Karcz, Z., The impact of hierarchical fracture networks on flow partitioning in carbonate reservoirs: Examples based on a jurassic carbonate ramp analog from the high atlas, Morocco - SPE 135135, in *Proceedings SPE Annual Technical Conference and Exhibition*, 2010, Society of Petroleum Engineers.

Ahmed Elfeel, M., Agada, S., Maier, C., and Geiger, S., Integrating Discrete Fracture Models for Static and Dynamic Calibration of Fractured Reservoirs, in *Proceedings 76th EAGE Conference and Exhibition*, 2014, Amsterdam, Netherlands, 2014.

Ahmed Elfeel, M., Couples, G. D., Geiger, S., and Ma, J., 2010, Upscaled Multi-Phase Flow Properties of Fracture Corridors, *SPE Caspian Carbonates Technology Conference: Atyrau, Kazakhstan*, Society of Petroleum Engineers.

Ahmed Elfeel, M., and Geiger, S., 2012, Static and Dynamic Assessment of DFN Permeability Upscaling, SPE 154369, *SPE Europec/EAGE Annual Conference*: Copenhagen, Denmark, Society of Petroleum Engineers.

Al-Ameri, M. B., and Shebl, H. T., 2011, Reservoir Rock Typing of a Giant Carbonate Field - SPE 148073, *SPE Reservoir Characterisation and Simulation Conference and Exhibition*: Abu Dhabi, UAE, Society of Petroleum Engineers.

Al-Dhahli, A., 2013, Pore- to field-scale modelling of three-phase flow processes in heterogeneous reservoirs with arbitrary wettability. *PhD: Heriot-Watt University*.

Al-Dhahli, A., van Dijke, M. I., and Geiger, S., 2013a, Accurate Modelling of Pore-Scale Films and Layers for Three-Phase Flow Processes in Clastic and Carbonate Rocks with Arbitrary Wettability: Transport in Porous Media, p. 1-28.

Al-Dhahli, A. R. S., Geiger, S., and Dijke, M. I. J. v., 2013b, Three-Phase Pore-Network Modeling for Reservoirs With Arbitrary Wettability: *SPE Journal*, v. 18, no. 2, p. pp. 285-295.

Al-Kobaisi, M., Kazemi, H., Ramirez, B., Ozkan, E., and Atan, S., 2009, A Critical Review for Proper Use of Water/Oil/Gas Transfer Functions in Dual-Porosity Naturally Fractured Reservoirs: Part II: *SPE Res Eval & Eng*, v. 12, no. 2, p. 211-217.

Al Shamsi, H. A., Al-Katheeri, A. B., Al Ameri, A. F., Abdulrahman, A. S., Sajeel, K., and Al Yaaqoobi, A., 2012, Immiscible WAG Injection Pilots Performance and Lessons Learnt in Carbonate Reservoir. Onshore Abu Dhabi Oil Field, United Arab Emirates - SPE 162165, *Society of Petroleum Engineers*.

Amaefule, J. O., Altunbay, M., Tiab, D., Kersey, D. G., and Keelan, D. K., 1993, Enhanced Reservoir Description: Using Core and Log Data to Identify Hydraulic (Flow) Units and Predict Permeability in Uncored Intervals/Wells - SPE 026436, *SPE Annual Technical Conference and Exhibition*: Houston, Texas, 1993, Society of Petroleum Engineers.

Arayni, F. A., Obeidi, A., Brahmakulam, J., and Ramamoorthy, R., 2013, Pulsed-Neutron Monitoring of the First CO2 Enhanced-Oil-Recovery Pilot in the Middle East: *SPE RESERVOIR EVALUATION & ENGINEERING*, v. 16, no. 1, p. pp. 72-84.

Awan, A. R., Teigland, R., and Kleppe, J., 2008, A survey of North Sea enhanced-oil-recovery projects initiated during the years 1975 to 2005: *SPE RESERVOIR EVALUATION & ENGINEERING*, v. 11, no. 3, p. 497-512.

Barenblatt, G. I., Iu, P. Z., and Kochina, I. N., 1960, Basic concepts in the theory of seepage of homogeneous liquids in fissured rocks [strata]: *PMM* vol.24, no.5, 1960, pp. 852-864 (Russian), v. 24, p. 1286-1303.

Bear, 1972, Dynamics of fluids in porous media. Pt.1-2 / by J. Bear, Elsevier, 1972.

Beckner, B., Chan, H., McDonald, A., Wooten, S., and Jones, T., Simulating naturally fractured reservoirs using a subdomain method, in *Proceedings SPE Symposium on Reservoir Simulation*, 1991, Society of Petroleum Engineers.

Behbahani, H., and Blunt, M., 2005, Analysis of imbibition in mixed-wet rocks using pore-scale modeling: *SPE Journal*, v. 10, no. 4, p. 466-474.

Bennion, D., Thomas, F., Schulmeister, B., and Ma, T., A Correlation of Water and Gas-Oil Relative Permeability Properties for Various Western Canadian Sandstone and Carbonate Oil Producing Formations - Paper 2002-066, in *Proceedings Canadian International Petroleum Conference*, 2002.

Berkowitz, B., 2002, Characterizing flow and transport in fractured geological media: A review: *ADVANCES IN WATER RESOURCES*, v. 25, no. 8-12, p. 861-884.

Biryukov, D., and Kuchuk, F. J., 2012, Transient pressure behavior of reservoirs with discrete conductive faults and fractures: *Transport in Porous Media*, v. 95, no. 1, p. 239-268.

Blunt, M. J., 2000, An empirical model for three-phase relative permeability: *SPE Journal*, v. 5, no. 4, p. 435-445.

Bogdanov, I., Mourzenko, V., Thovert, J. F., and Adler, P., 2003, Effective permeability of fractured porous media in steady state flow: *WATER RESOURCES RESEARCH*, v. 39, no. 1.

Bonnet, E., Bour, O., Odling, N. E., Davy, P., Main, I., Cowie, P., and Berkowitz, B., 2001, Scaling of fracture systems in geological media: *Reviews of Geophysics*, v. 39, no. 3, p. 347-383.

Botros, F. E., Hassan, A. E., Reeves, D. M., and Pohll, G., 2008, On mapping fracture networks onto continuum: *WATER RESOURCES RESEARCH*, v. 44, no. 8.

Bourbiaux, B., Basquet, R., Cacas, M.-C., Daniel, J.-M., and Sarda, S., An integrated workflow to account for multi-scale fractures in reservoir simulation models: implementation and benefits - SPE 78489, in *Proceedings Abu Dhabi International Petroleum Exhibition and Conference*, 2002, Society of Petroleum Engineers.

Bourbiaux, B., Granet, S., Landereau, P., Noetinger, B., Sarda, S., and Sabathier, J., Scaling up matrix-fracture transfers in dual-porosity models: theory and application, in *Proceedings SPE annual technical conference*, 1999.

BP, 2012, *BP statistical review of world energy*.

Brodie, J., Jhaveri, B., Moulds, T., and Hetland, S. M., SPE 154008 Review of Gas Injection Projects in BP, 2012, Volume 1, New York, Curran, p. 589-605.

Bulnes, A., and Fitting Jr, R., 1945, An introductory discussion of the reservoir performance of limestone formations: *Transactions of the AIME*, v. 160, no. 01, p. 179-201.

Burchette, T. P., 2012, Carbonate rocks and petroleum reservoirs: a geological perspective from the industry: *Geological Society, London*, Special Publications, v. 370, no. 1, p. 17-37.

Caers, J., 2005, Petroleum geostatistics, Richardson, TX: *Society of Petroleum Engineers*.

Carlson, C., 1981, Simulation of relative permeability hysteresis to the nonwetting phase, *SPE Annual Conference San Antonio*, TX: San Antonio, TX.

Casciano, C., Ruvo, L., Volpi, B., and Masserano, F., 2004, Well test simulation through Discrete Fracture Network modelling in a fractured carbonate reservoir: *PETROLEUM GEOSCIENCE*, v. 10, no. 4, p. 331-342.

Chandra, V., Steele, R., Corbett, P., Geiger, S., Barnett, A., Wright, P., and Mangione, A., In press, Evaluating the Impact of Late Burial Corrosion on Reservoir Permeability Distribution and Reservoir Performance in a Mature Carbonate Field Using Near Wellbore Upscaling.: *Geological Society, London*, Special Publications, v. Fundamental Controls on Fluid Flow in Carbonates.

Chang, M.-M., 1993, Deriving the shape factor of a fractured rock matrix: *National Inst. for Petroleum and Energy Research*, Bartlesville, OK (United States).

Chiaramonte, L., Zoback, M. D., Friedmann, J., and Stamp, V., 2008, Seal integrity and feasibility of CO 2 sequestration in the Teapot Dome EOR pilot: geomechanical site characterization: *ENVIRONMENTAL GEOLOGY*, v. 54, no. 8, p. 1667-1675.

Chilingar, G. V., and Yen, T., 1983, Some notes on wettability and relative permeabilities of carbonate reservoir rocks, II: *Energy Sources*, v. 7, no. 1, p. 67-75.

Choquette, P. W., and Pray, L. C., 1970, Geologic nomenclature and classification of porosity in sedimentary carbonates: *AAPG BULLETIN*, v. 54, no. 2, p. 207-250.

Christensen, J. R., Stenby, E. H., and Skauge, A., 2001, Review of WAG Field Experience: *SPE RESERVOIR EVALUATION & ENGINEERING*, v. 4, no. 2, p. 97-106.

Christie, M., Demyanov, V., and Erbas, D., 2006, Uncertainty quantification for porous media flows: *Journal of Computational Physics*, v. 217, p. 143-158.

Christie, M. A., Glimm, J., Grove, J. W., Higdon, D. M., Sharp, D. H., and Wood-Schultz, M. M., 2005, Error Analysis and Simulations of Complex Phenomena: *LOS ALAMOS SCIENCE*, v. 29, p. 6-25.

Clerke, E., Funk, J., and Shtepani, E., 2013, Spontaneous Imbibition of Water into Oil Saturated M 1 Bimodal Limestone - IPTC 17162, *6th Interna-*

tional Petroleum Technology Conference: Beijing, China, 2013, International Petroleum Technology Conference.

Coats, K. H., 1989, Implicit compositional simulation of single-porosity and dual-porosity reservoirs: paper SPE, v. 18427, p. 6-8.

Cooper, S. P., Goodwin, L. B., and Lorenz, J. C., 2006, Fracture and fault patterns associated with basement cored anticlines: The example of Teapot Dome, Wyoming: *AAPG BULLETIN*, v. 90, no. 12, p. 1903-1920.

Corbett, P., Geiger-Boschung, S., Borges, L., Garayev, M., Mosquera, J. G., and Valdez, R., Limitations in Numerical Well Test Modelling of Fractured Carbonate Rocks - SPE 130252, in *Proceedings 72nd EAGE Conference & Exhibition*2010.

Cottereau, N., Garcia, M. H., Gosselin, O. R., and Vigier, L., 2010, Effective Fracture Network Permeability: Comparative Study of Calculation Methods, *SPE EUROPEC/EAGE Annual Conference and Exhibition*: Barcelona, Spain, Society of Petroleum Engineers.

de Swaan, A., 1978, Theory of waterflooding in fractured reservoirs: *SPE Journal*, v. 18, no. 02, p. 117-122.

Dean, R., and Lo, L., 1988, Simulations of naturally fractured reservoirs: *SPE Reservoir Engineering*, v. 3, no. 02, p. 638-648.

Dehghan, A., Ghorbanizadeh, S., and Ayatollahi, S., 2012, Investigating the Fracture Network Effects on Sweep Efficiency during WAG Injection Process: *Transport in Porous Media*, v. 93, no. 3, p. 577.

Delorme, M., Oliveira Mota, R., Khvoenkova, N., Fourno, A., and Notinger, B., 2013, A methodology to characterize fractured reservoirs constrained by statistical geological analysis and production: a real field case study: *Geological Society, London*, Special Publications, v. 374.

Dershowitz, B., LaPointe, P., Eiben, T., and Wei, L., 2000, Integration of Discrete Feature Network Methods With Conventional Simulator Approaches: *SPE RESERVOIR EVALUATION & ENGINEERING*, no. 04.

Dershowitz, W. S., 1984, Rock joint systems. *PhD:Massachusetts Institute of Technology.*

Dershowitz, W. S., Einstein, H. H., La Pointe, P. R., Eiben, T., Wadleigh, E., and Ivanova, V., 1998, Fractured Reservoir Discrete Fracture Network Technologies: *National Petroleum Technology Office*.

Di Donato, G., Huang, W., and Blunt, M., Streamline-based dual porosity simulation of fractured reservoirs, in *Proceedings SPE Annual Technical Conference and Exhibition*, 2003, Society of Petroleum Engineers.

Di Donato, G., Lu, H., Tavassoli, Z., and Blunt, M. J., 2007, Multirate-Transfer Dual-Porosity Modeling of Gravity Drainage and Imbibition: *SPE Journal*, v. 12, no. 1, p. pp. 77-88.

Dougherty, E. L., 1972, Application of optimization methods to oilfield problems: Proved, probable, possible, *47th Annual Fall Meeting of the Society of Petroleum Engineers* (October 08, 1972-October 11, 1972): San Antonio, Texas.

Durlofsky, L. J., 1991, Numerical calculation of equivalent grid block permeability tensors for heterogeneous porous media: *WATER RESOURCES RESEARCH*, v. 27, no. 5, p. 699-708.

Er, V., Babadagli, T., and Xu, Z. H., 2010, Pore-Scale Investigation of the Matrix-Fracture Interaction During CO2 Injection in Naturally Fractured Oil Reservoirs: *ENERGY & FUELS*, v. 24, p. 1421-1430.

Fernø, M., Haugen, A., and Graue, A., 2011, Wettability effects on the matrix fracture fluid transfer in fractured carbonate rocks: *JOURNAL OF PETROLEUM SCIENCE AND ENGINEERING*, v. 77, no. 1, p. 146-153.

Gang, T., and Kelkar, M., 2008, History Matching for Determination of Fracture Permeability and Capillary Pressure: *SPE RESERVOIR EVALUATION & ENGINEERING*, v. 11, no. 5, p. 813-822.

Ganzer, L., Simulating fractured reservoirs using adaptive dual continuum - SPE 75233, in *Proceedings SPE/DOE Improved Oil Recovery Symposium*, 2002, Society of Petroleum Engineers.

Garcia, M. H., Gouth, F. M., and Gosselin, O. R., 2007, Fast and Efficient Modeling and Conditioning of Naturally Fractured Reservoir Models Using Static and Dynamic Data, *EUROPEC/EAGE Conference and Exhibition*: London, U.K., Society of Petroleum Engineers.

Garcia, R. G., 2005, Reservoir simulation of CO2 sequestration and enhanced oil recovery in the Tensleep Formation, Teapot Dome field. *MSc: Texas A&M University*.

Geiger, S., Dentz, M., and Neuweiler, I., 2013, A Novel Multi-Rate Dual-Porosity Model for Improved Simulation of Fractured and Multiporosity Reservoirs: *SPE Journal*, v. 18, no. 4, p. pp. 670-684.

Geiger, S., MatthÃ€i, S. K., Niessner, J., and Helmig, R., 2009, Black-Oil Simulations for Three-Component, Three-Phase Flow in Fractured Porous Media: *SPE Journal*, v. 14, no. 2, p. 338-354.

Gilman, J. R., 1986, An Efficient Finite-Difference Method for Simulating Phase Segregation in the Matrix Blocks in Double-Porosity Reservoirs: *SPE Reservoir Engineering*, v. 1, no. 4, p. 403-413.

Gilman, J. R., and Kazemi, H., 1983, Improvements in simulation of naturally fractured reservoirs: *SPE Journal*, v. 23, no. 04, p. 695-707.

Gilman, J. R., and Kazemi, H., 1988, Improved Calculations for Viscous and Gravity Displacement in Matrix Blocks in Dual-Porosity Simulators: *Journal of Petroleum Technology*, v. 40, no. 1, p. 60-70.

Golder Associates Inc., 2010, FracMan 7.40 Manual

Gomes, J., Ribeiro, M., Strohmenger, C., Naghban, S., and Kalam, M., Carbonate Reservoir Rock Typing-The Link between Geology and SCAL, in *Proceedings Abu Dhabi International Petroleum Exhibition and Conference*, 2008.

Gong, B., Karimi-Fard, M., and Durlofsky, L. J., 2008, Upscaling discrete fracture characterizations to dual-porosity, dual-permeability models for efficient simulation of flow with strong gravitational effects: *SPE Journal*, v. 13, no. 1, p. 58-67.

Gurpinar, O. M., and Kossack, C. A., 2000, Realistic Numerical Models for Fractured Reservoirs: *SPE Journal*, v. 5, no. 4, p. 485-491.

Haggerty, R., Fleming, S. W., Meigs, L. C., and McKenna, S. A., 2001, Tracer tests in a fractured dolomite: 2. Analysis of mass transfer in single-well injection-withdrawal tests: *WATER RESOURCES RESEARCH*, v. 37, no. 5, p. 1129-1142.

Haggerty, R., and Gorelick, S. M., 1995, Multiple-rate mass-transfer for modeling diffusion and surface-reactions in media with pore-scale heterogeneity, *WATER RESOURCES RESEARCH*, Volume 31, p. 2383-2400.

Hagoort, J., 1980, Oil Recovery by Gravity Drainage: *SPE Journal*, v. 20, no. 3, p. 139-150.

Hajizadeh, Y., Demyanov, V., Mohamed, L., and Christie, M., 2011, Comparison of Evolutionary and Swarm Intelligence Methods for History Matching and Uncertainty Quantification in Petroleum Reservoir Models: *STUDIES IN COMPUTATIONAL INTELLIGENCE*, v. 366, p. 209-240.

Haugen, A., Fernø, M. A., and Graue, A., 2008, Numerical Simulation and Sensitivity Analysis of In-Situ Fluid Flow in MRI Laboratory Waterfloods of Fractured Carbonate Rocks at Different Wettabilities SPE-116145, *SPE Annual Technical Conference and Exhibition*: Denver, Colorado, USA, Society of Petroleum Engineers.

Hill, A., and Thomas, G., 1985, A new approach for simulating complex fractured reservoirs: *Scientific SoftwareIntercomp*.

Hollis, C., Vahrenkamp, V., Tull, S., Mookerjee, A., Taberner, C., and Huang, Y., 2010, Pore system characterisation in heterogeneous carbonates: An al-

ternative approach to widely-used rock-typing methodologies: *Marine and Petroleum Geology*, v. 27, no. 4, p. 772-793.

Hoteit, H., and Firoozabadi, A., 2006, Compositional modeling by the combined discontinuous Galerkin and mixed methods: *SPE Journal*, v. 11, no. 01, p. 19-34.

Hubbert, M. K., 1956, Darcy's law and the field equations of the flow of underground fluids.

Hui, M.-H., Mallison, B. T., Fyrozjaee, M. H., and Narr, W., 2013, The Upscaling of Discrete Fracture Models for Faster, Coarse-Scale Simulations of IOR and EOR Processes for Fractured Reservoirs - SPE 166075, *SPE Annual Technical Conference and Exhibition*: New Orleans, Louisiana, USA, Society of Petroleum Engineers.

Hui, M.-H., Mallison, B. T., and Lim, K.-T., An innovative workflow to model fractures in a giant carbonate reservoir - IPTC 12572, in *Proceedings International Petroleum Technology Conference*, 2008.

IEA, 2014, FAQs: Oil: `http://www.iea.org/aboutus/faqs/oil/`

Imbt, W. C., and Ellison Jr, S. P., 1947, Porosity in limestone and dolomite petroleum reservoirs.

Jackson, C. P., Hoch, A. R., and Todman, S., 2000, Self-consistency of a heterogeneous continuum porous medium representation of a fractured medium: *WATER RESOURCES RESEARCH*, v. 36, no. 1, p. 189-202.

Jakobsson, N. M., and Christian, T. M., 1994, Historical Performance of Gas Injection of Ekofisk - SPE 28933, *SPE Annual Technical Conference and Exhibition*: New Orleans, Louisiana, Copyright 1994, Society of Petroleum Engineers.

Jennings, J. W., and Ward, W. B., 2000, Geostatistical Analysis of Permeability Data and Modeling of Fluid-Flow Effects in Carbonate Outcrops: *SPE RESERVOIR EVALUATION & ENGINEERING*, v. 3, no. 4, p. 292-303.

Jiang, Z., Al-Dhahli, A., van Dijke, M. I. J., Geiger, S., and Ma, J., 2013a, Multi-scale Pore-network Modelling of WAG in Carbonates, *IOR 2013* - From Fundamental Science to Deployment St. Petersburg, Russia.

Jiang, Z., van Dijke, M., Sorbie, K., and Couples, G., 2013b, Representation of multi-scale heterogeneity via multi-scale pore networks: *WATER RESOURCES RESEARCH*.

Juanes, R., Samper, J., and Molinero, J., 2002, A general and efficient formulation of fractures and boundary conditions in the finite element method: *International Journal for Numerical Methods in Engineering*, v. 54, no. 12, p. 1751-1774.

Kalam, M. Z., Negahban, S., Al-Rawahi, A. S., and Hosani, I. A., 2011, Miscible Gas Injection Tests in Carbonates and its impact on Field Development - SPE 148374, *SPE Reservoir Characterisation and Simulation Conference and Exhibition*: Abu Dhabi, UAE, Society of Petroleum Engineers.

Karimi-Fard, M., Durlofsky, L., and Aziz, K., 2004, An efficient discrete-fracture model applicable for general-purpose reservoir simulators: *SPE Journal*, v. 9, no. 02, p. 227-236.

Karimi-Fard, M., Gong, B., and Durlofsky, L. J., 2006, Generation of coarse-scale continuum flow models from detailed fracture characterizations: *WATER RESOURCES RESEARCH*, v. 42, no. 10.

Katsuaki, K., and Yuichi, I., 2006, Spatial correlation structures of fracture systems for deriving a scaling law and modeling fracture distributions: *Computers and Geosciences*, v. 32, p. 1079-1095.

Kazemi, A., Shaikhina, D. S., Pickup, G. E., and Corbett, P. W. M., 2012, Comparison of Upscaling Methods in a Heterogeneous Carbonate Model - SPE 154499, *SPE Europec/EAGE Annual Conference*: Copenhagen, Denmark, Society of Petroleum Engineers.

Kazemi, H., and Gilman, J., 1993, Multiphase flow in fractured petroleum reservoirs: *Flow and contaminant transport in fractured rock*, v. 6, p. 19.

Kazemi, H., Gilman, J. R., and Elsharkawy, A. M., 1992, Analytical and Numerical Solution of Oil Recovery From Fractured Reservoirs With Empirical Transfer Functions: *SPE Reservoir Engineering*, v. 7, no. 2, p. 219-227.

Kazemi, H., Merrill, L. S., Porterfield, J. L., and Zeman, P. R., 1976, Numerical simulation, of water-oil flow in naturally fractured reservoirs, *SPE Journal*.

Kerans, C., Lucia, F. J., and Senger, R., 1994, Integrated characterization of carbonate ramp reservoirs using Permian San Andres Formation outcrop analogs: *AAPG BULLETIN*, v. 78, no. 2, p. 181-216.

Killough, J. E., 1976, Reservoir simulation with history-dependent saturation functions, *SPE Journal*, Volume 16, p. 37-48.

Kim, J. G., and Deo, M. D., 2000, Finite element, discrete-fracture model for multiphase flow in porous media: *AIChE Journal*, v. 46, no. 6, p. 1120-1130.

King, M. J., Burn, K. S., Wang, P., Muralidharan, V., Alvarado, F. E., Ma, X., and Datta-Gupta, A., 2006, Optimal Coarsening of 3D Reservoir Models for Flow Simulation: *SPE RESERVOIR EVALUATION & ENGINEERING*, no. 08.

Land, C. S., 1968, Calculation of imbibition relative permeability for two- and three-phase flow from rock properties (SPE 1942), *SPE Journal*, p. 149-156.

Larsen, J. A., and Skauge, A., 1998, Methodology for Numerical Simulation With Cycle-Dependent Relative Permeabilities: *SPE JOURNAL*, v. 3, no. 2, p. 163-173.

Lee, J., 1982, Well testing, New York: *Society of Petroleum Engineers*.

Lichaa, P. M., Alpustun, H., Abdul, J. H., Nofal, W. A., and Fuseni, A. B., 1993, Wettability Evaluation of a Carbonate Reservoir Rock: *Advances in Core Evaluation III, Reservoir Management*, v. 327.

Lie, K. A., Krogstad, S., Ligaarden, I. S., Natvig, J. R., Nilsen, H. M., and Skaflestad, B., 2012, Open-source MATLAB implementation of consistent discretisations on complex grids: *COMPUTATIONAL GEOSCIENCES*, v. 16, no. 2, p. 297-322.

Lim, K., and Aziz, K., 1995, Matrix-fracture transfer shape factors for dual-porosity simulators: *JOURNAL OF PETROLEUM SCIENCE AND ENGINEERING*, v. 13, no. 3, p. 169-178.

Long, J., Remer, J., Wilson, C., and Witherspoon, P., 1982, Porous media equivalents for networks of discontinuous fractures: *WATER RESOURCES RESEARCH*, v. 18, no. 3, p. 645-658.

Lu, H., DiDonato, G., and Blunt, M. J., 2008, General Transfer Functions for Multiphase Flow in Fractured Reservoirs: *SPE Journal*, v. 13, no. 3, p. pp. 289-297.

Lucia, F., 1983, Petrophysical parameters estimated from visual descriptions of carbonate rocks: a field classification of carbonate pore space: *Journal of Petroleum Technology*, v. 35, no. 3, p. 629-637.

Lucia, F. J., 1995, Rock-fabric/petrophysical classification of carbonate pore space for reservoir characterization: *AAPG BULLETIN*, v. 79, no. 9, p. 1275-1300.

Maier, C., and Geiger, S., 2013, Combining Unstructured Grids, Discrete Fracture Representation and Dual-Porosity Models for Improved Simulation of Naturally Fractured Reservoirs - SPE 166049, *SPE Reservoir Characterisation and Simulation Conference and Exhibition:* Abu Dhabi, UAE, Society of Petroleum Engineers.

Maier, C., Schmid, K. S., Elfeel, M. A., and Geiger, S., 2013, Multi-Rate Mass-Transfer Dual-Porosity Modeling Using the Exact Analytical Solution for Spontaneous Imbibition SPE 164926, *SPE Europec/EAGE Annual Conference:* London, United Kingdom, Society of Petroleum Engineers.

Mäkel, G., 2007, The modelling of fractured reservoirs: Constraints and potential for fracture network geometry and hydraulics analysis: *Geological Society, London*, Special Publications, v. 292, no. 1, p. 375-403.

Mallison, B., Hui, M., and Narr, W., Practical Gridding Algorithms for Discrete Fracture Modeling Workflows, in *Proceedings 12th European Conference on the Mathematics of Oil Recovery*, 2010.

Mani, V., and Mohanty, K. K., 1998, Pore-Level Network Modeling of Three-Phase Capillary Pressure and Relative Permeability Curves.

Manrique, E. J., Muci, V. E., and Gurfinkel, M. E., 2007, EOR field experiences in carbonate reservoirs in the United States: *SPE RESERVOIR EVALUATION & ENGINEERING*, v. 10, no. 6, p. 667-686.

Margolin, G., Berkowitz, B., and Scher, H., 1998, Structure, flow, and generalized conductivity scaling in fracture networks: *WATER RESOURCES RESEARCH*, v. 34, no. 9, p. 2103-2121.

Mattax, C. C., and Kyte, J., 1962, Imbibition oil recovery from fractured water-drive reservoir: *SPE Journal*, v. 2, no. 02, p. 177-184.

Matthäi, S. K., Aydin, A., Pollard, D. D., and Stephen, G. R., 1998, Simulation of transient well-test signatures for geologically realistic faults in sandstone reservoirs: *SPE Journal*, v. 3, no. 01, p. 62-76.

Matthäi, S. K., and Bazrafkan, S., Simulation of Gas Oil Gravity Drainage: Comparison of the Dual Continuum with the Discrete-Fracture and Matrix Approach, in *Proceedings Second EAGE Workshop on Naturally Fractured Reservoirs*, 2013.

Matthäi, S. K., Mezentsev, A. A., and Belayneh, M., 2007, Finite Element Node-Centered Finite-Volume Two-Phase-Flow Experiments With Fractured Rock Represented by Unstructured Hybrid-Element Meshes: *SPE RESERVOIR EVALUATION & ENGINEERING*, no. 12.

Matthäi, S. K., and Nick, H. M., 2009, Upscaling two-phase flow in naturally fractured reservoirs: *AAPG BULLETIN*, v. 93, no. 11, p. 1621-1632.

Mohamed, L., Christie, M., and Demyanov, V., 2010, Comparison of Stochastic Sampling Algorithms for Uncertainty Quantification: *SPE Journal*, v. 15, no. 1, p. 31-38.

Montaron, B., 2008, Carbonate Evolution: *Oil and Gas Middle East*, Volume August 2008, p. 26-32.

Muggeridge, A., Cockin, A., Webb, K., Frampton, H., Collins, I., Moulds, T., and Salino, P., 2014, Recovery rates, enhanced oil recovery and technological limits: Philosophical Transactions of the Royal Society A: *Mathematical, Physical and Engineering Sciences*, v. 372, no. 2006, p. 20120320.

Müller, C., Siegesmund, S., and Blum, P., 2010, Evaluation of the representative elementary volume (REV) of a fractured geothermal sandstone reservoir: *Environmental Earth Sciences*, v. 61, no. 8, p. 1713-1724.

Narr, Schechter, and Thompson, 2006, Naturally fractured reservoir characterization / by Wayne Narr, David W. Schechter and Laird B. Thompson, *Society of Petroleum Engineers*

Nelson, R. A., 2001, Geologic analysis of naturally fractured reservoirs, *Gulf Professional Publishing*.

Neuman, S. P., 2005, Trends, prospects and challenges in quantifying flow and transport through fractured rocks: *HYDROGEOLOGY JOURNAL*, v. 13, no. 1, p. 124-147.

Neuman, S. P., and Di Federico, V., 2003, Multifaceted nature of hydrogeologic scaling and its interpretation: *REVIEWS OF GEOPHYSICS*, v. 41, p. 4-1-4-31.

Niemi, A., Kontio, K., Kuusela-Lahtinen, A., and Poteri, A., 2000, Hydraulic characterization and upscaling of fracture networks based on multiple-scale well test data: *WATER RESOURCES RESEARCH*, v. 36, no. 12, p. 3481-3497.

O'Neill, N., 1988, Fahud Field Review: A Switch From Water to Gas Injection: *SPE Journal of Petroleum Technology*, v. 40, no. 5, p. 609-618.

Oak, M., Baker, L., and Thomas, D., 1990, Three-phase relative permeability of Berea sandstone: *Journal of Petroleum Technology*, v. 42, no. 8, p. 1054-1061.

Oda, M., 1985, Permeability tensor for discontinuous rock masses: *Geotechnique*, v. 35, no. 4, p. 483.

Odling, N. E., 1997, Scaling and connectivity of joint systems in sandstones from western Norway: *Journal of Structural Geology*, v. 19, no. 10, p. 1257-1271.

Oliver, D. S., and Chen, Y., 2011, Recent progress on reservoir history matching: a review: *COMPUTATIONAL GEOSCIENCES*, v. 15, no. 1, p. 185-221.

Olson, J. E., Qiu, Y., Holder, J., and Rijken, P., Constraining the spatial distribution of fracture networks in naturally fractured reservoirs using fracture mechanics and core measurements, in *Proceedings SPE Annual Technical Conference and Exhibition*, New Orleans, LA, Sept, 2001.

Øren, P. E., and Bakke, S., 2003, Reconstruction of Berea sandstone and pore-scale modelling of wettability effects: *JOURNAL OF PETROLEUM SCIENCE AND ENGINEERING*, v. 39, no. 3, p. 177-199.

Panda, M. N., Ambrose, J. G., Beuhler, G., and McGuire, P. L., 2009, Optimized EOR Design for the Eileen West End Area, Greater Prudhoe Bay: *SPE RESERVOIR EVALUATION & ENGINEERING*, v. 12, no. 1, p. 25-32.

Penuela, G., Hughes, R., Civan, F., and Wiggins, M., Time-dependent shape factors for secondary recovery in naturally fractured reservoirs - SPE 75234, in *Proceedings SPE/DOE Improved Oil Recovery Symposium*, 2002, Society of Petroleum Engineers.

Piri, M., and Blunt, M. J., 2005, Three-dimensional mixed-wet random pore-scale network modeling of two-and three-phase flow in porous media. I. Model description: *Physical Review E*, v. 71, no. 2, p. 026301.

Pirker, B., and Heinemann, Z. E., Method to Preliminary Estimation of the Reserves and Production Forecast for Dual Porosity Fractured Reservoirs, in *Proceedings Europec/EAGE Conference and Exhibition*, 2008, Society of Petroleum Engineers.

Pirker, B., Mittermeir, G. M., and Heinemann, Z. E., Numerically Derived Type Curves for Assessing Matrix Recovery Factors SPE 107074, in *Proceedings EUROPEC/EAGE Conference and Exhibition*, 2007, Society of Petroleum Engineers.

Pirson, S. J., 1953, Performance of fractured oil reservoirs: *AAPG BULLETIN*, v. 37, no. 2, p. 232-244.

Pizarro, J. O. D. E. S., and Branco, C. C. M., 2012, Planning and implementing an EOR project for the pre-salt Lula field, *World Oil*, Volume 233.

Pruess, K., and Narasimhan, T. N., 1985, A Practical Method for Modeling Fluid and Heat Flow in Fractured Porous Media: *SPE Journal*, v. 25, no. 1, p. 14-26.

Quandalle, P., and Sabathier, J. C., 1989, Typical Features of a Multipurpose Reservoir Simulator: *SPE Reservoir Engineering*, v. 4, no. 4, p. 475-480.

Ramirez, B., Kazemi, H., Al-kobaisi, M., Ozkan, E., and Atan, S., 2009, A Critical Review for Proper Use of Water/Oil/Gas Transfer Functions in Dual-Porosity Naturally Fractured Reservoirs: Part I: *SPE RESERVOIR EVALUATION & ENGINEERING*, v. 12, no. 2, p. pp. 200-210.

Rangel-German, E. R., and Kovscek, A. R., 2006, Time-dependent matrix-fracture shape factors for partially and completely immersed fractures: *JOURNAL OF PETROLEUM SCIENCE AND ENGINEERING*, v. 54, no. 3, p. 149-163.

Rawahi, A., Hafez, H. H., Al-yafei, A., Ghori, S. G., Putney, K., and Matthews, T. R., 2012, Maximize the Ultimate Recovery by Designing & Optimizing a CO2 Miscible Gas Injection Pilot in Giant Carbonate Oil Reservoir, Abu Dhabi SPE-162277, *Abu Dhabi International Petroleum Conference and Exhibition*: Abu Dhabi, UAE, Society of Petroleum Engineers.

Renard, P., and deMarsily, G., 1997, Calculating equivalent permeability: A review: *ADVANCES IN WATER RESOURCES*, v. 20, no. 5-6, p. 253-278.

Robinson, P. C., 1984, Connectivity, flow and transport in network models of fractured media, Connectivity, flow and transport in network models of fractured media. *PhD St. Catherine's College, Oxford University.*

Rojas, T., Demyanov, V., Christie, M., and Arnold, D., Reducing Uncertainty in Modelling Fluvial Reservoirs by using Intelligent Geological Priors, in *Proceedings Geostatistical Congress*, Olso 2012.

Rossen, R., and Shen, E., 1989, Simulation of gas/oil drainage and water/oil imbibition in naturally fractured reservoirs: *SPE Reservoir Engineering*, v. 4, no. 04, p. 464-470.

Rubin, B., 2007, Simulating Gravity Drainage and Reinfiltration With a Subdomain-Dual-Permeability Hybrid Fracture Model SPE 106191, *SPE Reservoir Simulation Symposium*: Houston, Texas, U.S.A., Society of Petroleum Engineers.

Ryazanov, A., van Dijke, M. I. J., and Sorbie, K., 2009, Two-phase pore-network modelling: existence of oil layers during water invasion: *Transport in Porous Media*, v. 80, no. 1, p. 79-99.

Sabathier, J. C., Bourbiaux, B. J., Cacas, M. C., and Sarda, S., 1998, A New Approach of Fractured Reservoirs (SPE 39825), *International Petroleum Conference and Exhibition of Mexico*: Villahermosa, Mexico, Society of Petroleum Engineers.

Sablok, R., and Aziz, K., 2008, Upscaling and Discretization Errors in Reservoir Simulation: *Petroleum Science and Technology*, v. 26, no. 10-11, p. 1161-1186.

Saidi, A., Simulation of naturally fractured reservoirs SPE 12270, in *Proceedings SPE Reservoir Simulation Symposium*, 1983, Society of Petroleum Engineers.

Saidi, A., 1996, Twenty years of gas injection history into well-fractured Haft Kel Field (Iran) - SPE 35309, *SPE International Petroleum Conference and Exhibition*, Villahermosa, Mexico.

Samier, P., Quettier, L., and Thiele, M., 2002, Applications of streamline simulations to reservoir studies: *SPE RESERVOIR EVALUATION & ENGINEERING*, v. 5, no. 04, p. 324-332.

Sarda, S., Bourbiaux, B. J., Cacas, M. C., and Sabathier, J. C., An Innovative Procedure to Compute Equivalent Block Size in a Dual-Porosity Model, 1997, *European Association of Geoscientists & Engineers*, p. 017.

Sarda, S., Jeannin, L., Basquet, R., and Bourbiaux, B., 2002, Hydraulic Characterization of Fractured Reservoirs: Simulation on Discrete Fracture Models: *SPE RESERVOIR EVALUATION & ENGINEERING*, no. 04.

Sarma, P., and Aziz, K., 2006, New Transfer Functions for Simulation of Naturally Fractured Reservoirs with Dual-Porosity Models: *SPE Journal*, v. 11, no. 3, p. pp. 328-340.

Sayers, C. M., and den Boer, L. D., 2012, Characterizing production-induced anisotropy of fractured reservoirs having multiple fracture sets: *Geophysical Prospecting*, v. 60, no. 5, p. 919-939.

Schlumberger, 2007, Schlumberger Market Analysis: `http://www.slb.com/carbonates.aspx`.

Schlumberger, 2012, ECLIPSE reservoir simulation software.

Schmid, K., and Geiger, S., 2012, Universal scaling of spontaneous imbibition for water-wet systems: *WATER RESOURCES RESEARCH*, v. 48, no. 3.

Schmid, K. S., and Geiger, S., 2013, Universal scaling of spontaneous imbibition for arbitrary petrophysical properties: Water-wet and mixed-wet states and Handy's conjecture: *JOURNAL OF PETROLEUM SCIENCE AND ENGINEERING*, v. 101, no. 0, p. 44-61.

Schwartz, B. C., 2006, Fracture Pattern Characterization of the Tensleep Formation, Teapot Dome, Wyoming. *MSc: West Virginia University.*

Senger, R., Lucia, F., Kerans, C., Ferris, M., and Fogg, G., Dominant control on reservoir-flow behavior in carbonate reservoirs as determined from outcrop studies, in *Proceedings 3rd International Reservoir Characterization Technical Conference*: Tulsa, Oklahoma, National Institute for Petroleum and Energy Research and US Department of Energy1991, Volume 1, p. 107-150.

Shahverdi, H., and Sohrabi, M., 2013, An Improved Three-Phase Relative Permeability and Hysteresis Model for the Simulation of a Water-Alternating-Gas Injection: *SPE Journal*, v. 18, no. 05, p. 841-850.

Skauge, A., and Sorbie, K. S., Status of Fluid Flow Mechanisms for Miscible and Immiscible WAG SPE 169747, in *Proceedings SPE EOR Conference at Oil and Gas West Asia*, 2014, Society of Petroleum Engineers.

Skauge, A., Veland, I., and Larsen, J. A., 1999, Factors Influencing Three Phase Flow Parameters in WAG Experiments: *SCA*-9932.

Smith, V. L., 2008, Modeling natural fracture networks | Establishing the groundwork for flow simulation at Teapot Dome, Wyoming. *MSc: WEST VIRGINIA UNIVERSITY.*

Snow, D. T., 1969, Anisotropie permeability of fractured media: *WATER RESOURCES RESEARCH*, v. 5, no. 6, p. 1273-1289.

Sohrabi, M., Tehrani, D. H., Danesh, A., and Henderson, G. D., 2004, Visualization of oil recovery by water-alternating-gas injection using high-pressure micromodels: *SPE Journal*, v. 9, no. 3, p. 290-301.

Sonier, F., Souillard, P., and Blaskovich, F. T., 1988, Numerical Simulation of Naturally Fractured Reservoirs: *SPE Reservoir Engineering*, v. 3, no. 4, p. 1114-1122.

Spiteri, E., Juanes, R., Blunt, M., and Orr, F., 2008, A new model of trapping and relative permeability hysteresis for all wettability characteristics: *SPE Journal*, v. 13, no. 3, p. 277-288.

Spiteri, E. J., and Juanes, R., 2006, Impact of relative permeability hysteresis on the numerical simulation of WAG injection: *JOURNAL OF PETROLEUM SCIENCE AND ENGINEERING*, v. 50, p. 115-139.

Stone, H., 1970, Probability model for estimating three-phase relative permeability: *Journal of Petroleum Technology*, v. 22, no. 2, p. 214-218.

Stone, H. L., 1973, Estimation of Three-Phase Relative Permeability and Residual Oil Data: *JOURNAL OF CANADIAN PETROLEUM TECHNOLOGY*, v. 12, no. 4, p. 53.

Suzuki, S., Daly, C., Caers, J. K., and Mueller, D., 2007, History Matching of Naturally Fractured Reservoirs Using Elastic Stress Simulation and Probability Perturbation Method: *SPE Journal*, v. 12, no. 1, p. pp. 118-129.

Tatomir, A., Szymkiewicz, A., Class, H., and Helmig, R., 2011, Modeling two phase flow in large scale fractured porous media with an extended multiple interacting continua method: *Computer Modeling in Engineering & Sciences(CMES)*, v. 77, no. 2, p. 81-111.

Tavassoli, Z., Carter, J. N., and King, P. R., 2004, Errors in History Matching: *SPE Journal*, v. 9, no. 3, p. 352-361.

Tecklenburg, J., Neuweiler, I., Dentz, M., Carrera, J., Geiger, S., Abramowski, C., and Silva, O., 2013, A Non-Local Two-Phase Flow Model For Immiscible Displacement in Highly Heterogeneous Porous Media And Its Parametrization: *ADVANCES IN WATER RESOURCES*.

Thomas, L. K., Dixon, T. N., and Pierson, R. G., 1983, Fractured Reservoir Simulation: *SPE Journal*, v. 23, no. 1, p. 42-54.

Ueda, Y., Murata, S., Watanabe, Y., and Funatsu, K., Investigation of the shape factor used in the dual-porosity reservoir simulator SPE 19469, in *Proceedings SPE Asia-Pacific Conference*, 1989, Society of Petroleum Engineers.

van Dijke, M. I. J., and Sorbie, K., 2006, Existence of fluid layers in the corners of a capillary with non-uniform wettability: *Journal of colloid and interface science*, v. 293, no. 2, p. 455-463.

van Dijke, M. I. J., Sorbie, K. S., Sohrabi, M., and Danesh, A., 2004, Three-phase flow WAG processes in mixed-wet porous media: Pore-scale network simulations and comparison with water-wet micromodel experiments: *SPE Journal*, v. 9, no. 2

van Dijkum, C. E., and Walker, T., 1991, Fractured Reservoir Simulation and Field Development, Natih Field, Oman. SPE 22917, *SPE Annual Technical Conference and Exhibition*: Dallas, Texas, 1991, Society of Petroleum Engineers.

van Heel, A. P., and Boerrigter, P. M., On the shape-factor in fractured reservoir simulation, in *Proceedings SPE Annual Technical Conference and Exhibition*, 2006, Society of Petroleum Engineers.

von Pattay, P. W., and Ganzer, L. J., Reservoir simulation model for fractured and partially fractured reservoirs based on PEBI grids SPE 66384, in *Proceedings SPE Reservoir Simulation Symposium*, 2001, Society of Petroleum Engineers.

Warren, J. E., and Root, P. J., 1963, The Behavior of Naturally Fractured Reservoirs, no. 09.

Wu, Y.-S., and Pruess, K., 1988, A Multiple-Porosity Method for Simulation of Naturally Fractured Petroleum Reservoirs: *SPE Reservoir Engineering*, v. 3, no. 1, p. 327-336.

Zhang, F., Skjervheim, J.-A., Reynolds, A. C., and Oliver, D. S., 2005, Automatic History Matching in a Bayesian Framework, Example Applications: *SPE RESERVOIR EVALUATION & ENGINEERING*, v. 8, no. 3, p. pp. 214-223.

Zhang, X., Morrow, N. R., and Ma, S., 1996, Experimental Verification of a Modified Scaling Group for Spontaneous Imbibition: *SPE Reservoir Engineering*, v. 11, no. 04, p. 280-285.

Zhou, D., Kamath, J., Zuo, L., and Chen, Y., 2013, Three-Phase Relative Permeability Modeling in the Simulation of WAG Injection - SPE 166138, SPE Annual Technical Conference and Exhibition: New Orleans, Louisiana, USA, 2013, Society of Petroleum Engineers.